AD-A191 110 PULSED POWER SIMULATION PROBLEMS IN MAGIC(U) MISSION 1/2
RESEARCH CORP ALEXANDRIA VA B COPLEN ET AL. 18 APR 87
MRC/WDC-R-124 DNA-TR-87-148 DNA001-84-C-0200

UNCLASSIFIED F/G 20/14 NL

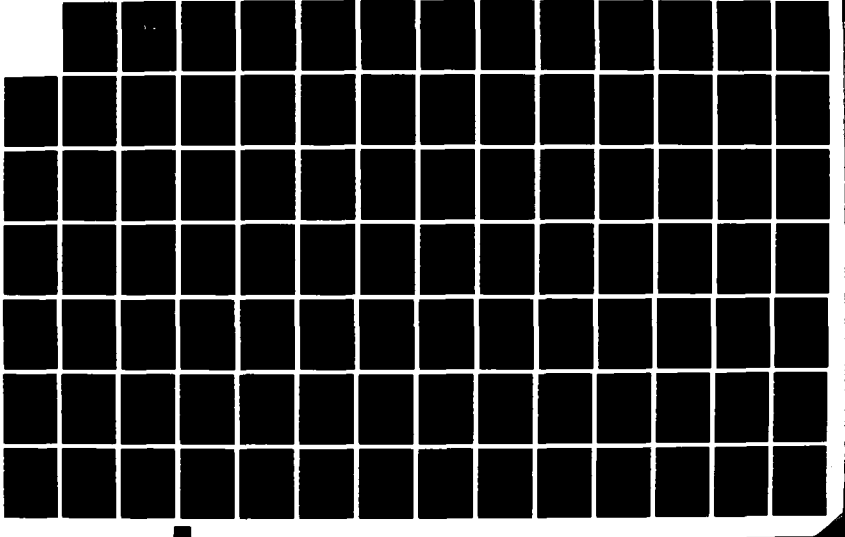

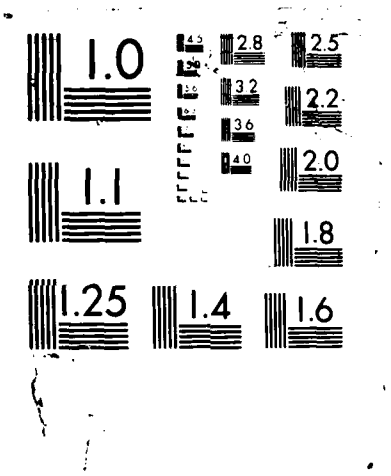
1.0
1.1
1.25
1.4
1.6
1.8
2.0
2.2
2.5
2.8
3.2
3.6
4.0

DNA-TR-87-148

PULSED POWER SIMULATION PROBLEMS IN MAGIC

B. Goplen
R. Worl
Mission Research Corporation
5503 Cherokee Avenue, Suite 201
Alexandria, VA 22312

18 April 1987

Technical Report

CONTRACT No. DNA 001-84-C-0208

Approved for public release;
distribution is unlimited.

THIS WORK WAS SPONSORED BY THE DEFENSE NUCLEAR AGENCY
UNDER RDT&E RMSS CODE B323084466 T99QMXLA00013 H2590D.

Prepared for
Director
DEFENSE NUCLEAR AGENCY
Washington, DC 20305-1000

Destroy this report when it is no longer needed. Do not return to sender.

PLEASE NOTIFY THE DEFENSE NUCLEAR AGENCY ATTN: TITL, WASHINGTON, DC 20305 1000, IF YOUR ADDRESS IS INCORRECT, IF YOU WISH IT DELETED *FROM THE DISTRIBUTION LIST, OR IF THE ADDRESSEE* IS NO LONGER EMPLOYED BY YOUR ORGANIZATION.

DISTRIBUTION LIST UPDATE

This mailer is provided to enable DNA to maintain current distribution lists for reports. We would appreciate your providing the requested information.

- ☐ Add the individual listed to your distribution list.
- ☐ Delete the cited organization/individual.
- ☐ Change of address.

NAME: _____

ORGANIZATION: _____

OLD ADDRESS	CURRENT ADDRESS
_____	_____
_____	_____
_____	_____

TELEPHONE NUMBER: (___) _____

SUBJECT AREA(s) OF INTEREST:

_____	_____
_____	_____
_____	_____

DNA OR OTHER GOVERNMENT CONTRACT NUMBER: _____

CERTIFICATION OF NEED-TO-KNOW BY GOVERNMENT SPONSOR (if other than DNA):

SPONSORING ORGANIZATION: _____

CONTRACTING OFFICER OR REPRESENTATIVE: _____

SIGNATURE: _____

CUT HERE AND RETURN

REPORT DOCUMENTATION PAGE

1a. REPORT SECURITY CLASSIFICATION UNCLASSIFIED	1b. RESTRICTIVE MARKINGS
2a. SECURITY CLASSIFICATION AUTHORITY N/A since Unclassified	3. DISTRIBUTION/AVAILABILITY OF REPORT Approved for public release; distribution is unlimited.
2b. DECLASSIFICATION/DOWNGRADING SCHEDULE N/A since Unclassified	
4. PERFORMING ORGANIZATION REPORT NUMBER(S) MRC/WDC-R-124	5. MONITORING ORGANIZATION REPORT NUMBER(S) DNA-TR-87-148
6a. NAME OF PERFORMING ORGANIZATION Mission Research Corp. — 6b. OFFICE SYMBOL (If applicable)	7a. NAME OF MONITORING ORGANIZATION Director Defense Nuclear Agency
6c. ADDRESS (City, State, and ZIP Code) 5503 Cherokee Avenue, Suite 201 Alexandria, VA 22312	7b. ADDRESS (City, State, and ZIP Code) Washington, DC 20305-1000
8a. NAME OF FUNDING/SPONSORING ORGANIZATION — 8b. OFFICE SYMBOL (If applicable) RAEV/Stobbs	9. PROCUREMENT INSTRUMENT IDENTIFICATION NUMBER DNA 001-84-C-0208
8c. ADDRESS (City, State, and ZIP Code)	10. SOURCE OF FUNDING NUMBERS PROGRAM ELEMENT NO. 62715H — PROJECT NO. T99QMXL — TASK NO. A — WORK UNIT ACCESSION NO DH008390

11. TITLE (Include Security Classification)
PULSED POWER SIMULATION PROBLEMS IN MAGIC

12. PERSONAL AUTHOR(S)
Goplen, Bruce; Worl, Richard

13a. TYPE OF REPORT	13b. TIME COVERED	14. DATE OF REPORT (Year, Month, Day)	15. PAGE COUNT
Technical	FROM 840419 TO 870418	870418	166

16. SUPPLEMENTARY NOTATION
This work was sponsored by the Defense Nuclear Agency under RDT&E RMSS Code B323084466 T99QMXLA00013 H2590D.

17 COSATI CODES			18. SUBJECT TERMS (Continue on reverse if necessary and identify by block number)
FIELD	GROUP	SUB-GROUP	
20	15		Pulsed Power Simulation, Electromagnetic Fields, MAGIC (Code)
12	5		

19. ABSTRACT (Continue on reverse if necessary and identify by block number)

This report documents canonical pulsed power simulation problems designed to be performed with the two-and-one-half dimensional, particle-in-cell code, MAGIC. The problems were created to furnish new users of MAGIC with experience in the application of simulation techniques to realistic pulsed power problems. The problems range from simple electromagnetic propagation to self-consistent diode operation. Each problem is presented in three parts: (1) a problem description, complete and self-contained, (2) a suggested approach, including actual input data, and (3) an analytical solution, allowing comparison with simulation results.

20 DISTRIBUTION/AVAILABILITY OF ABSTRACT	21 ABSTRACT SECURITY CLASSIFICATION
☐ UNCLASSIFIED/UNLIMITED ☒ SAME AS RPT. ☐ DTIC USERS	UNCLASSIFIED
22a. NAME OF RESPONSIBLE INDIVIDUAL Sandra E. Young	22b. TELEPHONE (Include Area Code) (202) 325-7042 — 22c. OFFICE SYMBOL DNA/CSTI

DD FORM 1473, 84 MAR — 83 APR edition may be used until exhausted. All other editions are obsolete.

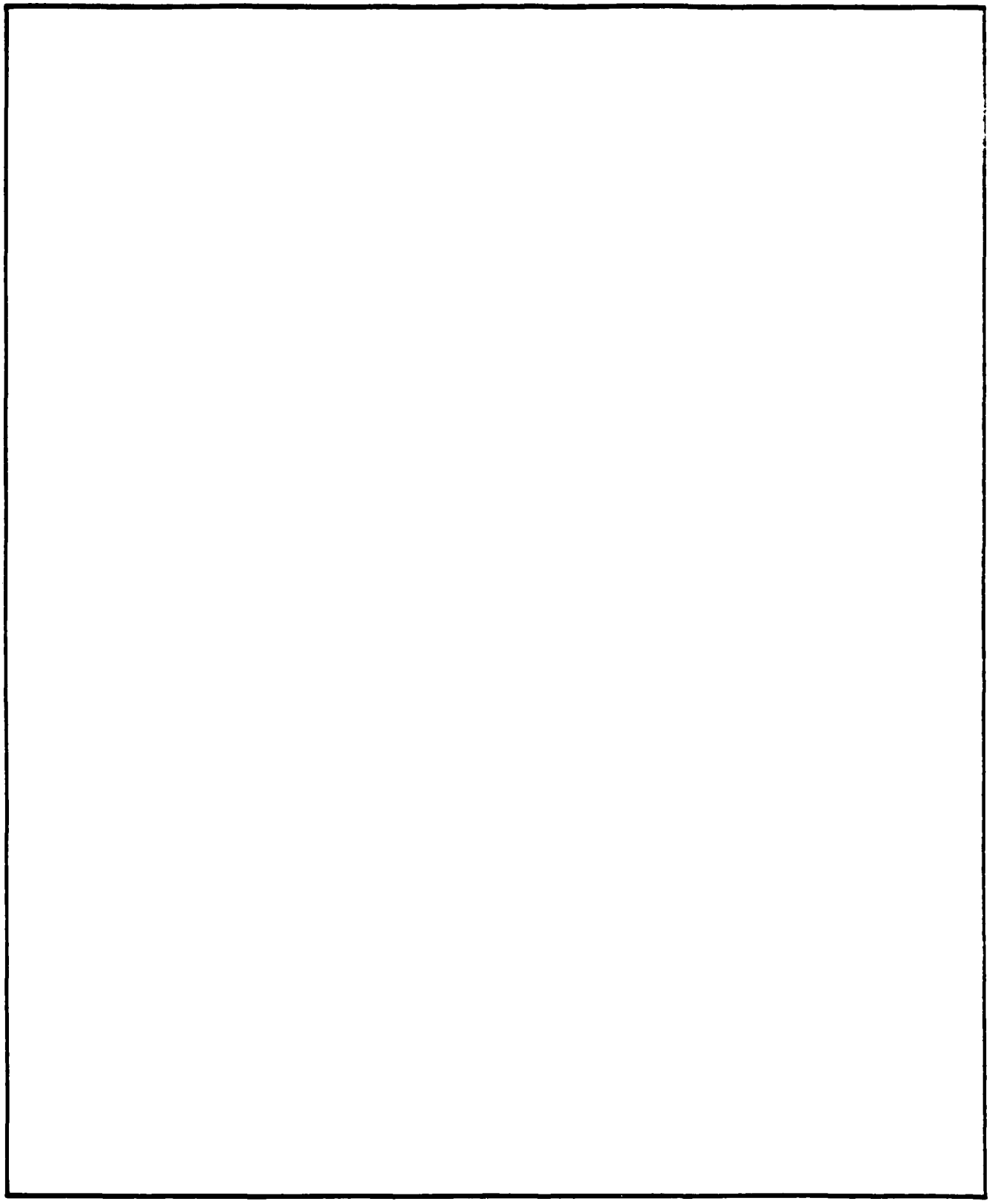

PREFACE

Although the MAGIC code† is designed to be user friendly, our experience has been that a new user will typically require several years to become proficient in its use. This simply reflects that performing particle-in-cell (PIC) code simulations on complex physical problems is an art. Specifically, it requires an intimate knowledge of mathematical models and their application in particular physical regimes, it requires judgment in the trade-offs which are necessary to perform practical simulations, and it requires the ability to interpret results and to recognize failures due to modeling errors, algorithm incompatibilities, numerical instabilities, et cetera, as well as outright code errors.

The purpose of the canonical problems presented in this report is to accelerate the learning process. Specifically, we have developed twenty-two simulation problems which relate to pulsed power transport. These problems are divided into the following three sets:

(1) Electromagnetic Propagation - simulating a coaxial line in cold test.

(2) Particle Kinematics - simulating gyrokinetics, space-charge limiting, and magnetic insulation.

(3) Power Transport - simulating self-consistent pulsed power transport processes.

These three sets of problems are described in this report in Sections 1, 2, and 3, respectively. The problems are intended to be solved sequentially, since many of the effects are interrelated and the problems gradually increase in level of difficulty.

† B. Goplen, R. E. Clark, J. McDonald, and W. M. Bollen, "User's Manual for MAGIC/ Version-September 1993," Mission Research Corporation Report, MRC/WDC-R-068, September 1993.

The individual problems were drawn from several sources; however, most were developed specifically for the present application. Similarly, the authors are responsible for most of the analytical solutions: exceptions, such as the B x ∇B drift and field emission, are denoted by references.

For each of the problems, we have included selected simulation results, and have also included complete copies of the input data used. All simulations described in this report were performed with one version (June 1993) of MAGIC. For future versions of the code, certain data commands may change in detail; however, it should be possible at any time to obtain equivalent results.

Clearly it is not possible to treat computational pulsed power transport in a comprehensive manner by performing a few simulation problems. However, it should be possible for a new user to work all of these problems in a relatively short time period (say, three months); this was considered to be an important constraint. A second constraint was imposed by available computer time: the exercises would need to be affordable. Thus, a maximum limit of five minutes CPU time on the CRAY 1 was set for any simulation. This effectively precluded realistic self-consistent problems. Because of such constraints, this experience can, at best, offer some exposure to the major ideas.

Finally, the authors wish to thank James Benford of Physics International Company for suggesting the canonical problem approach, and John Brandenburg of MRC for assistance with the analytical solutions in Problems 2.6 and 3.6.

TABLE OF CONTENTS

TABLE OF CONTENTS (Continued)

TABLE OF CONTENTS (Continued)

TABLE OF CONTENTS (Continued)

LIST OF ILLUSTRATIONS

LIST OF ILLUSTRATIONS (Continued)

LIST OF ILLUSTRATIONS (Continued)

LIST OF ILLUSTRATIONS (Continued)

LIST OF TABLES

LIST OF TABLES

SECTION 1
ELECTROMAGNETIC FIELDS

The first problem set consists of purely electromagnetic field problems. Since Maxwell's equations in the absence of space charge are linear, this greatly simplifies the interpretation of results and provides an ideal means of introducing PIC simulation concepts. Similarly, Section 2 will begin by studying the motion of single particles in specified electromagnetic fields, which is also easy to check analytically. The more complex nonlinear processes involving space charge will be deferred until Section 3.

The electromagnetic field problems are all based upon a coaxial transmission line geometry. They are designed to offer some exposure to the variety of algorithms, models, and boundary conditions available in the code.

1.1 COAXIAL LINE.

1.1.1 Problem Description.

Consider the section of coaxial transmission line illustrated in Figure 1.1. The inner and outer radii and length of the section are defined to be

$$r_i = 0.10 \text{ m}$$
$$r_0 = 0.20 \text{ m} \qquad (1.1)$$
$$L = 0.60 \text{ m} .$$

It is assumed that the walls are perfectly conducting and that no free-charge (e.g., from field emission) can be created.

For the simulation, we introduce at the inlet an incident voltage pulse representing a transverse electromagnetic (TEM) wave traveling from left to right. The pulse is defined to reach a peak voltage ϕ^+_p of 10^6 V during a linear rise-time τ of 1 nsec and to be constant thereafter. Thus, the incident wave equation is

$$\phi^+(t) = \begin{cases} \phi^+_p(t/\tau) & , \ 0 < t < \tau \\ \phi^+_p & , \ \tau \leq t < \infty . \end{cases} \qquad (1.2)$$

In general, the wave at a boundary consists of both incident and scattered parts, or

$$\phi = \phi^+ + \phi^- . \qquad (1.3)$$

However, for this simulation, we want the scattered wave to vanish ($\phi^- = 0$), so that the inlet wave will consist purely of incident wave. At the outlet, the exact opposite is to be the case. We want the incident

wave to vanish ($\phi^+ = 0$), so the outlet wave will consist purely of scattered wave. This is the simplest choice of boundary conditions which will allow us to watch an electromagnetic wave propagating through the coaxial line.

During the simulation, we wish to measure the voltage $\phi(t)$ and the current $I(t)$ as a function of time at three axial locations: $z = 0$, $L/2$, L. We also desire to examine the radial dependence of the fields E_r, E_z, and B_θ at the same three axial locations at the end of the simulation, which is to cover a time span of ten nsec.

1.1.2 Suggested Approach.

All data sequences and conventions are described in the September 1983 version of the MAGIC User's Manual[†]. Input data is entered in the form of commands, each of which contains a key word followed by arguments and parameters and is terminated by a slash. The input data for this particular problem are given in Table 1.1. For this first problem, we shall briefly discuss all of the input data in the order of appearance in Table 1.1. (Note that the order of commands is generally arbitrary.) In subsequent problems, only important variations or newly introduced commands will be discussed. The reader must refer to the Manual for a detailed description of command parameters.

The TITLE command (see Table 1.1) provides a unique problem identification on all output, while the COMMENT command allows the user to record arbitrary comments. The cylindrical (z,r) coordinate system is specified by the SYSTEM command, which identifies the spatial coordinates ($x_1 = z$, $x_2 = r$). To resolve the spatial coordinates, we shall use a uniform grid with $\delta_r = \delta_z = 0.01$ m. The spatial grid must be sufficiently fine to resolve the wave front and associated wavelengths. The z-axis

[†] B. Goplen, R. E. Clark, J. McDonald, and W. M. Bollen, "User's Manual for MAGIC/Version-September 1983," Mission Research Corporation Report, MRC/WDC-R-068, September 1983.

is specified by a X1GRID command and the r-axis by a X2GRID command. Note that the first cell (outer boundary) in MAGIC is unusable - thus the simulation boundary must begin at spatial index 2 rather than 1. We use the FIELDS command to specify a centered-difference field algorithm with 500 time steps of 2×10^{-11} sec each, for a total duration of 10^{-8} sec. The COURANT command specifies a test for compliance with the Courant stability criterion.

The CONDUCTOR command is used to specify the conducting surfaces. The two conducting segments are arbitrarily named CATHODE and ANODE. Note the definition of the surface normal flags - the convention is that the unit vector must lie normal to the surface and point to the interior of the simulation.

The VOLTAGE command is used to specify the incident voltage pulse at the inlet. In particular, the option which zeros out scattered waves at the inlet ($\phi^- = 0$) is specified by setting IVOL(1) to zero. (For this problem, there should be no physically meaningful scattered wave.) Both the temporal and radial distributions of the incident pulse must be specified, and these are simply given the arbitrary names, TEMPORAL and RADIAL, respectively. All functions in MAGIC are entered as input data using FUNCTION commands. Thus, the temporal function in Equation (1.2) is entered in the form of numerical data.

The radial distribution is determined as follows. It can be shown that this system of two separate conductors will support a TEM wave.† This wave propagates axially at the speed of light, has only two transverse components (E_r and B_θ), and has a transverse field distribution given by the static solution,

† J. D. Jackson, Classical Electrodynamics, John Wiley and Sons, New York, 1967 (p. 243).

$$\nabla^2 \phi = 0 \ , \tag{1.4}$$

which in cylindrical coordinates yields the results,

$$E_r = - \frac{\phi}{r \ell n(r_o/r_i)} \ . \tag{1.5}$$

In this equation, ϕ is the anode voltage. For the radial distribution, MAGIC requires only the relative dependence (r^{-1}), since the voltage normalization is specified by the temporal function. The radial function is entered using a power term option.

Finally, the LOOKBACK command is used to specify the outlet boundary condition and will allow outgoing waves to escape at the outlet. The phase velocity factor is assumed to be unity.

To measure simulation results†, we specify time histories of the radial electric field integral (voltage) at inlet, midpoint, and outlet, using the OBSERVE command. Six magnetic field measurements (cathode and anode at the same axial locations) are also specified. To record the spatial variation of these same fields, range plots are specified using the RANGE command. The OUTPUT command is used to specify output on system graphics rather than the internal MAGIC line printer graphics.

The START command is used to initiate the simulation, and the STOP command will terminate execution after completing the simulation.

1.1.3 Analytical Solution.

Axial propagation in a coaxial cable can be considered in terms of an equivalent transmission line. Transmission line equations for TEM

† The input data provided for these problems will generally produce copious output; for reasons of space, only selected simulation results are included in this report.

propagation involve axial and temporal derivatives of anode voltage, ϕ, and anode current, I. The equations are

$$\partial_z \phi = L' \partial_t I$$

and (1.6)

$$\partial_z I = C' \partial_t \phi \quad .$$

For a coaxial line, the capacitance and inductance per unit length are

$$C' = \frac{2\pi\varepsilon_o}{\ell n(r_o/r_i)}$$

and (1.7)

$$L' = \frac{\mu_o \ell n(r_o/r_i)}{2\pi} \quad ,$$

where ε_o and μ_o are the free-space permitivity and permeability, respectively. Division of the two relations in Equation (1.6) yields

$$\phi = IZ \quad , \tag{1.8}$$

where the line impedance, Z, is

$$Z = (L'/C')^{1/2} = Z_o \ell n(r_o/r_i) \tag{1.9}$$

with

$$Z_o = \frac{1}{2\pi} (\mu_o/\varepsilon_o)^{1/2} \approx 59.96 \text{ ohms} \quad . \tag{1.10}$$

By Ampere's law, the azimuthal magnetic field is related to the anode current by the expression,

$$B_\vartheta = \frac{\mu_o I}{2\pi r} \quad , \tag{1.11}$$

whereas the radial electric field is given by Equation (1.5). Making use of Equations (1.5) and (1.11) in (1.8), we find that

$$\frac{E_r}{B_\Theta} = (\mu_o \varepsilon_o)^{-1/2} = c \ , \tag{1.12}$$

as expected.

Figure 1.2 presents simulation results for the inlet voltage as a function of time. Note that the imposition of the boundary condition $\phi^- = 0$ forces the total wave to be exactly equal to the incident wave, or $\phi = \phi^+$. The voltage at the outlet is presented in Figure 1.3. Note the following: (1) the time delay correctly represents a wave velocity c, (2) the outlet voltage is invariant ($\phi = 10^6$ V) at late time, and (3) formation of a foot near the leading edge and a ripple near the peak. This result, also in evidence for the outlet magnetic field in Figure 1.4, is a consequence of numerical diffusion in the code.

Figures 1.5, 1.6, and 1.7 present electric and magnetic field distributions. All illustrate the r^{-1} behavior of the TEM wave predicted in Equation (1.5). The result in Figure 1.5 was imposed as a boundary condition; however, the very similar result for the outlet field in Figure 1.6 is not so constrained. Comparison suggests the potential accuracy of the method in purely electromagnetic applications.

As a final check, we compute using Equations (1.8) and (1.11) the magnetic fields at r = 0.105 m and 0.195 m. (Note that the azimuthal magnetic field is defined at half-grid rather than full-grid points). The resulting analytical results, $B = 4.58 \times 10^{-2}$ and 2.47×10^{-2} T, are given exactly (to three significant figures) by the code.

Table 1.1. Input data for Problem 1.1.

```
title * problem 1.1 * /
comment * base problem * /
system 2 /
x1grid 1 62 2 0.0 60 0.01 0.6 /
x2grid 1 12 2 0.1 10 0.01 0.1 /
fields 1 1 500 2.0e-11 /
courant 0 0 /
conductor cathode 1 2  2 62  2 /
conductor anode  -1 2 12 62 12 /
voltage temporal radial twod 0 0 0 2 2 2 12 2 /
function temporal 0 3 0.0 0.0 1.0e-9 1.0e6 1.0 1.0e6 /
function radial 5  -1 1 /
lookback 1 -1 62 2 62 12 /
observe   1 twod 1 0.0 1.0 2  2 2  2 12
            twod 1 0.0 1.0 2 32 2 32 12
            twod 1 0.0 1.0 2 62 2 62 12
            twod 1 0.0 1.0 6  2 2  2 2
            twod 1 0.0 1.0 6 32 2 32 2
            twod 1 0.0 1.0 6 61 2 61 2
            twod 1 0.0 1.0 6 2 11 2 11
            twod 1 0.0 1.0 6 32 11 32 11
            twod 1 0.0 1.0 6 61 11 61 11 /
range 250 1 2  2 2  2 12 1
          1 2 32 2 32 12 1
          1 2 62 2 62 12 1
          1 6  2 2  2 12 1
          1 6 32 2 32 12 1
          1 6 61 2 61 12 1 /
output 0 /
start /
stop /
```

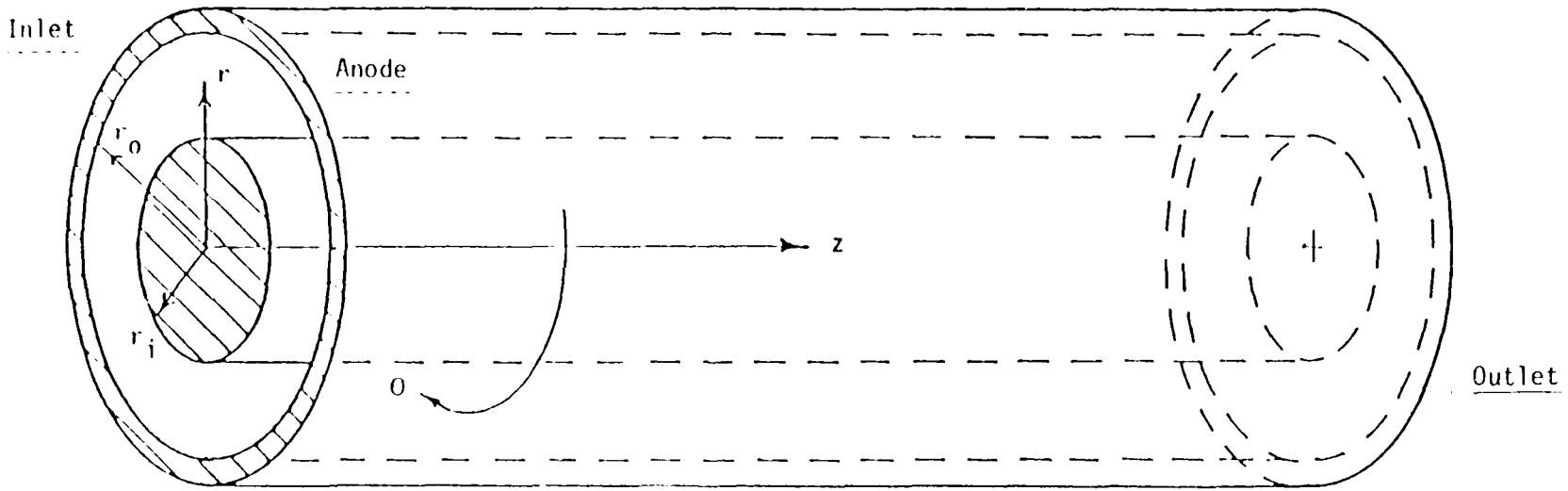

Figure 1.1. Coaxial transmission line.

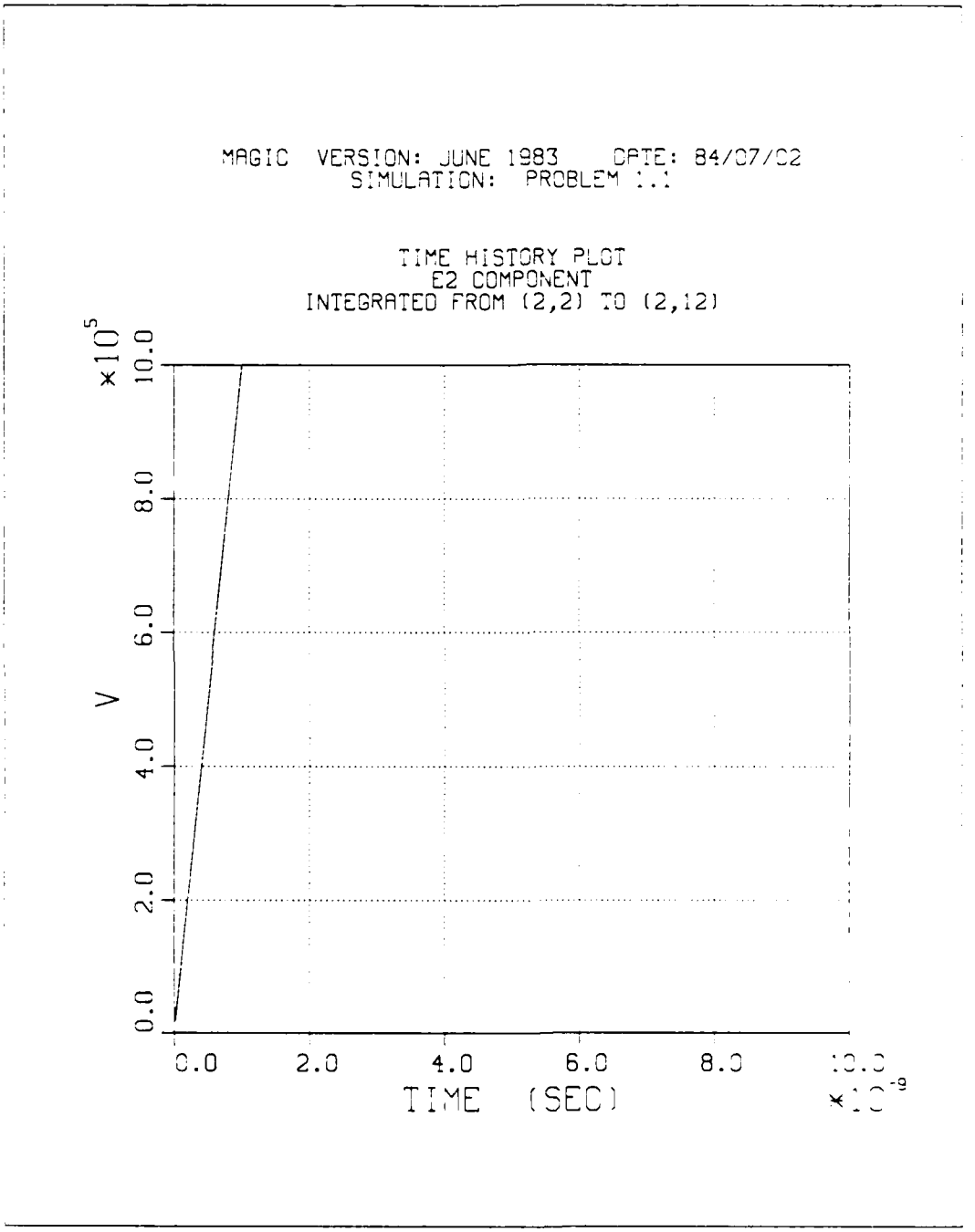

Figure 1.2. Inlet voltage vs. time, Problem 1.1.

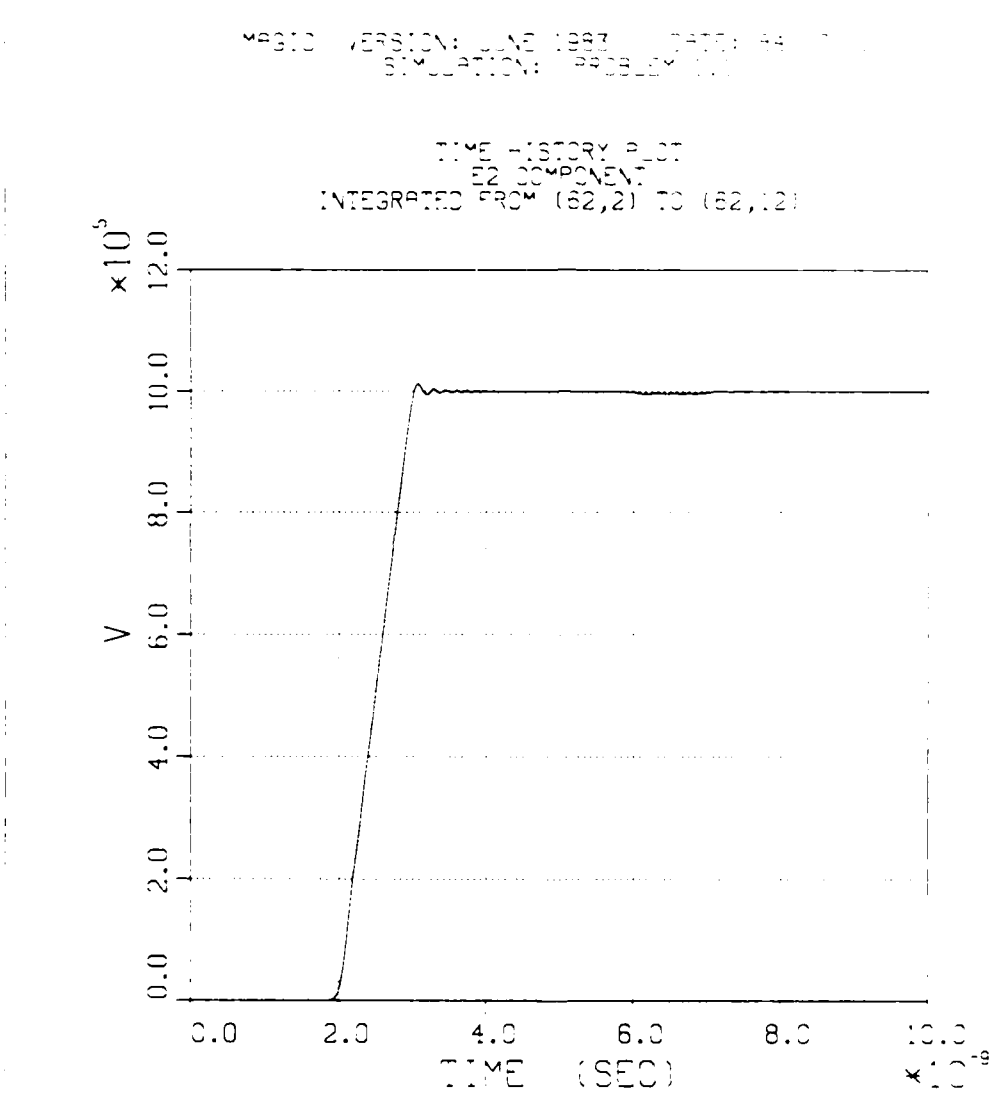

Figure 1.3. Outlet voltage vs. time, Problem 1.1.

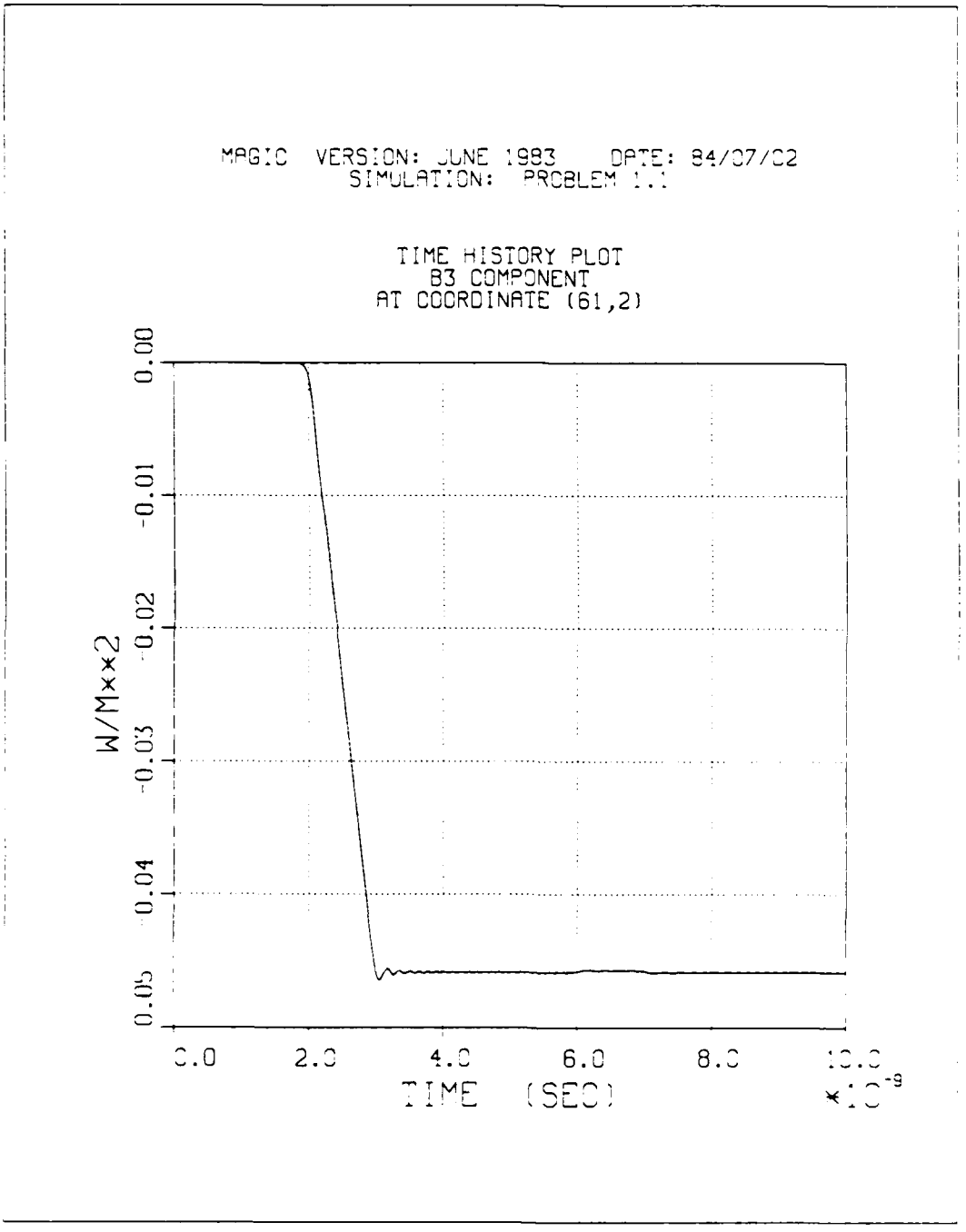

Figure 1.4. Magnetic field vs. time, Problem 1.1.

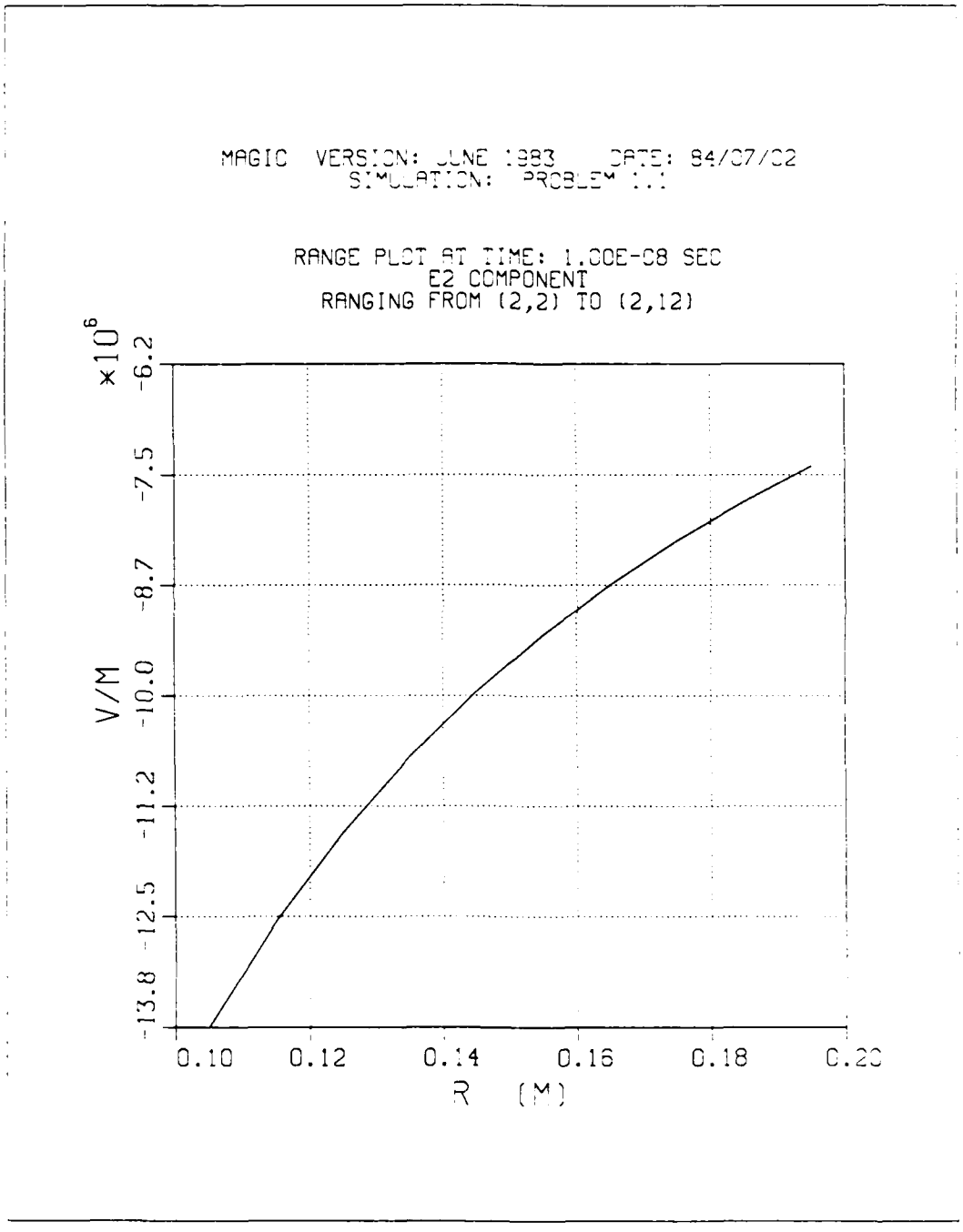

Figure 1.5. Inlet electric field vs. radius, Problem 1.1.

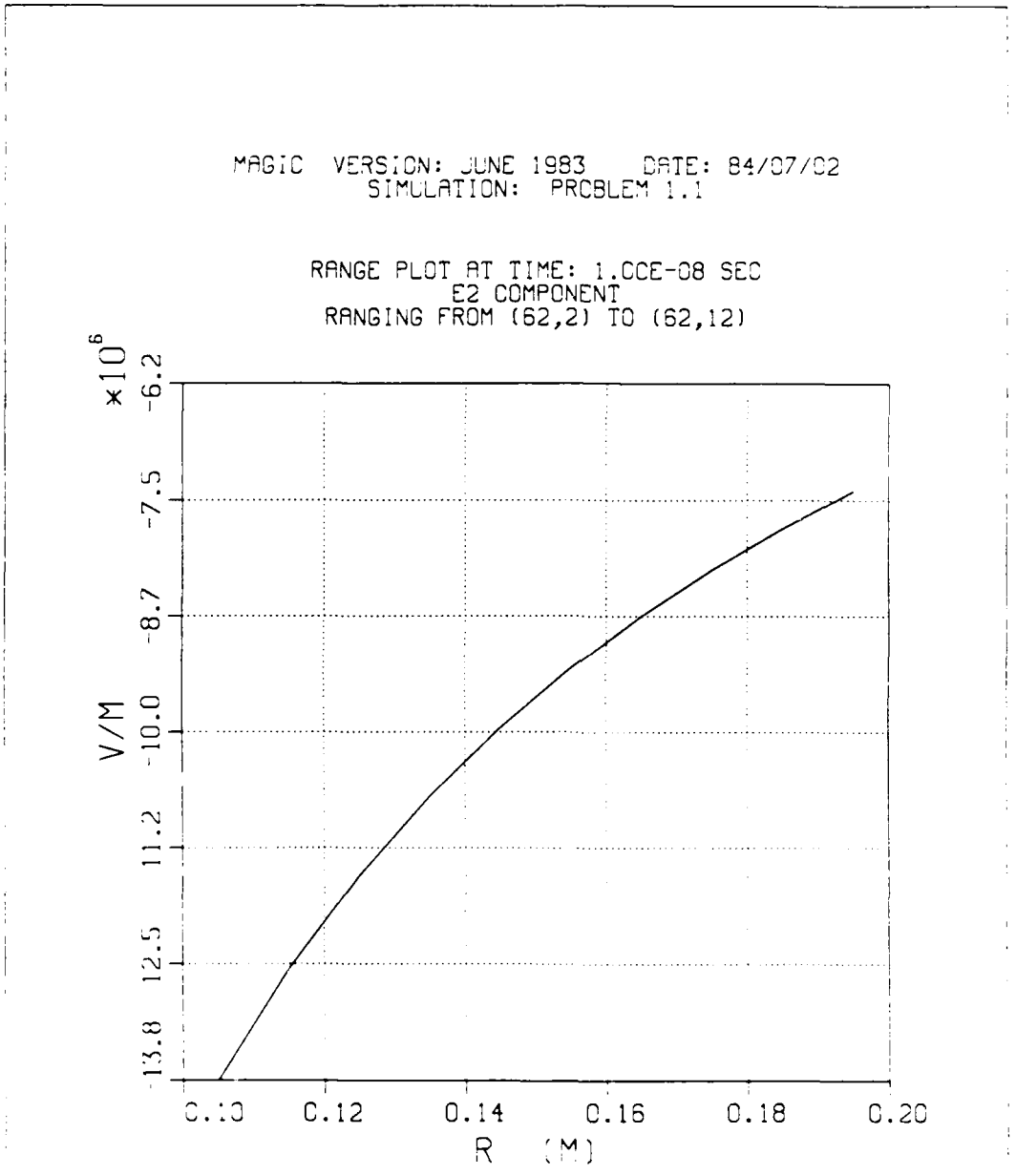

Figure 1.6. Outlet electric field vs. radius, Problem 1.1.

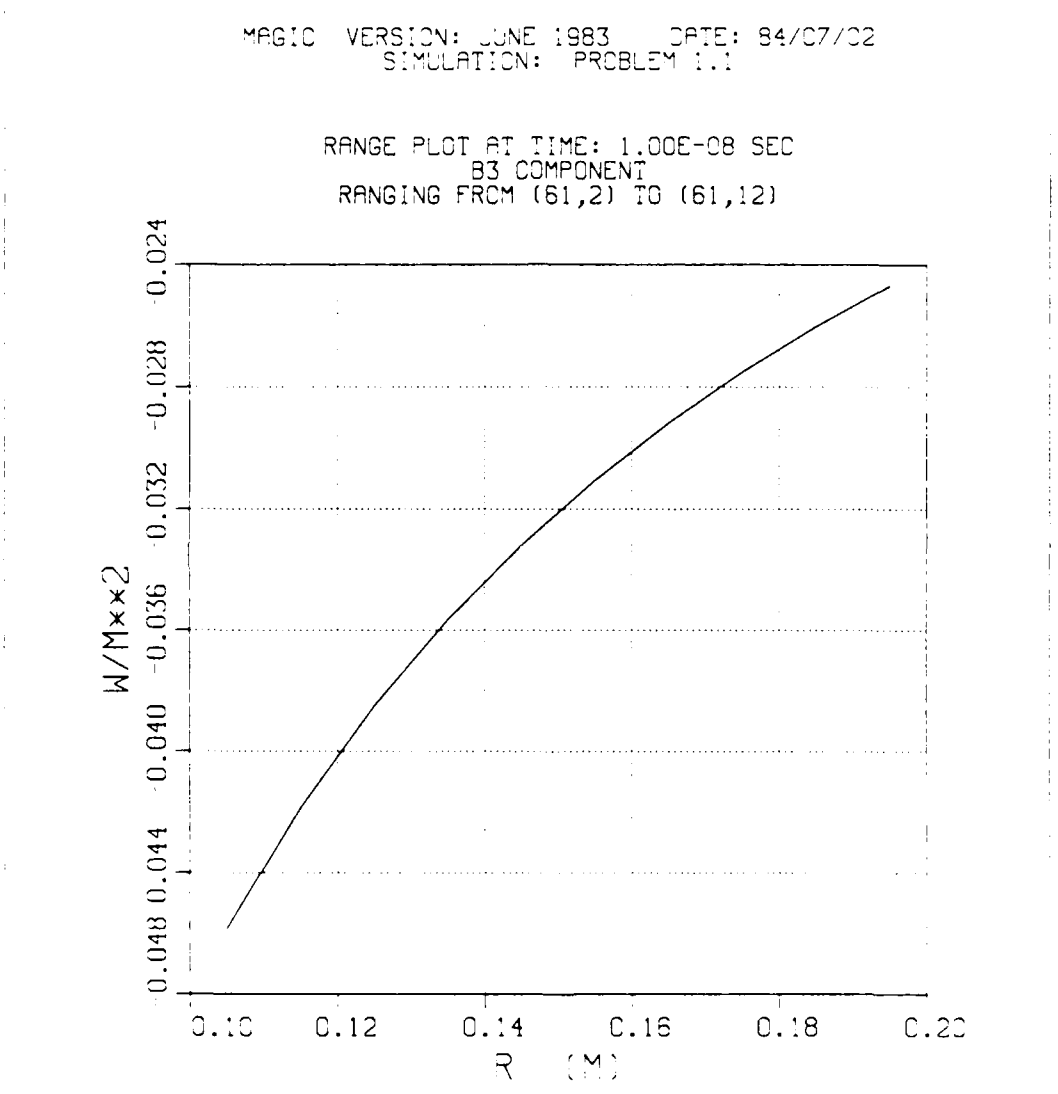

Figure 1.7. Outlet magnetic field vs. radius, Problem 1.1.

1.2 SCATTERED WAVE REFLECTION AT INLET.

1.2.1 Problem Description.

This problem demonstrates the application of the previously described (zero scattered wave) inlet boundary condition for a case in in which there is a physically meaningful scattered wave impinging on it, i.e., $\phi^- \neq 0$. To create a scattered wave, we shall simply short out the two conductors at the previous outlet. This should produce a scattered wave equal in magnitude to the incident wave ($\phi^- = -\phi^+$). In this problem, we will see that the selected inlet boundary condition ($\phi^- = 0$) is the wrong boundary condition for this case.

1.2.2 Suggested Approach.

Using the input data for Problem 1.1, simply replace the LOOKBACK command at the outlet with a CONDUCTOR command. This is labeled 'SHORT' in Table 1.2.

1.2.3 Analytical Solution.

To understand (or predict) what will happen in this problem, it is necessary to understand the effect of an impedance mismatch. Thus, we consider a two-region problem, with the inlet at impedance Z_1 and the outlet at Z_2.

As before, the incident pulse is defined by a peak voltage, ϕ^+, and associated current, I^+, which are related by the inlet impedance according to

$$\phi^+ = I^+ Z_1 \ . \tag{1.13}$$

At the mismatch, scattering occurs. The scattered wave, described in terms of peak voltage and current, ϕ^- and I^-, propagates in both directions from the discontinuity at the speed of light. The voltage-current relationship must be satisfied on both sides of the discontinuity. Thus, solving for the scattered voltage and current in terms of the incident pulse, one obtains

$$\phi^- = \phi^+ \frac{Z_2 - Z_1}{Z_1 + Z_2}$$

$$I^- = I^+ \frac{Z_1 - Z_2}{Z_1 + Z_2} \quad . \tag{1.14}$$

Then the total voltage and current are given by

$$\phi = \phi^+ \frac{2Z_2}{Z_1 + Z_2}$$

$$I = I^+ \frac{2Z_1}{Z_1 + Z_2} \quad . \tag{1.15}$$

For a short circuit ($Z_2 = 0$), the total voltage vanishes and the current doubles. Note that the transient results should reflect the retarded time between mismatch and measurements as well as the rise-time of the incident pulse.

Figure 1.9 illustrates the simulation result at the inlet boundary. Note that imposition of the condition $\phi^- = 0$ forces the total wave to be equal to the incident wave, or $\phi = \phi^+$. Physically, we expect the voltage at the inlet to vanish at 5 nsec.

The reason for the discrepancy is clear in Figure 1.9, which illustrates voltage vs. time at midpoint (L/2). Note the passage of the incident wave ϕ^+ beginning at 1 nsec. At 3 nsec, the scattered wave from the short circuit (traveling from right to left) begins to cancel the incident wave. Between 4 and 5 nsec, cancellation is complete ($\phi^+ + \phi^- = 0$) and the voltage vanishes. So far, the result is physically correct. However, by 5 nsec the scattered wave from the short circuit (ϕ^-) has reached the inlet, has itself been rescattered (since $\phi^- = 0$), and the second scattered wave has returned to the midpoint. This process will simply repeat forever - of course, we have picked the spatial dimensions and wave rise-time to produce the even pattern shown in Figure 1.9.

This result is, of course, nonphysical and potentially catastrophic. This is illustrated even more clearly in the plot of magnetic field vs. time. This result, shown in Figure 1.10, indicates that the magnetic field will increase without limit. (This result is similarly predicted, with careful attention to signs.) Thus, it is crucially important for simulation purposes to separate experimental measurements into incident and scattered waves. Application of the total wave will produce satisfactory results only if the choice of boundary condition is consistent with the internal dynamics. Otherwise, scattered waves will be trapped in the simulation. In Problem 1.3, we consider a boundary condition which avoids this particular difficulty.

Table 1.2. Input data for Problem 1.2.

```
title * problem 1.2 * /
comment * scattered wave reflection * /
system 2 /
x1grid 1 62 2 0.0 60 0.01 0.6 /
x2grid 1 12 2 0.1 10 0.01 0.1 /
fields 1 1 500 2.0e-11 /
courant 0 0 /
conductor cathode 1 2  2 62  2 /
conductor anode  -1 2 12 62 12 /
conductor short -1 62 2 62 12 /
voltage temporal radial twod 0 0 0 2 2 2 12 2 /
function temporal 0 3 0.0 0.0 1.0e-9 1.0e6 1.0 1.0e6 /
function radial 5  -1 1 /
observe   1 twod 1 0.0 1.0 2  2 2  2 12
            twod 1 0.0 1.0 2 32 2 32 12
            twod 1 0.0 1.0 2 62 2 62 12
            twod 1 0.0 1.0 6  2 2  2 2
            twod 1 0.0 1.0 6 32 2 32 2
            twod 1 0.0 1.0 6 61 2 61 2
            twod 1 0.0 1.0 6 2 11 2 11
            twod 1 0.0 1.0 6 32 11 32 11
            twod 1 0.0 1.0 6 61 11 61 11 /
range 250 1 2  2 2  2 12 1
          1 2 32 2 32 12 1
          1 2 62 2 62 12 1
          1 6  2 2  2 12 1
          1 6 32 2 32 12 1
          1 6 61 2 61 12 1 /
output 0 /
start /
stop /
```

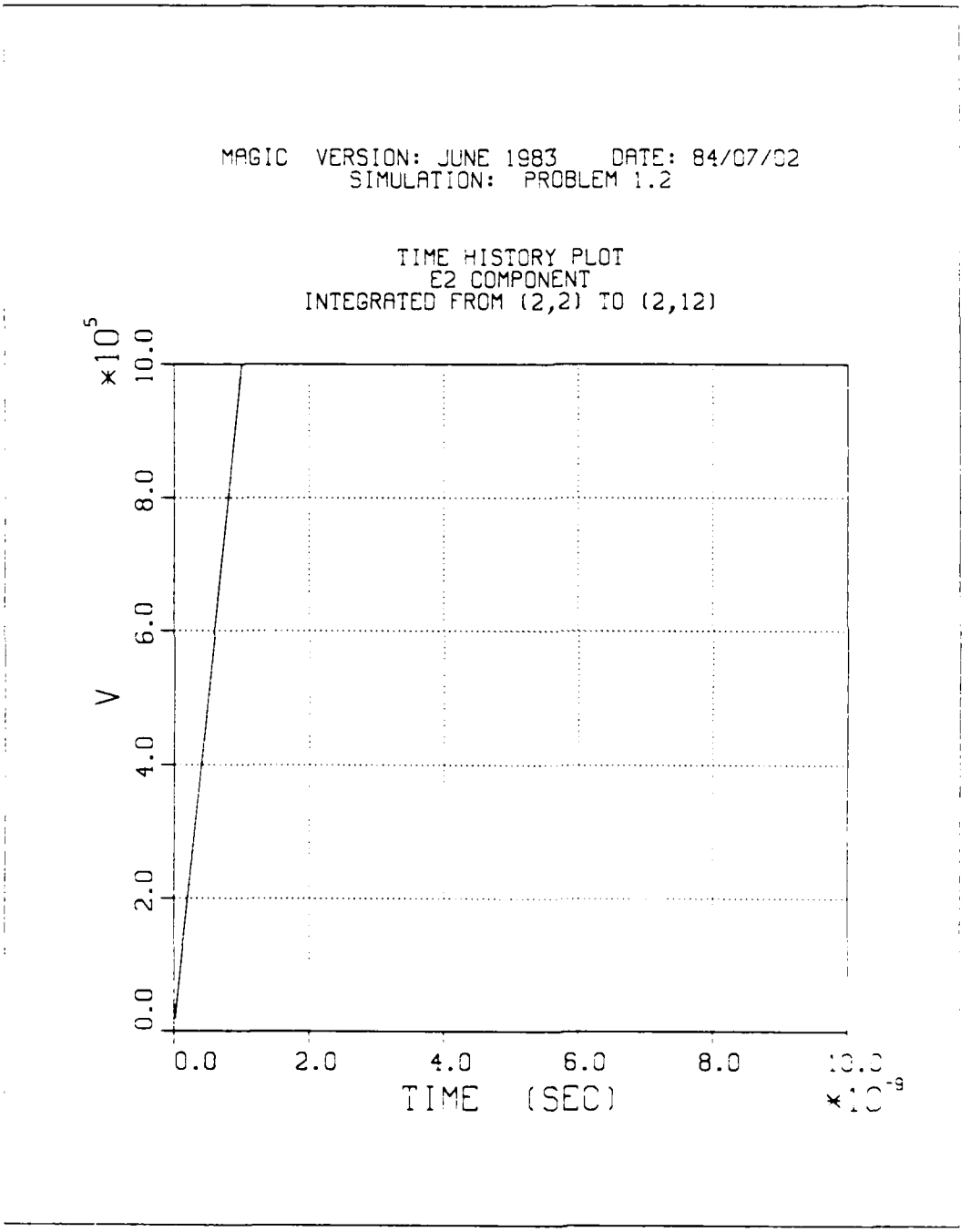

Figure 1.8. Inlet voltage vs. time, Problem 1.2.

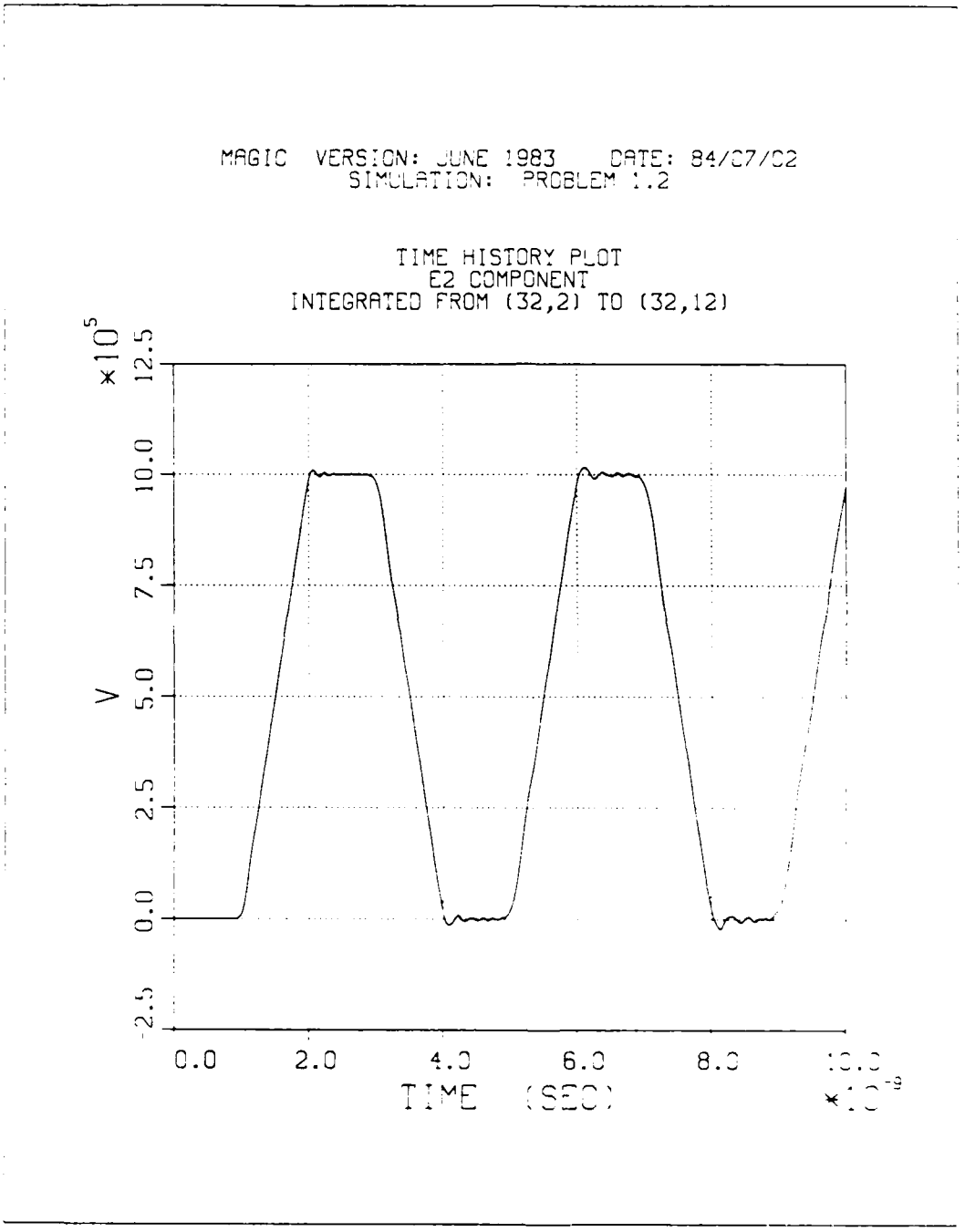

Figure 1.9. Midpoint voltage vs. time, Problem 1.2.

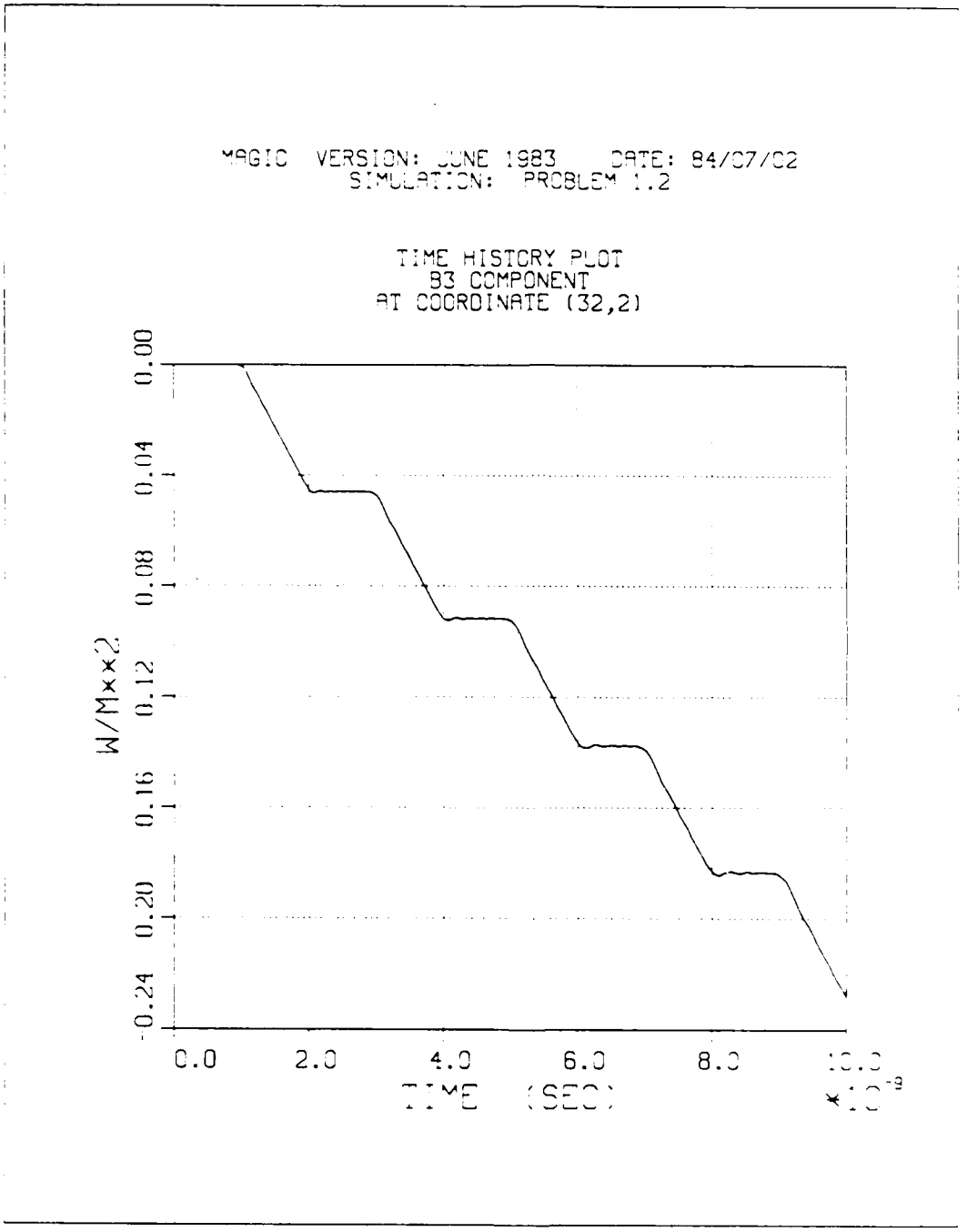

Figure 1.10. Midpoint magnetic field vs. time, Problem 1.2.

1.3 SCATTERED WAVE ABSORPTION AT INLET.

1.3.1 Problem Description.

The problem is to repeat the short circuit simulation in Problem 1.2, but to use an inlet boundary condition which allows the scattered waves to exit through the inlet rather than forcing them to zero. This is accomplished by absorbing the scattered wave at the inlet.

1.3.2 Suggested Approach.

The input data from Problem 1.2 can be duplicated exactly except for the VOLTAGE command. Here, the option flag (which doubles as a surface alignment flag) should be set to +1; also the phase velocity factor should be set to unity. The input data is shown in Table 1.3.

1.3.3 Analytical Solution.

Selected results from this simulation are shown in Figures 1.11, 1.12, and 1.13, which correspond to similar plots from Problem 1.2. Whereas, in Figure 1.8 the total voltage is maintained at the incident wave value ($\phi = \phi^+$), in Figure 1.11 the scattered wave is correctly accounted for ($\phi = \phi^+ + \phi^-$). Note that the time lapse until the voltage begins to drop is perfectly consistent with the leading edge of the incident pulse reaching the short circuit, scattering, and returning to the inlet.

The voltage and current near midpoint (L/2) are shown in Figures 1.12 and 1.13. From Equation (1.15), we expect the voltage to vanish and the current to double, precisely as the figures illustrate. Again, note the consistency of the time lapses with waves traveling at the speed of light.

In summary, this inlet boundary condition, which allows scattered waves to escape upstream (absorption), is generally superior to that used in Problems 1.1 and 1.2. However, it suffers from two defects: (1) the phase velocity for the scattered wave must be known (see Problem 1.5), and (2) the incident wave must be clearly distinguishable from any scattered waves.

Table 1.3. Input data for Problem 1.3.

```
title * problem 1.3 * /
comment * scattered wave absorption * /
system 2 /
x1grid 1 62 2 0.0 60 0.01 0.6 /
x2grid 1 12 2 0.1 10 0.01 0.1 /
fields 1 1 500 2.0e-11 /
courant 0 0 /
conductor cathode 1 2  2 62  2 /
conductor anode  -1 2 12 62 12 /
conductor short -1 62 2 62 12 /
voltage temporal radial twod 0 1.0 1 2 2 2 12 2 /
function temporal 0 3 0.0 0.0 1.0e-9 1.0e6 1.0 1.0e6 /
function radial 5  -1 1 /
observe   1 twod 1 0.0 1.0 2  2 2  2 12
            twod 1 0.0 1.0 2 32 2 32 12
            twod 1 0.0 1.0 2 61 2 61 12
            twod 1 0.0 1.0 6  2 2  2 2
            twod 1 0.0 1.0 6 32 2 32 2
            twod 1 0.0 1.0 6 61 2 61 2
            twod 1 0.0 1.0 6 2 11 2 11
            twod 1 0.0 1.0 6 32 11 32 11
            twod 1 0.0 1.0 6 61 11 61 11 /
range 250 1 2  2 2  2 12 1
          1 2 32 2 32 12 1
          1 2 61 2 61 12 1
          1 6  2 2  2 12 1
          1 6 32 2 32 12 1
          1 6 61 2 61 12 1 /
output 0 /
start /
stop /
```

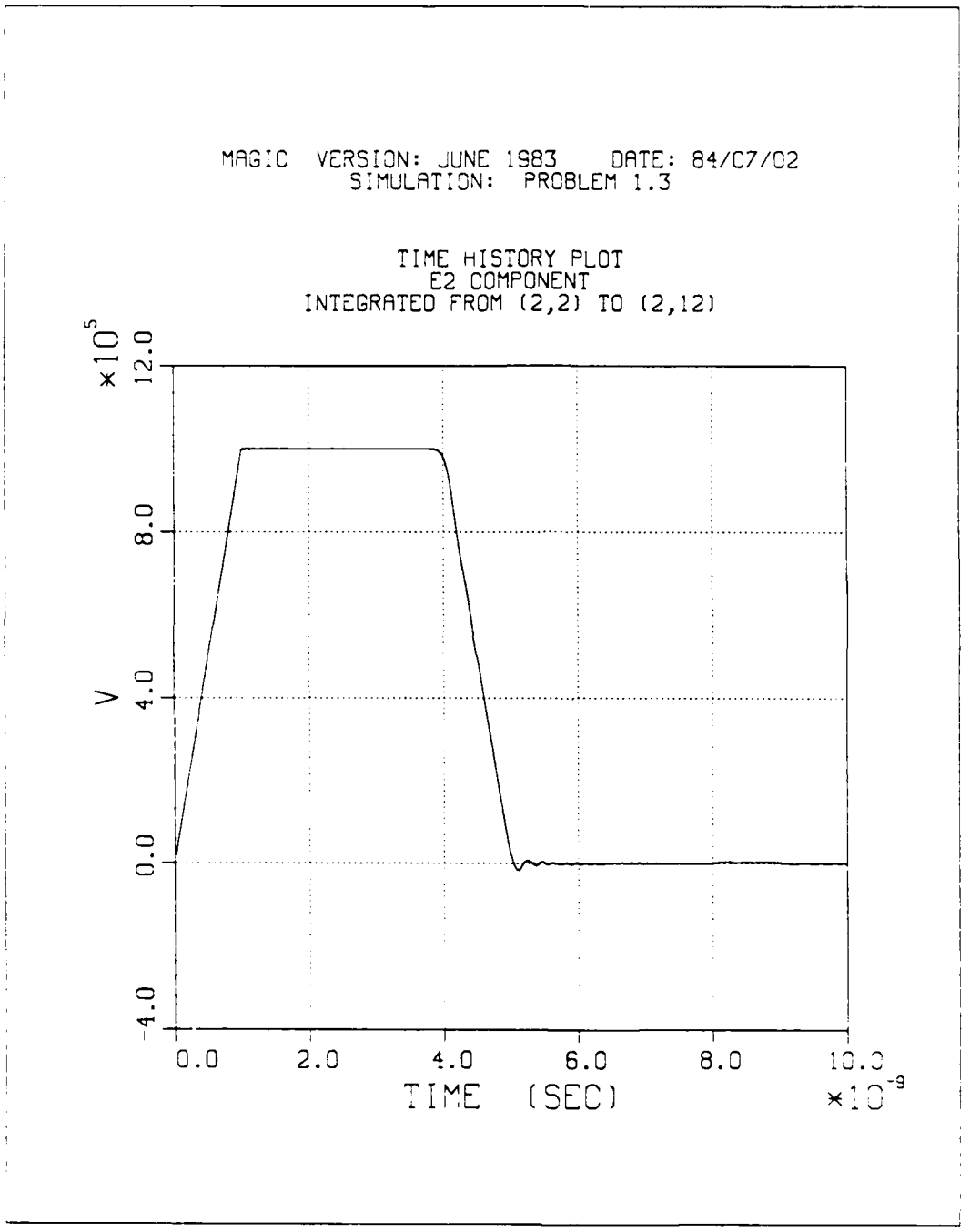

Figure 1.11. Inlet voltage vs. time, Problem 1.3.

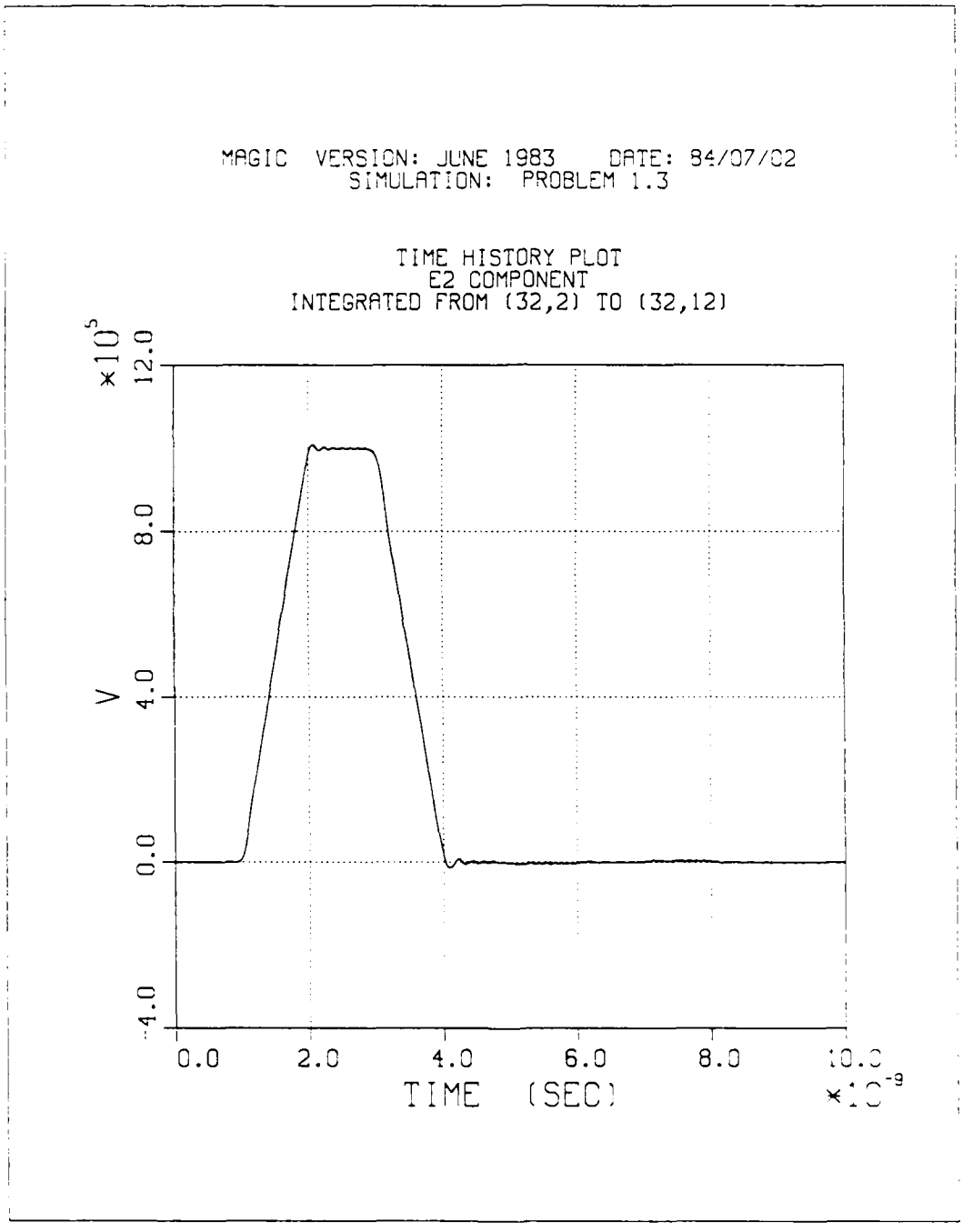

Figure 1.12. Midpoint voltage vs. time, Problem 1.3.

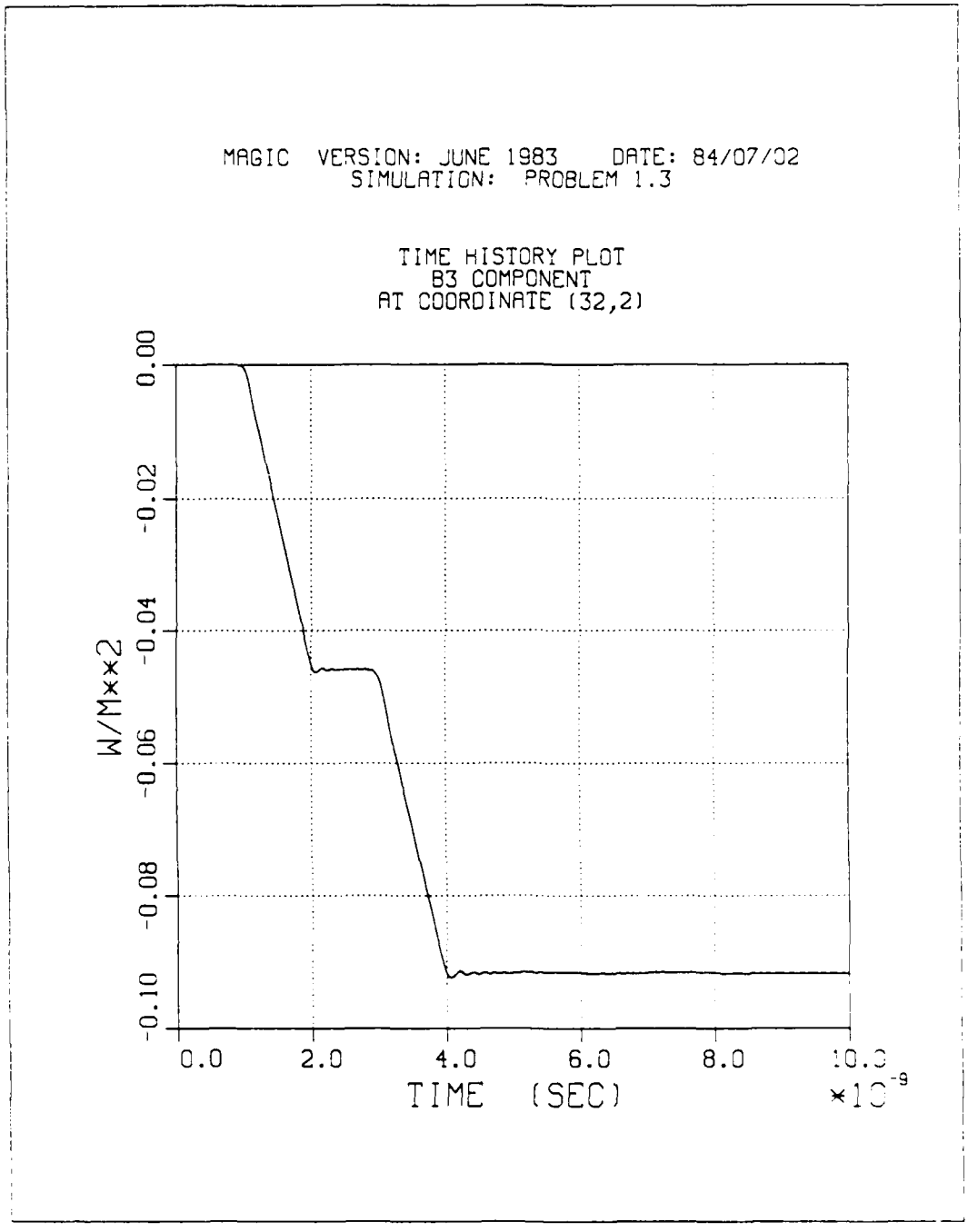

Figure 1.13. Midpoint magnetic field vs. time, Problem 1.3.

1.4 SCATTERED WAVE ABSORPTION AT INLET AND OUTLET.

1.4.1 Problem Description.

Repeat the previous simulation, allowing scattered waves to be absorbed at both inlet and outlet.

1.4.2 Suggested Approach.

The input data from Problem 1.3 can be duplicated exactly, except for the CONDUCTOR command which specifies the short. This should be replaced with a LOOKBACK command, as shown in Table 1.4.

1.4.3 Analytical Solution.

Results from this simulation, as shown in Figures 1.14 and 1.15, closely duplicate those from Problem 1.1. Note, however, that the inlet voltage in Figure 1.14 does not exactly reproduce the incident wave, due to a very small but non-zero scattered component originating from numerical diffusion.

Table 1.4. Input data for Problem 1.4.

```
title * problem 1.4 * /
comment * lookback reinstated * /
system 2 /
x1grid 1 62 2 0.0 60 0.01 0.6 /
x2grid 1 12 2 0.1 10 0.01 0.1 /
fields 1 1 500 2.0e-11 /
courant 0 0 /
conductor cathode 1 2  2 62  2 /
conductor anode  -1 2 12 62 12 /
voltage temporal radial twod 0 1.0 1 2 2 2 12 2 /
function temporal 0 3 0.0 0.0 1.0e-9 1.0e6 1.0 1.0e6 /
function radial 5  -1 1 /
lookback 1 -1 62 2 62 12 /
observe   1 twod 1 0.0 1.0 2  2 2  2 12
            twod 1 0.0 1.0 2 32 2 32 12
            twod 1 0.0 1.0 2 61 2 61 12
            twod 1 0.0 1.0 6  2 2  2 2
            twod 1 0.0 1.0 6 32 2 32 2
            twod 1 0.0 1.0 6 61 2 61 2
            twod 1 0.0 1.0 6 2 11 2 11
            twod 1 0.0 1.0 6 32 11 32 11
            twod 1 0.0 1.0 6 61 11 61 11 /
range 250 1 2  2 2  2 12 1
          1 2 32 2 32 12 1
          1 2 61 2 61 12 1
          1 6  2 2  2 12 1
          1 6 32 2 32 12 1
          1 6 61 2 61 12 1 /
output 0 /
start /
stop /
```

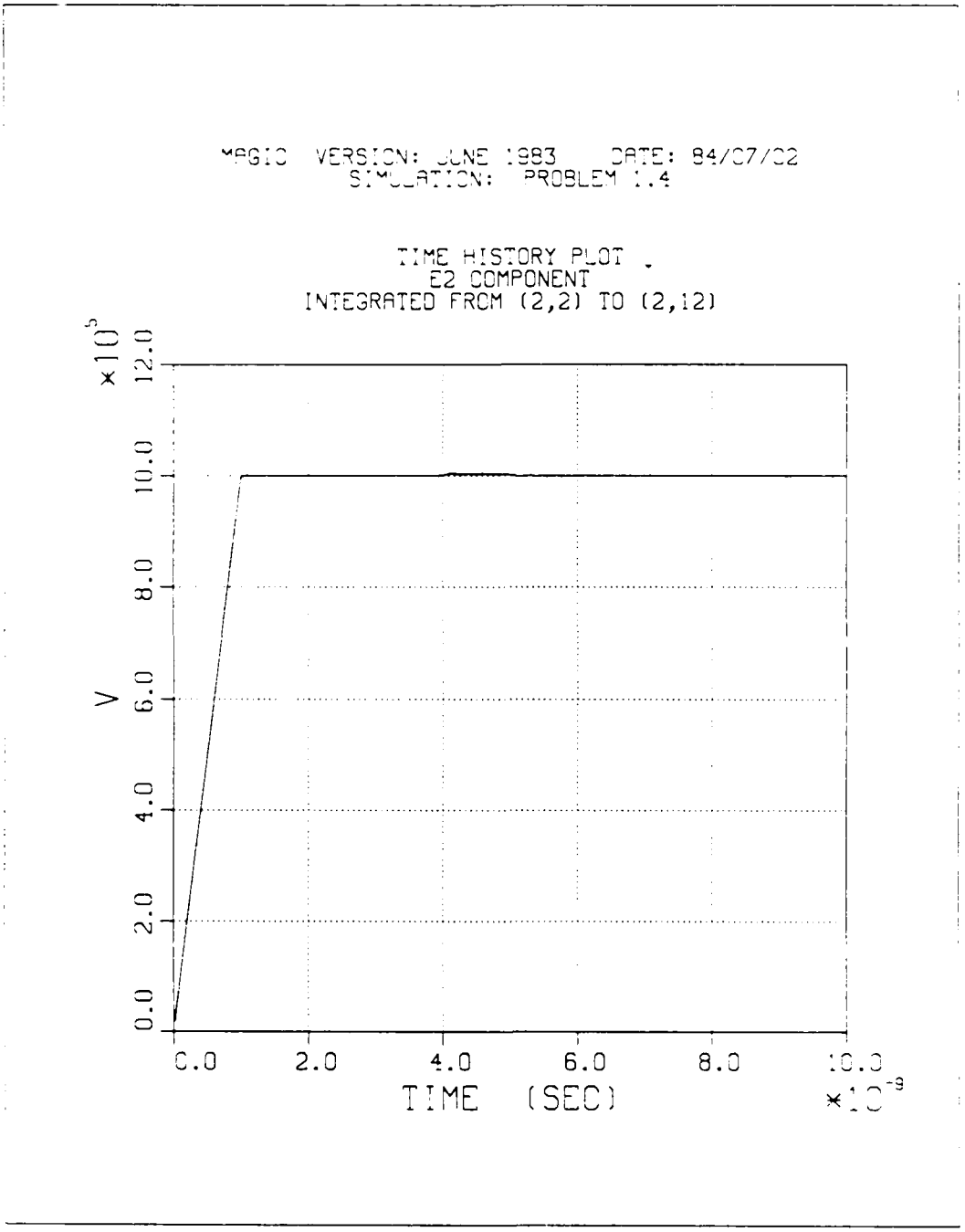

Figure 1.14. Inlet voltage vs. time, Problem 1.4.

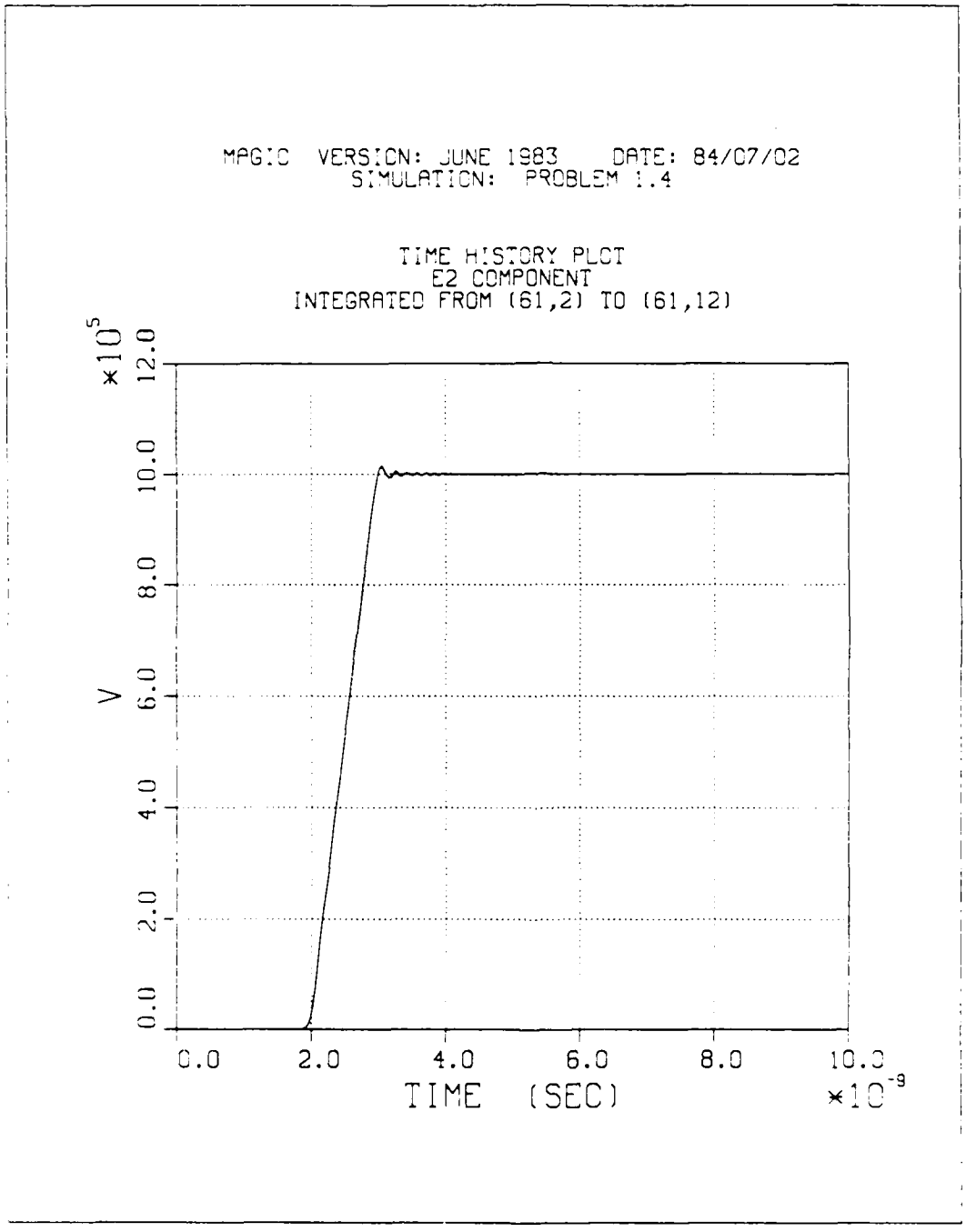

Figure 1.15. Outlet voltage vs. time, Problem 1.4.

1.5 PHASE VELOCITY AT OUTLET.

1.5.1 Problem Description.

For simulations in which the phase velocity is accurately known (e.g., c for a TEM wave), the boundary conditions specified by the VOLTAGE and LOOKBACK commands give excellent results. In many cases of interest (e.g., a plasma region or a waveguide), however, the phase velocity may not be known. Such cases will produce artificial reflections from the boundaries. To demonstrate this effect, we repeat the preceding simulation with an incorrect phase velocity value, v/c = 0.8.

1.5.2 Suggested Approach.

The input data from Problem 1.4 can be duplicated exactly, with the phase velocity factor in the LOOKBACK command changed from 1.0 to 0.8. The new input data is shown in Table 1.5.

1.5.3 Analytical Solution.

The inlet and outlet voltages from this simulation are shown in Figures 1.16 and 1.17 respectively. Note that the timing of the scattered wave at the inlet and the absence of peak voltage at the outlet both suggest an error in the outlet boundary condition. It is possible to characterize this effect in terms of an effective impedance. By inverting Equation (1.15), we obtain the expression,

$$Z_2 = Z_1 \frac{\phi}{2\phi^+ - \phi} . \qquad (1.16)$$

From Equation (1.9), the cable impedance is 41.6 Ω. Thus, using voltages from Figure 1.16 of $\phi^+ = 10^6$ V and $\phi = 8.9 \times 10^5$ V, we obtain $Z_2 = 33$ Ω. Note that this result (which can also be shown analytically from the boundary condition model itself) depends upon time step and axial cell size in addition to phase velocity.

Table 1.5. Input data for Problem 1.5.

```
title * problem 1.5 * /
comment * lookback phase velocity * /
system 2 /
x1grid 1 62 2 0.0 60 0.01 0.6 /
x2grid 1 12 2 0.1 10 0.01 0.1 /
fields 1 1 500 2.0e-11 /
courant 0 0 /
conductor cathode 1 2  2 62  2 /
conductor anode  -1 2 12 62 12 /
voltage temporal radial twod 0 1.0 1 2 2 2 12 2 /
function temporal 0 3 0.0 0.0 1.0e-9 1.0e6 1.0 1.0e6 /
function radial 5  -1 1 /
lookback 0.8 -1 62 2 62 12 /
observe   1 twod 1 0.0 1.0 2  2 2  2 12
            twod 1 0.0 1.0 2 32 2 32 12
            twod 1 0.0 1.0 2 61 2 61 12
            twod 1 0.0 1.0 6  2 2  2 2
            twod 1 0.0 1.0 6 32 2 32 2
            twod 1 0.0 1.0 6 61 2 61 2
            twod 1 0.0 1.0 6 2 11 2 11
            twod 1 0.0 1.0 6 32 11 32 11
            twod 1 0.0 1.0 6 61 11 61 11 /
range 250 1 2  2 2  2 12 1
          1 2 32 2 32 12 1
          1 2 61 2 61 12 1
          1 6  2 2  2 12 1
          1 6 32 2 32 12 1
          1 6 61 2 61 12 1 /
output 0 /
start /
stop /
```

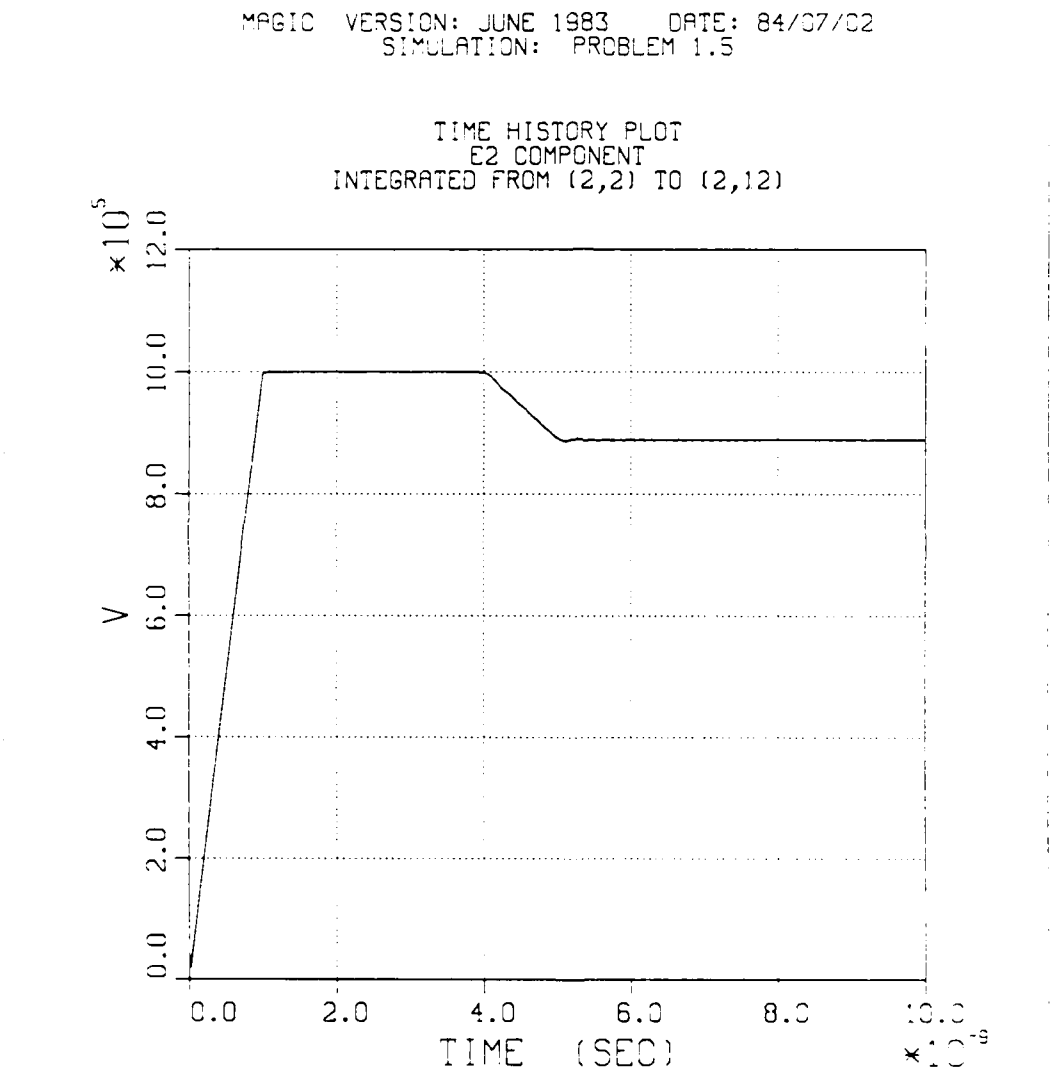

Figure 1.16. Inlet voltage vs. time, Problem 1.5.

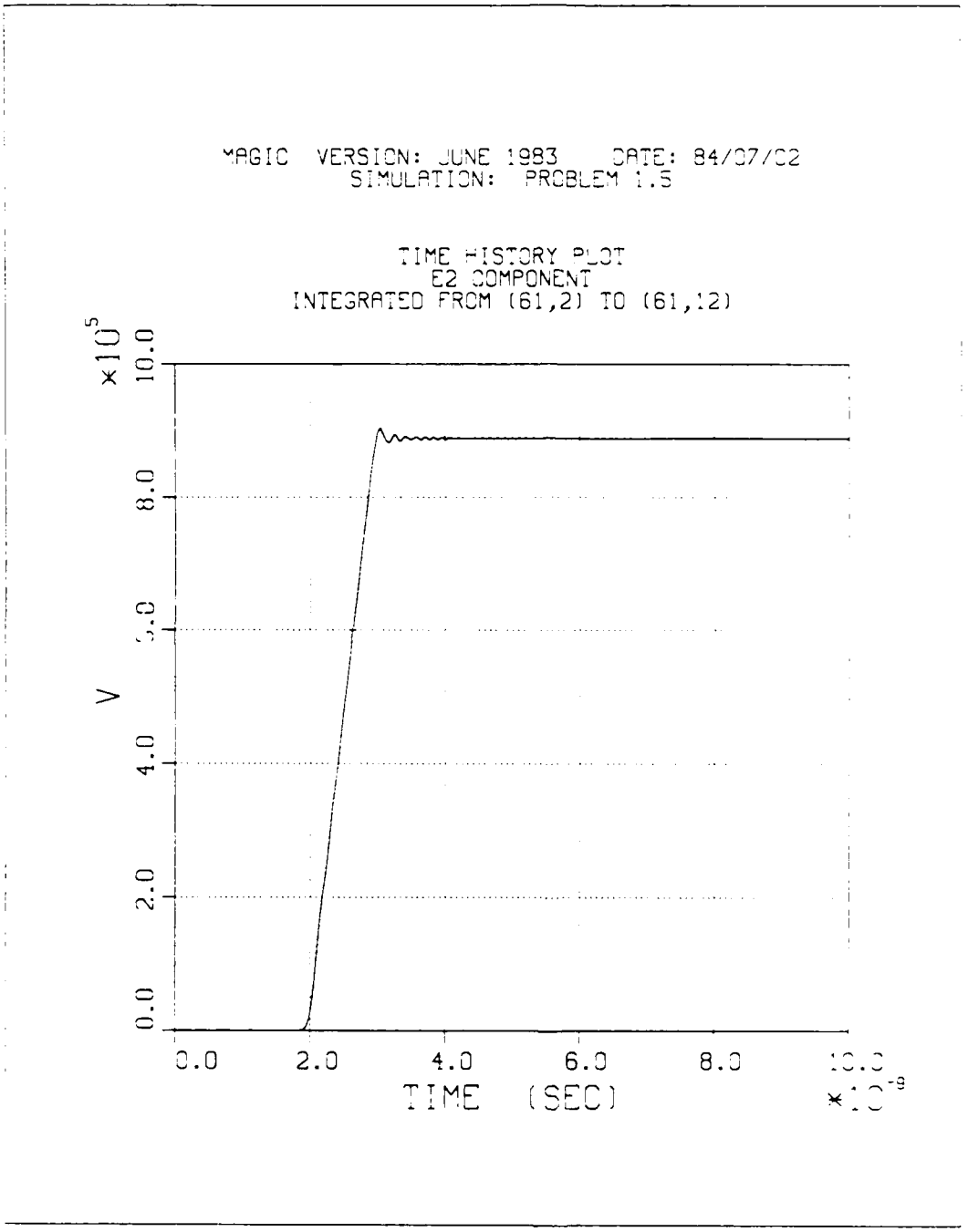

Figure 1.17. Outlet voltage vs. time, Problem 1.5.

1.6 COAXIAL LINE WITH MISMATCH.

1.6.1 Problem Description.

The preceding problems have explored the effects of various boundary conditions and artificial impedance effects which can result in simulations. In this problem, we consider a physical mismatch: the anode radius is to be reduced from 0.20 m to 0.15 m from the axial midpoint (L/2) onward. This coaxial line, illustrated in Figure 1.18, has the dimensions,

$$\begin{aligned} r_i &= 0.10 \text{ m} \\ r_s &= 0.15 \text{ m} \\ r_o &= 0.20 \text{ m} \\ L &= 0.60 \text{ m} . \end{aligned} \tag{1.17}$$

1.6.2 Suggested Approach.

We suggest using the spatial grid, etc., from the preceding simulations, with a few of the boundaries and measurements altered. For example, the CONDUCTOR command for the anode surface can be altered to produce the desired geometry using the continuation option. (The input data for the first line segment is produced in its entirety, including alphanumeric, surface normal flag, and spatial line indices. Only the end point indices are specified for the remaining contiguous line segments.) In addition, the spatial line indices for the LOOKBACK command and various output commands must be modified to reflect the smaller radius. The input data for this problem is shown in Table 1.6.

1.6.3 Analytical Solution.

This is a classic example of the two-region impedance mismatch. From Equations (1.9) and (1.17), the impedances of the inlet and outlet regions are

$$Z_1 = 41.56\ \Omega$$
$$Z_2 = 24.31\ \Omega\ , \tag{1.18}$$

respectively. Making use of Equation (1.15), we obtain the total steady-state voltage and current,

$$\Phi = 7.38 \times 10^5\ V$$
$$I = 3.03 \times 10^4\ A\ . \tag{1.19}$$

The simulation results for inlet and outlet voltage are shown in Figures 1.19 and 1.20, respectively, with the corresponding magnetic fields in Figures 1.21 and 1.22. By applying Equation (1.11) to the magnetic field (both voltage and field data time averaged over final 1 nsec), we obtain the simulation results,

$$\Phi = 7.38 \times 10^5\ V$$
$$I = 3.04 \times 10^4\ A\ , \tag{1.20}$$

which compare favorably with the analytical results. The electric and magnetic field distributions (vs. radius) should also be checked to confirm the existence of TEM waves at inlet and outlet.

Table 1.6. Input data for Problem 1.6.

```
title * problem 1.6 * /
comment * impedance mismatch * /
system 2 /
x1grid 1 62 2 0.0 60 0.01 0.6 /
x2grid 1 12 2 0.1 10 0.01 0.1 /
fields 1 1 500 2.0e-11 /
courant 0 0 /
conductor cathode 1 2  2 62  2 /
conductor anode  -1 2 12 32 12 32 7 62 7 /
voltage temporal radial twod 0 1.0 1 2 2 2 12 2 /
function temporal 0 3 0.0 0.0 1.0e-9 1.0e6 1.0 1.0e6 /
function radial 5  -1 1 /
lookback 1 -1 62 2 62 12 /
observe   1 twod 1 0.0 1.0 2  2 2  2 12
            twod 1 0.0 1.0 2 31 2 31 12
            twod 1 0.0 1.0 2 61 2 61 7
            twod 1 0.0 1.0 6  2 2  2 2
            twod 1 0.0 1.0 6 31 2 31 2
            twod 1 0.0 1.0 6 61 2 61 2
            twod 1 0.0 1.0 6 2 11 2 11
            twod 1 0.0 1.0 6 31 11 31 11
            twod 1 0.0 1.0 6 61 6 61 6 /
range 250 1 2  2 2  2 12 1
          1 2 31 2 31 12 1
          1 2 61 2 61 7 1
          1 6  2 2  2 12 1
          1 6 31 2 31 12 1
          1 6 61 2 61 7 1 /
output 0 /
start /
stop /
```

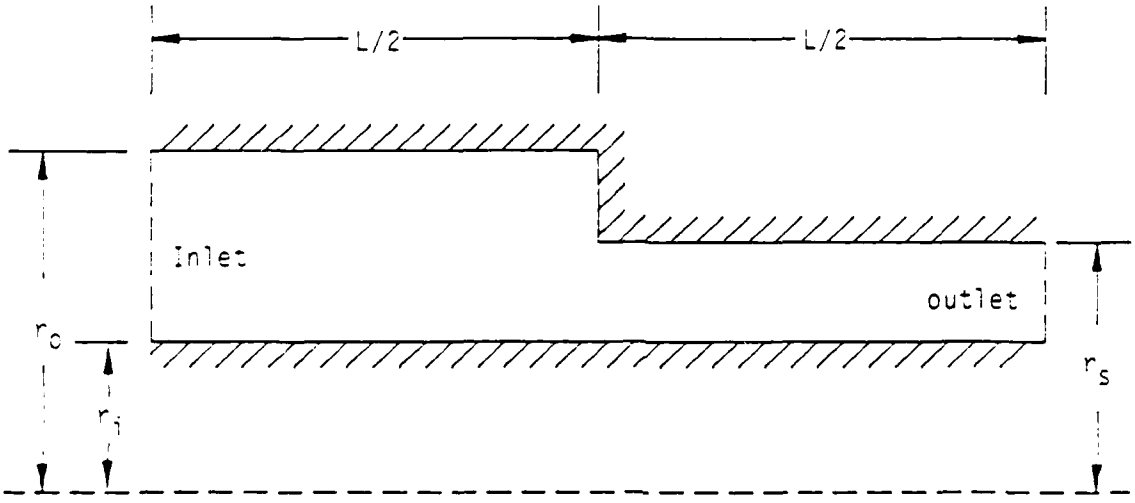

Figure 1.18. Section of coaxial line with mismatch.

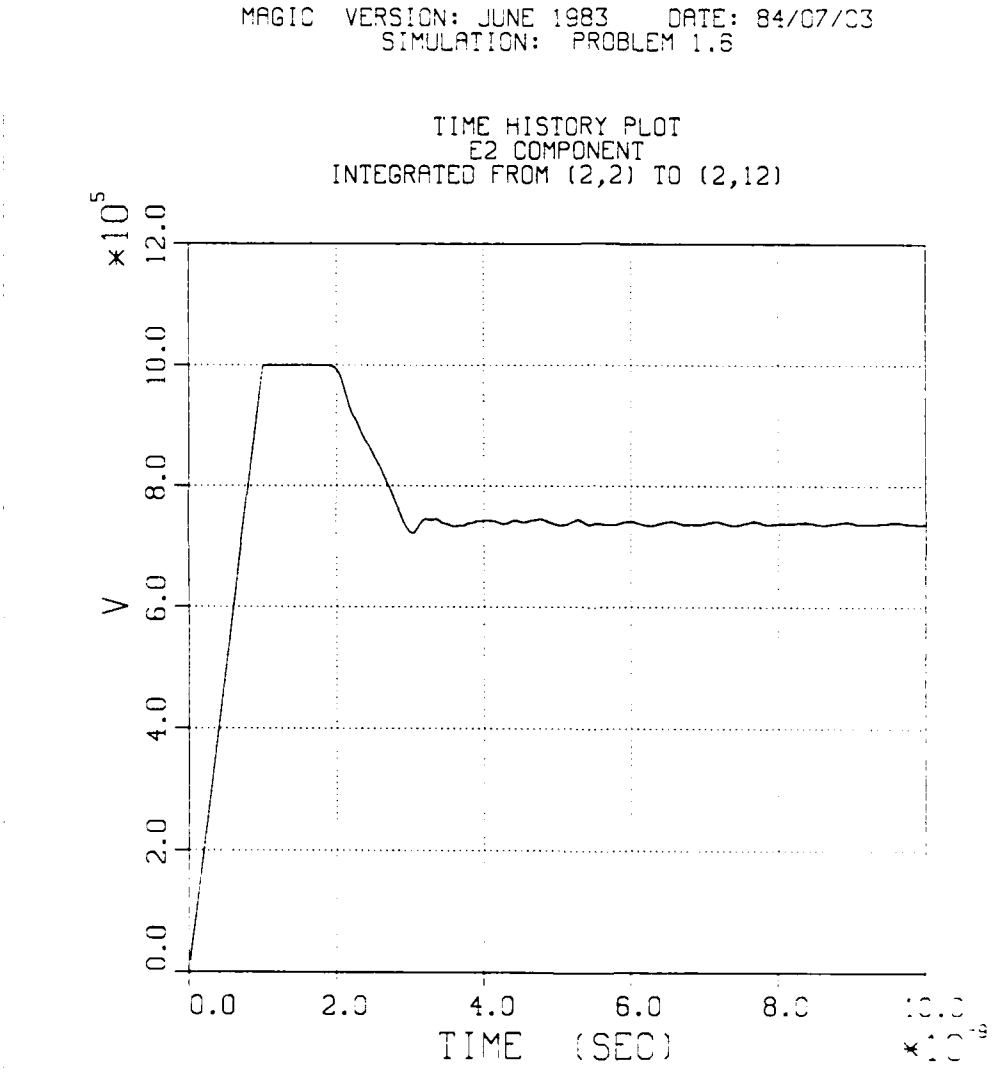

Figure 1.19. Inlet voltage vs. time, Problem 1.6.

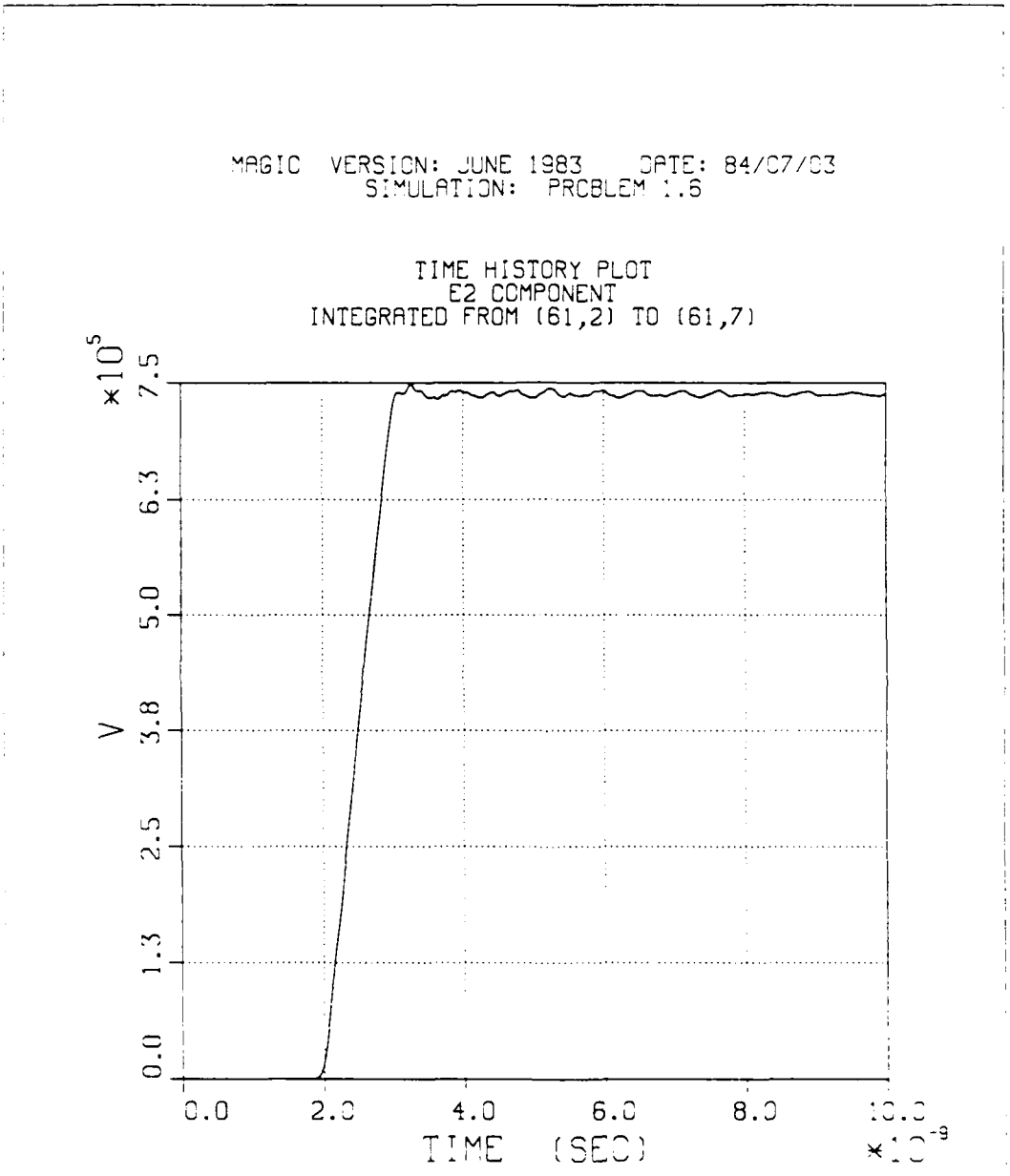

Figure 1.20. Outlet voltage vs. time, Problem 1.6.

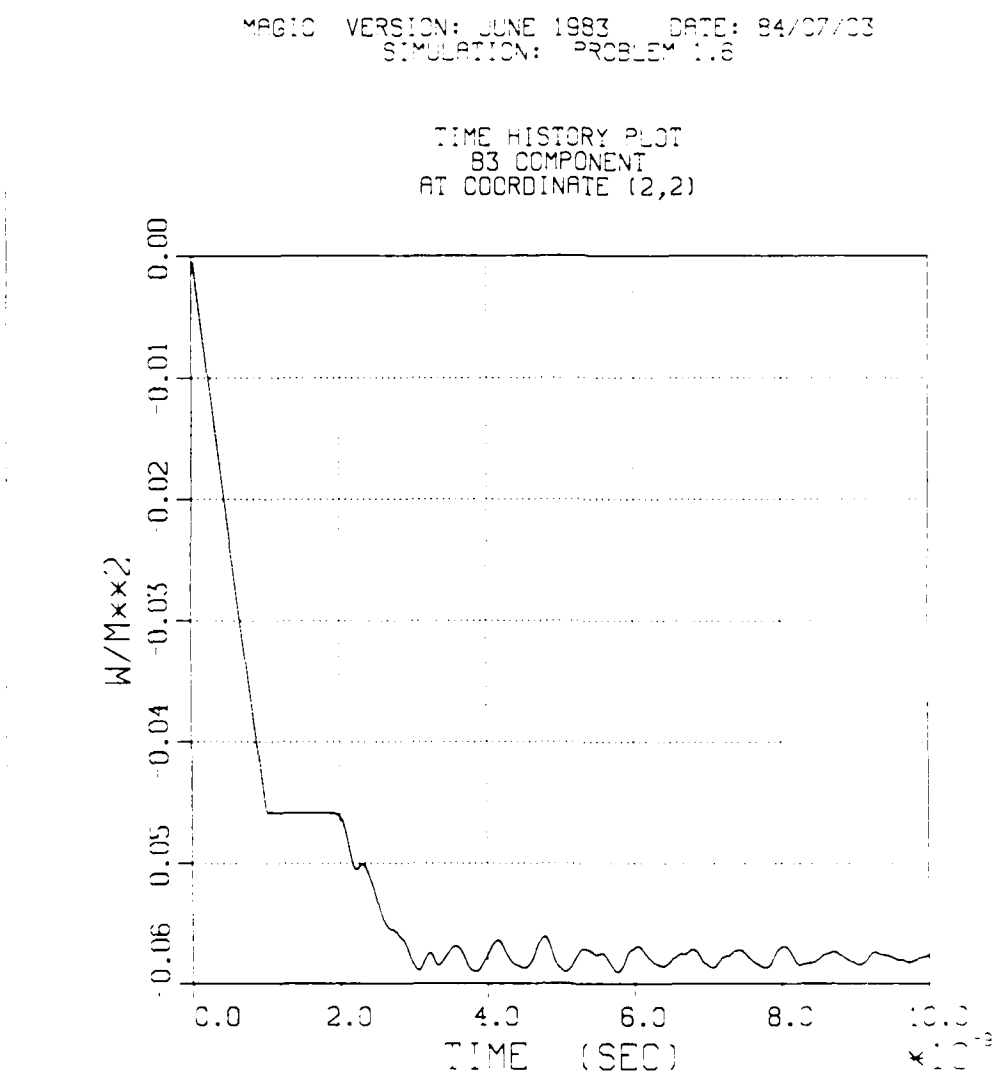

Figure 1.21. Inlet magnetic field vs. time, Problem 1.6.

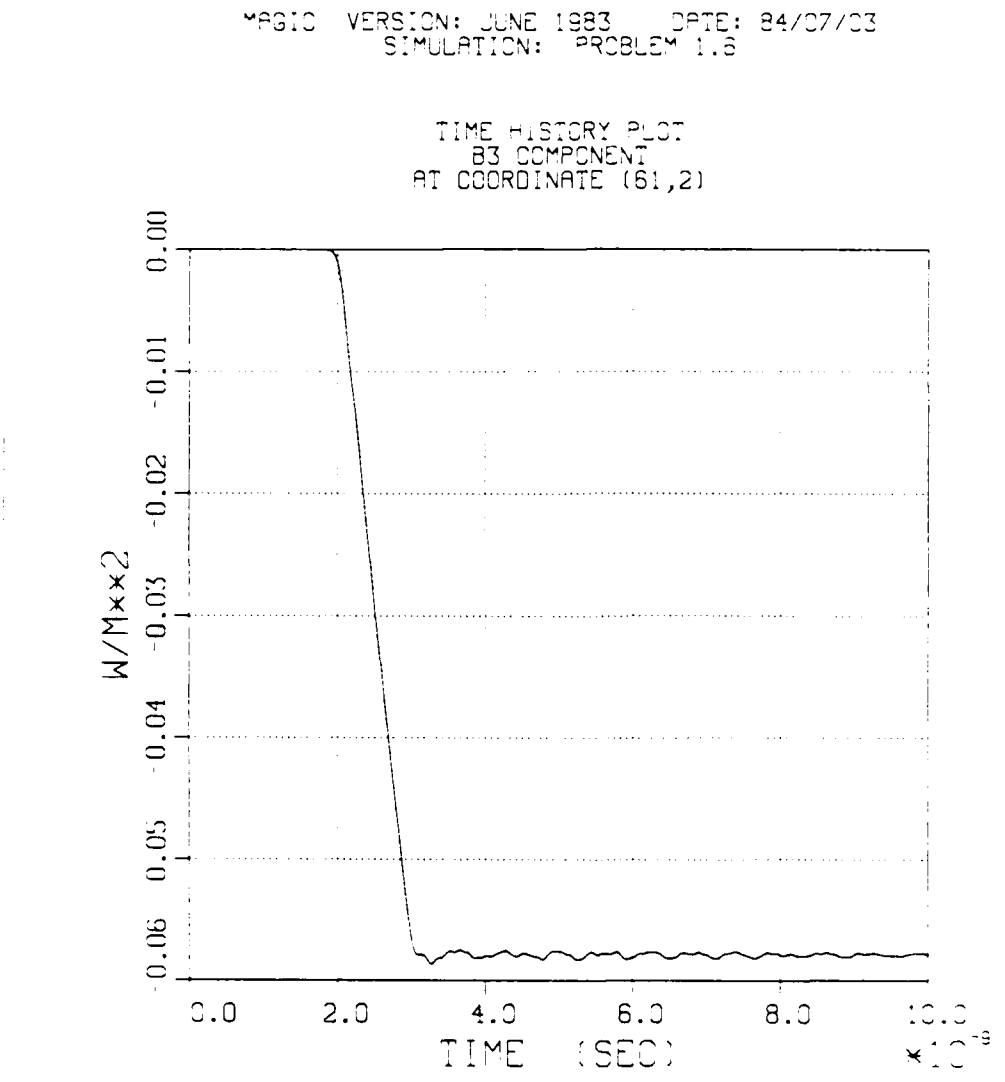

Figure 1.22. Outlet magnetic field vs. time, Problem 1.6.

1.7 REDUCED TIME STEP.

1.7.1 Problem Description.

We want to explore the electromagnetic effects of using a smaller time step, well below the Courant criterion.

1.7.2 Suggested Approach.

Using input data from the preceding simulation, cut the time step in the FIELDS command in half. Also, double the number of time steps and all time step intervals that determine the frequency of output. The new input data is shown in Table 1.7.

1.7.3 Analytical Solution.

Figure 1.23 illustrates the calculated inlet magnetic field vs. time. This is one of the more sensitive results, and can be compared with the result of Figure 1.21. While there are slight discernible differences, the agreement is substantial. This is a characteristic of the centered-difference electromagnetic algorithm - results generally depend upon spatial differences but not upon temporal differences.

Table 1.7. Input data for Problem 1.7.

```
title * problem 1.7 * /
comment * reduced time step * /
system 2 /
x1grid 1 62 2 0.0 60 0.01 0.6 /
x2grid 1 12 2 0.1 10 0.01 0.1 /
fields 1 1 1000 1.0e-11 /
courant 0 0 /
conductor cathode 1 2  2 62  2 /
conductor anode  -1 2 12 32 12 32 7 62 7 /
voltage temporal radial twod 0 1.0 1 2 2 2 12 2 /
function temporal 0 3 0.0 0.0 1.0e-9 1.0e6 1.0 1.0e6 /
function radial 5  -1 1 /
lookback 1 -1 62 2 62 12 /
observe   1 twod 1 0.0 1.0 2  2 2  2 12
            twod 1 0.0 1.0 2 31 2 31 12
            twod 1 0.0 1.0 2 61 2 61 7
            twod 1 0.0 1.0 6  2 2  2 2
            twod 1 0.0 1.0 6 31 2 31 2
            twod 1 0.0 1.0 6 61 2 61 2
            twod 1 0.0 1.0 6 2 11 2 11
            twod 1 0.0 1.0 6 31 11 31 11
            twod 1 0.0 1.0 6 61 6 61 6 /
range 250 1 2  2 2  2 12 1
          1 2 31 2 31 12 1
          1 2 61 2 61 7 1
          1 6  2 2  2 12 1
          1 6 31 2 31 12 1
          1 6 61 2 61 7 1 /
output 0 /
start /
stop /
```

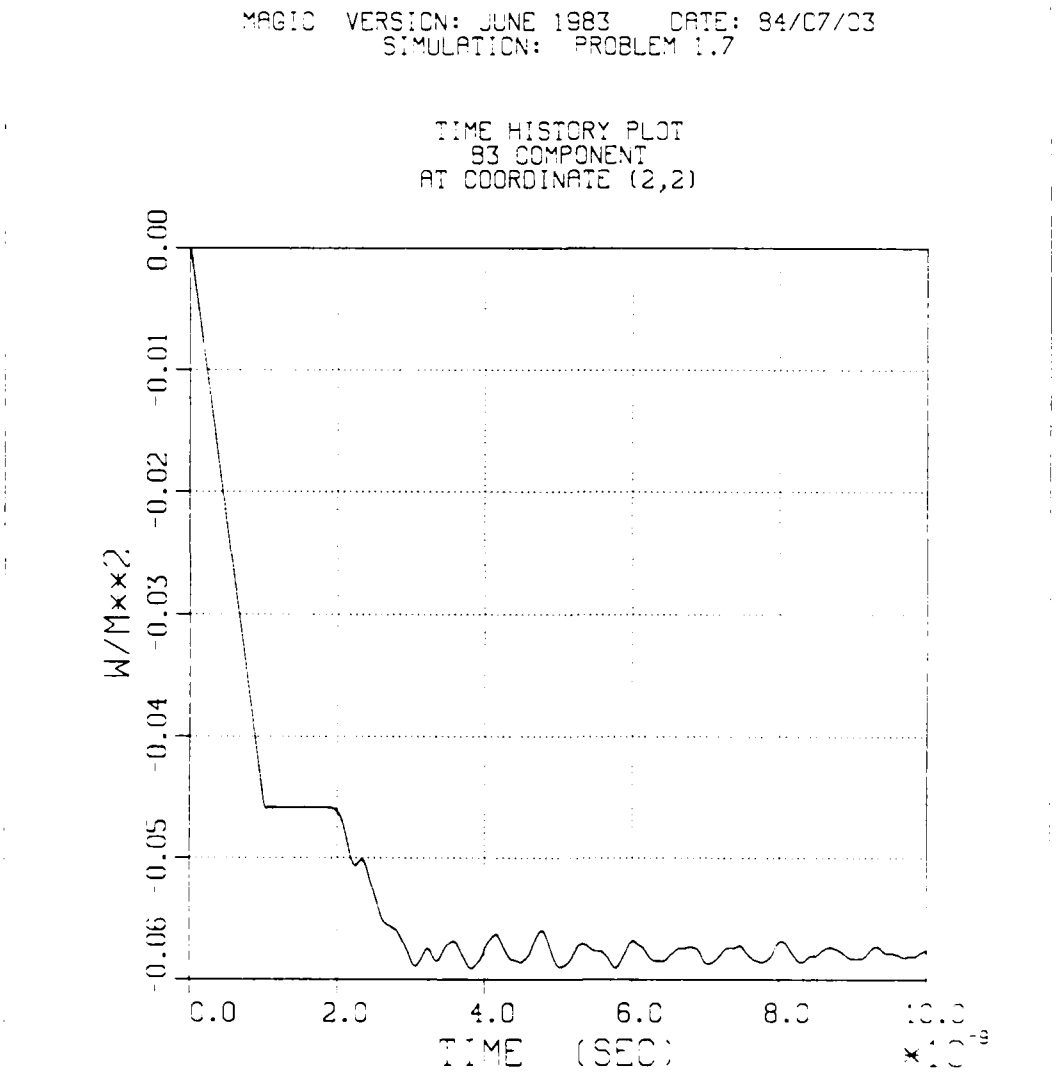

Figure 1.23. Inlet magnetic field vs. time, Problem 1.7.

1.8 TIME-BIASED ALGORITHM.

1.8.1 Problem Description.

As a final exercise, we wish to duplicate Problem 1.6 using the time-biased electromagnetic algorithm. This algorithm, which is implicit, is most useful in damping out the numerical noise associated with particle kinematics.

1.8.2 Suggested Approach.

From the User's Manual, we arbitrarily select time-biased coefficients for four iterations,

$$\begin{aligned} &\alpha_1 = \alpha_2 = 0.5 \ , \quad \alpha_3 = 0 \\ &\tau_i = 0.29912,\ 0.15022,\ 0.11111, \qquad i=1,\ldots,4 \ . \end{aligned} \tag{1.21}$$

From the Courant criterion,

$$\frac{1}{c^2 \delta t^2} > (\alpha_2^2 - 4\alpha_1\alpha_3) \left\{ \frac{1}{(\delta r)^2} + \frac{1}{(\delta z)^2} \right\} , \tag{1.22}$$

it is obviously possible to double the time step and to cut the number of time steps and output frequency in half. (Note that the running time will actually increase by about 100%; the time step is doubled, but four iterations are specified per step.) The input data for this simulation is given in Table 1.8.

1.8.3 Analytical Solution.

The calculated magnetic field at the inlet is shown in Figure 1.24. This result can be compared with Figures 1.21 and 1.23. While the mean results are in good agreement, the result in Figure 1.24 is relatively free of high-frequency (dispersion) numerical noise. This ability to damp high-frequency waves is a primary characteristic of the time-biased algorithm.

Table 1.8. Input data for Problem 1.8.

```
title * problem 1.8 * /
comment * time-biased field algorithm * /
system 2 /
x1grid 1 62 2 0.0 60 0.01 0.6 /
x2grid 1 12 2 0.1 10 0.01 0.1 /
fields 1 3 250 4.0e-11 0.5 0.5 0.0
              4 1.0 0.29912 0.15022 0.11111 /
courant 0 0 /
conductor cathode 1 2  2 62  2 /
conductor anode  -1 2 12 32 12 32 7 62 7 /
voltage temporal radial twod 0 1.0 1 2 2 2 12 2 /
function temporal 0 3 0.0 0.0 1.0e-9 1.0e6 1.0 1.0e6 /
function radial 5  -1 1 /
lookback 1 -1 62 2 62 12 /
observe   1 twod 1 0.0 1.0 2  2 2  2 12
            twod 1 0.0 1.0 2 31 2 31 12
            twod 1 0.0 1.0 2 61 2 61 7
            twod 1 0.0 1.0 6  2 2  2 2
            twod 1 0.0 1.0 6 31 2 31 2
            twod 1 0.0 1.0 6 61 2 61 2
            twod 1 0.0 1.0 6 2 11 2 11
            twod 1 0.0 1.0 6 31 11 31 11
            twod 1 0.0 1.0 6 61 6 61 6 /
range 125 1 2  2 2  2 12 1
          1 2 31 2 31 12 1
          1 2 61 2 61 7 1
          1 6  2 2  2 12 1
          1 6 31 2 31 12 1
          1 6 61 2 61 7 1 /
output 0 /
start /
stop /
```

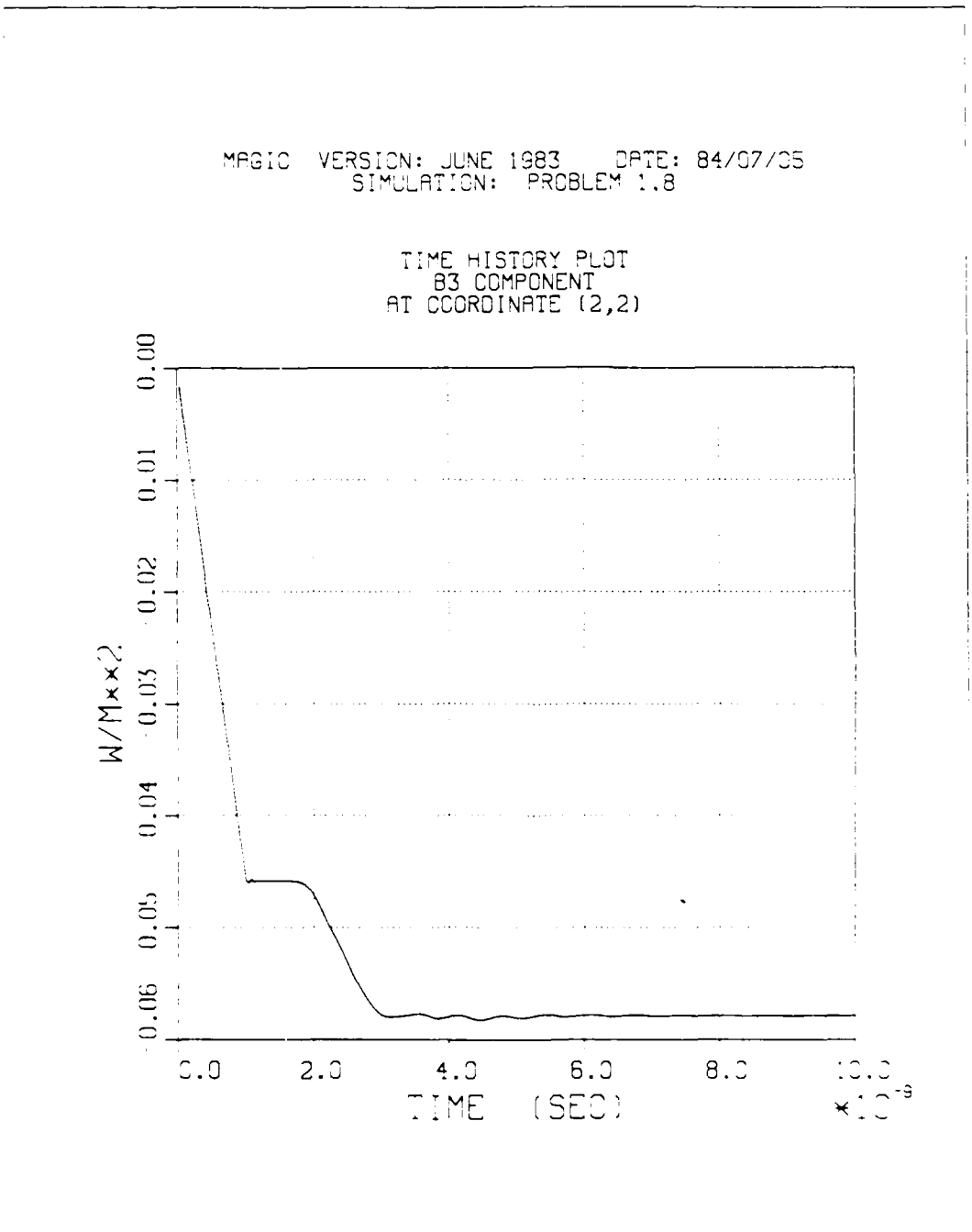

Figure 1.24. Inlet magnetic field vs. time, Problem 1.8.

SECTION 2
PARTICLE KINEMATICS

The problem set on particle kinematics is introduced by simulations involving the motion of a single particle in a prescribed electromagnetic field. Four problems were chosen to represent various physical effects, including relativistic motion, gyromagnetic motion, E x B drift, and B x ∇B drift. These single particle problems also demonstrate the extent to which the code can faithfully reproduce physical particle trajectories. Following the single-particle problems in this section are two fully self-consistent problems in one-dimension. These two problems cover field emission and magnetic insulation.

2.1 RELATIVISTIC TRAJECTORY.

2.1.1 Problem Description.

The first problem involves the relativistic motion of an electron in a constant electric field, specifically

$$\begin{aligned} \overline{E} &= \hat{y}E \\ \overline{B} &= 0 \ , \end{aligned} \tag{2.1}$$

where $E = -3 \times 10^7$ V/m. The initial conditions are given by

$$\begin{aligned} t = x = y = z &= 0 \\ \overline{p} &= \hat{x}p \ , \end{aligned} \tag{2.2}$$

where $p = 9 \times 10^8$ m/sec. Note that the relativistic equation of motion for a particle of charge -e and rest mass m is

$$\frac{d\overline{p}}{dt} = \frac{-e}{m}\left(\overline{E} + v \times \overline{B}\right) \tag{2.3}$$

where the momentum p and velocity v are related by

$$\overline{p} = \gamma\overline{v}$$

where

$$\gamma = \frac{1}{\left(1 - v^2/c^2\right)^{1/2}} \ . \tag{2.4}$$

This definition of momentum differs from the usual one by the omission of rest mass. However, it is consistent with the formalism and input data requirements of MAGIC.

2.1.2 Suggested Approach.

To test the particle kinematics algorithm, MAGIC allows the user to prescribe external fields causing forces on the particles. The FORCES command allows the prescription of any (or all six) field components as a triple product function in space and time. For problem 2.1, all fields except E_2 are zero, and

$$E_2(x_1,x_2,t) = f_1(x_1)\ f_2(x_2)\ f_t(t)\ . \tag{2.5}$$

The functions are identified by means of an option in the FORCES data sequence. Each separate function is specified in the usual way with a FUNCTION command. This capability provides a simple means of prescribing fields required for a particular kinematics test, e.g., $B \times \nabla B$, which clearly requires a spatial dependence.

When prescribed fields are used, it is still necessary to provide input data for all the usual data sequences, including the field algorithm and spatial grid. We suggest using a 1 x 1 x 1 mesh (i.e., one functional cell sufficiently large to contain the particle trajectory) surrounded by conducting boundaries. In this case, the field algorithm is essentially ignored, and the time step specified by the FIELDS command is used only for the particle kinematics. Output for these simulations can easily be obtained in the form of trajectory plots, which can be measured directly to verify analytical results. More precise measurements are available from the diagnostics which print out particle coordinates and momenta during the simulation.

This problem is easily set up by including three commands: FORCES with the prescribed field option to set the electric field, POPULATE to establish initial conditions for a single particle, and DIAGNOSE (KINEMAT) to print particle coordinates as a function of time.

(A trajectory plot should be specified with the TRAJECTORY command; however, it will not allow quantitative measurements. The object is to obtain x and y as a function of t, and to compare computed with analytical results at several points in time.) The input data for this simulation is shown in Table 2.1.

2.1.3 Analytical Solution.

This problem, although relativistic, is analytical (integrable). The Lagrangian is given by[†]

$$L = - mc^2\left(1 - \frac{\dot{x}^2 + \dot{y}^2}{c^2}\right)^{1/2} - eEy \ . \tag{2.6}$$

Application of the variational principle,

$$\frac{d}{dt}\left(\frac{\partial L}{\partial \dot{q}}\right) - \frac{\partial L}{\partial q} = 0 \ , \tag{2.7}$$

and integration yield the results,

$$\begin{aligned} \frac{\dot{x}}{\left(1 - \frac{\dot{x}^2 + \dot{y}^2}{c^2}\right)^{1/2}} &= p \\ \\ \frac{\dot{y}}{\left(1 - \frac{\dot{x}^2 + \dot{y}^2}{c^2}\right)^{1/2}} &= - \frac{eE}{m} t \ . \end{aligned} \tag{2.8}$$

By algebraic manipulation, we obtain the two integrals

$$x = p \int_0^t \frac{dt'}{\left\{\left[1 + \left(\frac{p}{c}\right)^2\right] + \left(- \frac{eE}{mc} t'\right)^2\right\}^{1/2}}$$

[†] H. Goldstein, Classical Mechanics, Addison-Wesley, New York, 1950 (p.206).

$$y = \int_0^t \frac{\left(-\frac{eE}{m} t'\right) dt'}{\left\{\left[1 + \left(\frac{p}{c}\right)^2\right] + \left(-\frac{eE}{mc} t'\right)^2\right\}^{1/2}} \quad . \tag{2.9}$$

These are integrated to give the trajectory equations,

$$x = -\frac{mc}{eE} p \ln \left\{ \frac{-\frac{eE}{mc} t + \left[1 + \left(\frac{p}{c}\right)^2 + \left(\frac{eE}{mc} t\right)^2\right]^{1/2}}{\left[1 + \left(\frac{p}{c}\right)^2\right]^{1/2}} \right\}$$

$$y = -\frac{mc^2}{eE} \left\{ \left[1 + \left(\frac{p}{c}\right)^2 + \left(\frac{eE}{mc} t\right)^2\right]^{1/2} - \left[1 + \left(\frac{p}{c}\right)^2\right]^{1/2} \right\} \quad . \tag{2.10}$$

Although there is no force in the x direction, this component of velocity, since initially non-zero, must decrease due to the increase in mass. Thus, x is sublinear in time. This effect appears in the simulation trajectory plot illustrated in Figure 2.1. Examining diagnostic results from the output listing, we find the calculated coordinates at t = 0.141 nsec to be

$$x = 8.97 \times 10^{-3} \text{ m}$$
$$y = 2.84 \times 10^{-2} \text{ m} \ . \tag{2.11}$$

The analytical result from Equation (2.10) at the same time yields

$$x = 9.06 \times 10^{-3} \text{ m}$$
$$y = 2.81 \times 10^{-2} \text{ m} \ . \tag{2.12}$$

This time period includes only 50 time steps in the kinematics; the accuracy of the numerical result will improve with resolution.

Table 2.1. Input data for Problem 2.1.

```
title *problem 2.1* /
comment *relativistic trajectory in constant electric field* /
system 1 /
x1grid 1 3 2 0.0 1 0.028 0.028 /
x2grid 1 3 2 0.0 1 0.028 0.028 /
conductor boundary +1 2 2 3 2 3 3 2 3 2 2 /
fields 1 1 50 2.82616e-12 /
courant 0 0 /
kinematics 1 0 0 0 0 /
forces  1 1 1 2 e2 null null /
function e2 1 0 -3.0e7 /
populate electrons 0 0.0 1 2 2 3 3 1.6e-19
                     0.0 0.0 1.0e8 0.0 0.0 /
diagnose prscrib  0  2
         kinemat  0 51 /
trajectory 50 50 1 0.0 0.028 0.0 0.028 /
timeout -1 0 /
start /
stop /
```

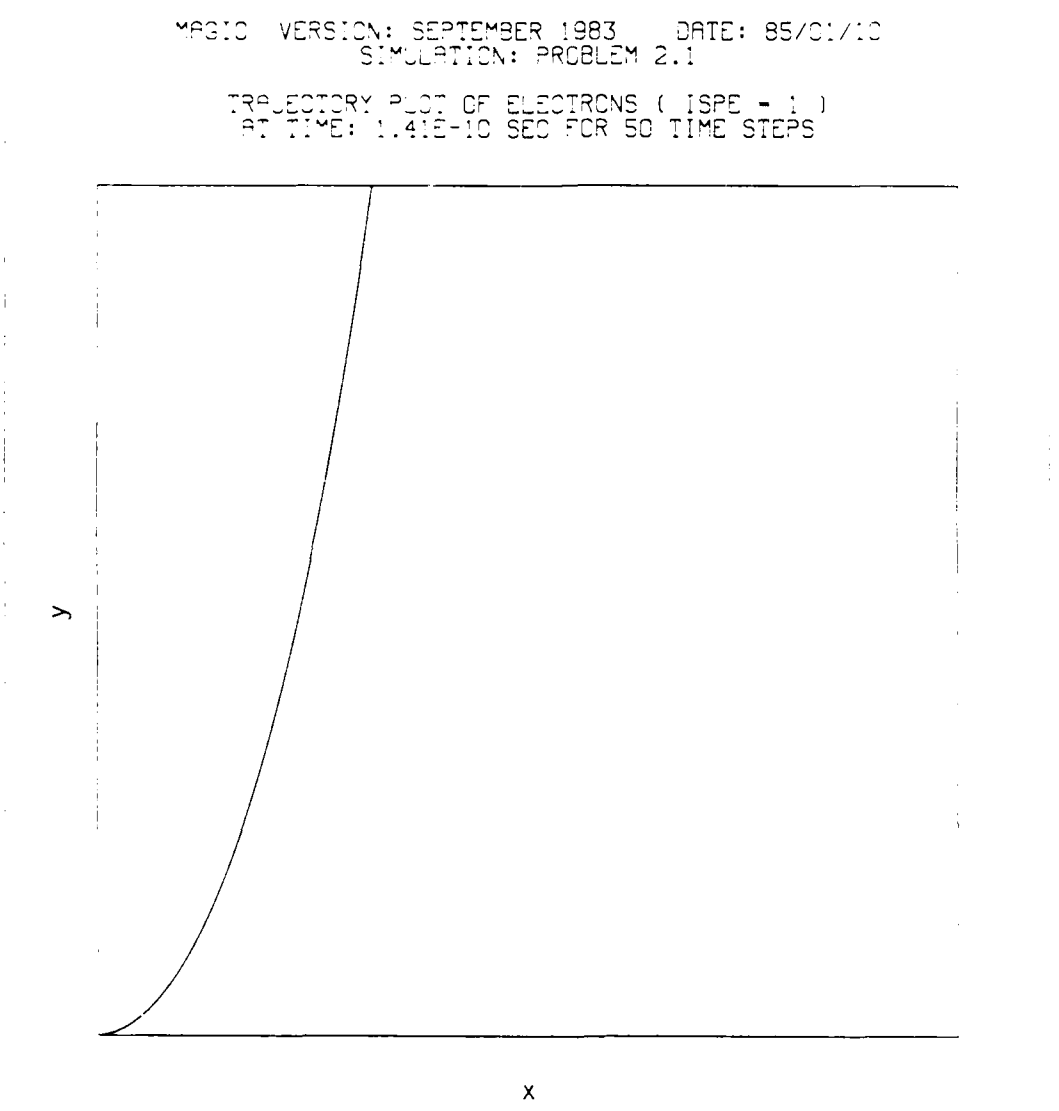

Figure 2.1. Trajectory plot, Problem 2.1.

2.2 GYROMAGNETIC MOTION.

2.2.1 Problem Description.

This problem involves simulating the trajectory of a relativistic electron in a high magnetic field,

$$\bar{B} = \hat{z}B \ , \tag{2.13}$$

where B = - 20 T. Initial conditions for the particle are

$$\begin{aligned} t &= x = y = z = 0 \\ p &= \hat{x}p \ , \end{aligned} \tag{2.14}$$

where $p = 9 \times 10^8$ m/sec.

2.2.2 Suggested Approach.

In this problem, the trajectory plot capability is appropriate to measure performance. One trick is to choose the kinematics time step such that an integer multiple equals the gyromagnetic period, i.e.,

$$k\delta t = \tau \ . \tag{2.15}$$

Then the orbit should close in k time steps. Conservation of momentum, etc., can be assessed using the previously described diagnostic capability. Input data for this simulation is shown in Table 2.2.

2.2.3 Analytical Solution.

In the absence of electric field (E = 0), the momentum magnitude (and thus γ) is constant. The gyromagnetic radius and period are given by

$$r = \frac{\gamma m v}{eB}$$

$$\tau = \frac{2\pi r}{v} = \frac{2\pi m}{eB} \quad . \tag{2.16}$$

For the momentum specified in Equation (2.14), the radius and period are 0.2558 mm and 5.65 psec, respectively.

It will be seen from the simulation trajectory plot in Figure 2.2 that the orbit has apparently closed in 100 time steps. Using the kinematics diagnostic data from the output listing, we estimate the effective radius to be 0.2559 mm. This degree of accuracy results from using a small time step (i.e., large number of steps to represent a single orbit). With a larger time step, the accuracy decreases and, in the limit, approaches a simple oscillating state.

Table 2.2. Input data for Problem 2.2.

```
title *problem 2.2* /
comment *gyromagnetic motion in constant magnetic field* /
system 1 /
x1grid 1 3 2 -5.0000e-4 1 0.001 0.001 /
x2grid 1 3 2 -7.5587e-4 1 0.001 0.001 /
conductor boundary +1 2 2 3 2 3 3 2 3 2 2 /
fields 1 1 100 5.65233e-14 /
courant 0 0 /
kinematics 1 0 0 0 0 /
forces  1 1 1 6 b3 null null /
function b3 1 0 -20.0 /
populate electrons 0 0.0 1 2 2 3 3 1.6e-19
                   0.5 0.75587 9.0e8 0.0 0.0 /
diagnose prscrib   0   2
         kinemat   0 101 /
trajectory 100 100 1 -0.0005 0.0005 -7.5587e-4 2.4413e-4 /
timeout -1 0 /
start /
stop /
```

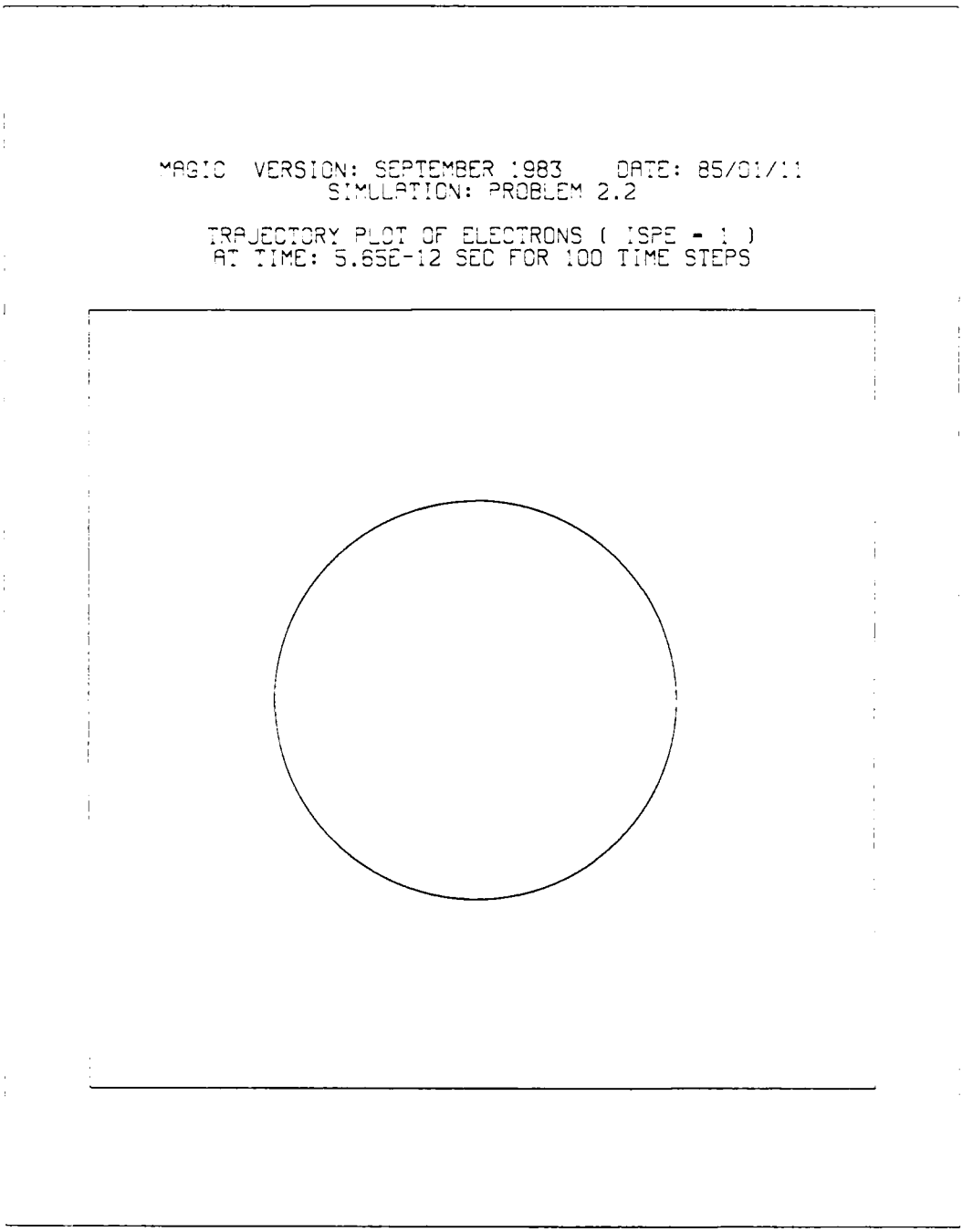

Figure 2.2. Trajectory plot, Problem 2.2.

2.3 DRIFT (E x B).

2.3.1 Problem Description.

This problem involves simulating an E x B drift where the constant fields obey the constraint,

$$\left|\frac{E}{cB}\right| < 1 \ . \tag{2.17}$$

This constraint is motivated by the reduction in normal electric field which results from space-charge limiting in magnetic insulation. We arbitrarily select field parameters from the preceding problems, i.e.,

$$\begin{aligned} \overline{B} &= \hat{z}B \\ \overline{E} &= \hat{y}E \ , \end{aligned} \tag{2.18}$$

where B = -20 T and E = -3 x 10^7 V/m. The particle initial conditions are

$$t = \overline{x} = \overline{p} = 0 \ . \tag{2.19}$$

2.3.2 Suggested Approach.

Using a trajectory plot (and diagnostic), measure the period, turning distance, and drift of the orbit. Input data for the simulation is shown in Table 2.3.

2.3.3 Analytical Solution.

For the specified fields (which satisfy the constraint of Equation (2.17)), a Lorentz transformation can be made to a frame, S', in which the electric field vanishes. This frame, illustrated in Figure 2.3, is defined by the velocity,

$$u = -\frac{E}{B} \ . \tag{2.20}$$

The only nonvanishing field in the S' frame is the magnetic field, which transforms according to

$$B' = \gamma^{-1} B$$

$$\gamma^{-1} = \left(1 - \frac{u^2}{c^2}\right)^{1/2} = \left[1 - \left(\frac{E}{cB}\right)^2\right]^{1/2} . \tag{2.21}$$

As illustrated in Figure 2.3b, the turning distance in this frame is related to gyromagnetic radius by

$$d' = 2r' = \frac{2p'}{eB'} = \frac{2mE\gamma^2}{eB^2} . \tag{2.22}$$

The period and drift are given by

$$\tau' = \frac{2\pi r'}{u} = \frac{2\pi m\gamma^2}{eB}$$

$$\ell' = 0 . \tag{2.23}$$

These parameters must be transformed back to the rest frame. Since the perpendicular dimension is Lorentz invariant, the turning distance is the same in either frame (i.e., d = d'). However, the period and drift are modified. Thus, the parameters of motion in the rest frame are

$$\tau = \frac{2\pi m\gamma^3}{eB}$$

$$d = \frac{2mE\gamma^2}{eB^2} \tag{2.24}$$

$$\ell = \frac{2\pi mE\gamma^3}{eB^2} = \pi\gamma d .$$

Using the initial conditions of Equation (2.18), we obtain the analytical results,

$$\begin{aligned} \tau &= 1.79\times10^{-12} \text{ sec} \\ d &= 8.53\times10^{-7} \text{ m} \\ \ell &= 2.68\times10^{-6} \text{ m} . \end{aligned} \tag{2.25}$$

Figure 2.4 presents a trajectory plot from the simulation. Note that the cycle appears to have repeated precisely three times in a simulation of duration, 3τ. The measured turning distance and drift are

$$\begin{aligned} d &= 8.5\times10^{-7} \text{ m} \\ \ell &= 2.7\times10^{-6} \text{ m} . \end{aligned} \tag{2.26}$$

These values were obtained by graphical measurement of the trajectory plots.

Table 2.3. Input data for Problem 2.3.

```
title *problem 2.3* /
comment *drift (e cross b) in constant electromagnetic field* /
system 1 /
x1grid 1 3 2 -4.81e-7 1 9.0e-6 9.0e-6 /
x2grid 1 3 2 -4.07e-6 1 9.0e-6 9.0e-6 /
conductor boundary +1 2 2 3 2 3 3 2 3 2 2 /
fields 1 1 300 1.78638e-14 /
courant 0 0 /
kinematics 1 0 0 0 0 /
forces  1 1 2 2 e2 null null 6 b3 null null /
function e2 1 0 -3.0e7 /
function b3 1 0 -20.0 /
populate electrons 0 0.0 1 2 2 3 3 1.6e-19
                   0.0534 0.4526 0.0 0.0 0.0 /
diagnose prscrib   0   2
         kinemat   0 301 /
trajectory 300 300 1 -4.81e-7 8.52e-6 -4.07e-6 4.93e-6 /
timeout -1 0 /
start /
stop /
```

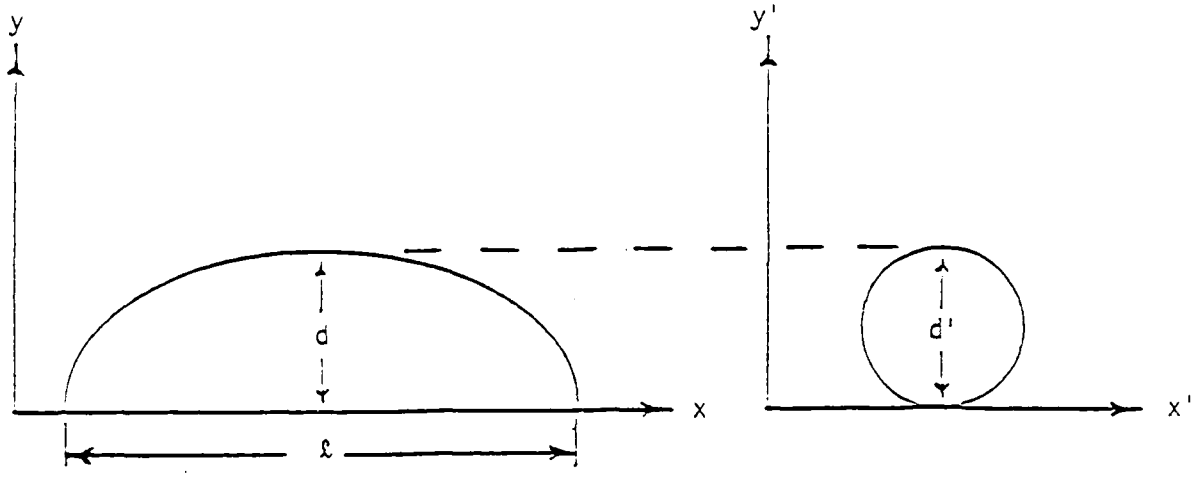

Figure 2.3. Lorentz transformation for E x B drift.

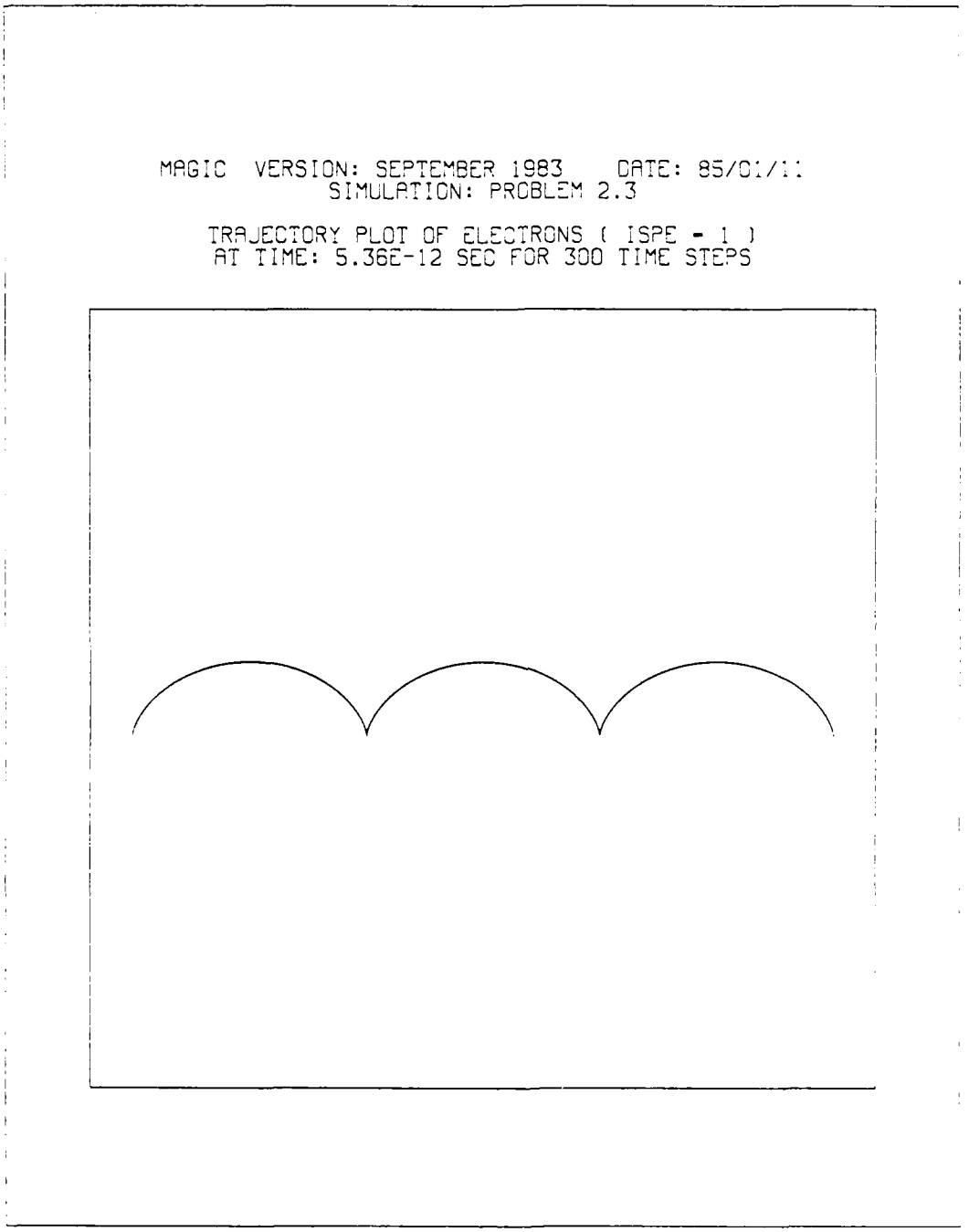

Figure 2.4. Trajectory plot, Problem 2.3.

2.4 DRIFT ($B \times \nabla B$).

2.4.1 Problem Description.

Spatial variations in the magnetic field will result in a variety of particle drifts. One drift of interest in plasma physics is that due to a transverse gradient in the magnetic field. Specifically, we consider the fields,

$$\overline{E} = 0$$

$$\overline{B} = \hat{z}B \ , \tag{2.27}$$

where $B = -\frac{0.2}{y}$.

The particle initial conditions are

$$t = x = z = 0$$

$$y = 10^{-2} \text{ m} \tag{2.28}$$

$$\overline{p} = \hat{x}p_o \ ,$$

where $p_o = 9 \times 10^8$ m/sec.

2.4.2 Suggested Approach.

The field prescription option in the FORCES command along with the appropriate FUNCTION command can easily be used to provide the 1/y dependence in the magnetic field (see function no. 5 in the User's Manual). Input data for this simulation is shown in Table 2.4.

2.4.3 Analytical Solution.

This problem can also be solved analytically, at least for the case of weak spatial gradients†. The solution involves expansion of the magnetic field (or gyromagnetic frequency) about the slowly moving orbital center, or

$$\bar{\omega}(\bar{r}) = - \frac{e}{\gamma mc} \bar{B}(\bar{r}) \simeq \bar{\omega}_o \left[1 + \left(\frac{1}{B} \frac{\partial B}{\partial y}\right) \hat{y} \cdot \bar{r}\right] . \tag{2.29}$$

The transverse velocity is written in two parts,

$$\bar{v} = \bar{v}_o + \bar{v}_d , \tag{2.30}$$

where v_o is the gyromagnetic velocity and v_d is a small drift velocity. Substitution into the frequency expansion yields the result,

$$\frac{d\bar{v}}{dt} \simeq \left[\bar{v}_d + \bar{v}_o(\hat{y} \cdot \bar{r}_o)\left(\frac{1}{B} \frac{\partial B}{\partial y} \right)\right] \times \bar{\omega}_o . \tag{2.31}$$

Thus, the drift velocity has a nonvanishing average value,

$$\langle \bar{v}_d \rangle = \left(\frac{1}{B} \frac{\partial B}{\partial y}\right) \bar{\omega}_o \times \langle \bar{r}_o(\hat{y} \cdot \bar{r}_o) \rangle , \tag{2.32}$$

or

$$\langle \bar{v}_d \rangle = \frac{r^2 \omega}{2B^2} (\bar{B} \times \bar{\nabla} \times \bar{B}) . \tag{2.33}$$

Using the parameters of Equations (2.27) and (2.28), we obtain the analytical value of the drift velocity,

† J. D. Jackson, Classical Electrodynamics, John Wiley and Sons, New York, 1967 (p. 415).

$$\langle v_d \rangle = 3.64 \times 10^6 \text{ m/sec.} \quad (2.34)$$

Simulation results are shown in the trajectory plot in Figure 2.5. In a period of 5.65 psec, we estimate the orbit differential motion to be 2.1×10^{-5} m. This would indicate a simulation drift velocity of

$$\langle v_d \rangle = 3.7 \times 10^6 \text{ m/sec.} \quad (2.35)$$

Table 2.4. Input data for Problem 2.4.

```
title *problem 2.4* /
comment *drift (b cross delb) in spatially varying
         magnetic field* /
system 1 /
x1grid 1 3 2 -0.00026 1 0.0006 0.0006 /
x2grid 1 3 2  0.00945 1 0.0006 0.0006 /
fields 1 1 500 5.65233e-14 /
conductor boundary +1 2 2 3 2 3 3 2 3 2 2 /
courant 0 0 /
kinematics 1 0 0 0 0 /
forces  1 1 1 6 null null b3x2 /
function b3x2 5 -1 -0.2 /
populate electrons 0 0.0 1 2 2 3 3 1.6e-19
                0.4339 0.9167 9.0e8 0.0 0.0 /
diagnose kinemat 0 501
         prscrib 0 501 /
trajectory 500 500 1 -0.00026 0.00034 0.00945 0.01005 /
timeout -1 0 /
start /
stop /
```

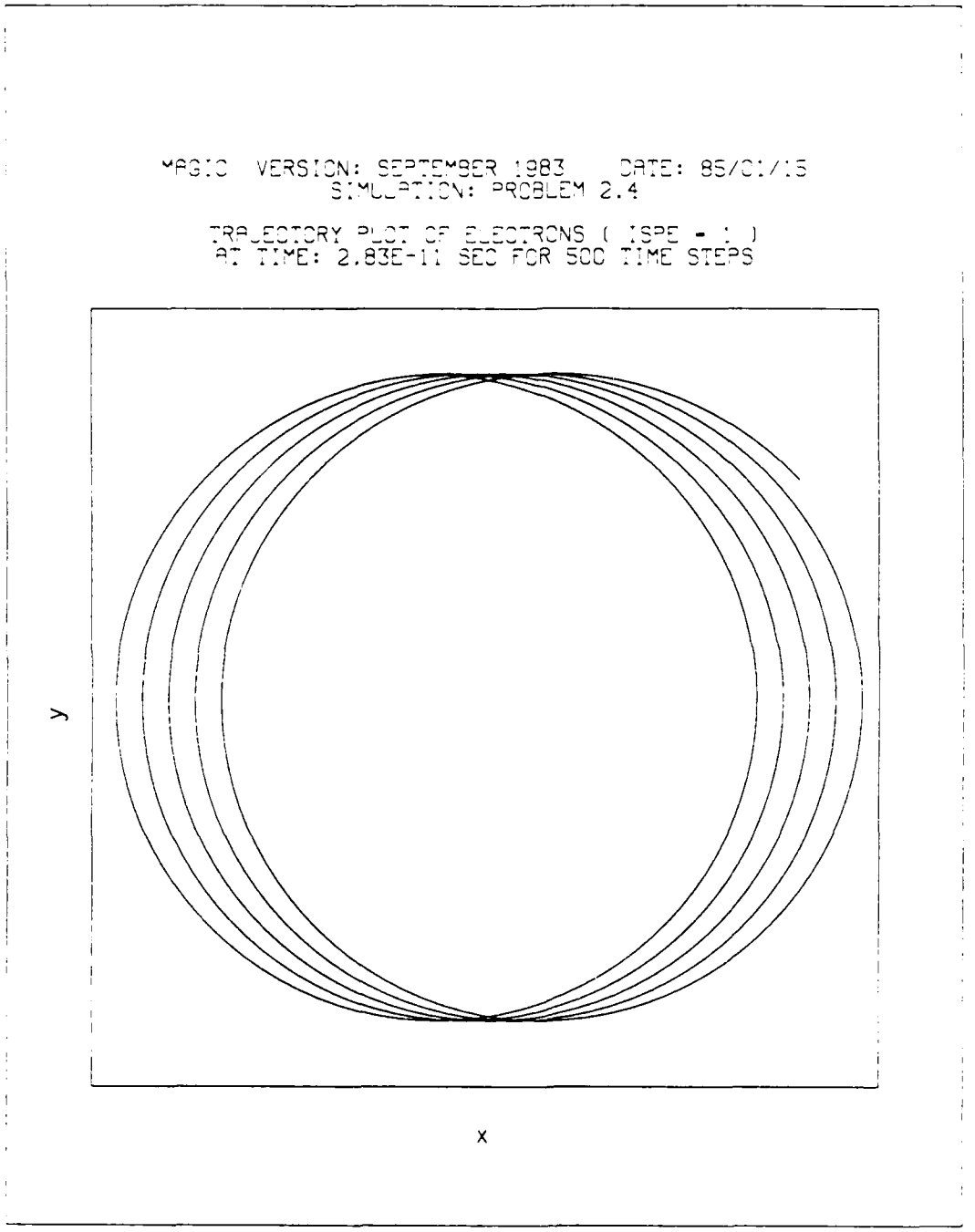

Figure 2.5. Trajectory plot, Problem 2.4.

2.5 FIELD EMISSION.

2.5.1 Problem Description.

Two infinite plates separated by distance, d, are maintained at a constant potential difference, V. We arbitrarily use the parameters,

$$d = 3 \times 10^{-2} \text{ m}$$
$$V = 1 \times 10^{5} \text{ V} \quad . \tag{2.36}$$

The cathode is assumed to break down; i.e., it continuously emits electrons which are received at the anode. We want to measure the final, steady-state voltage as a function of distance and the incident (cathode surface) current density as a function of time.

2.5.2 Suggested Approach.

The one-dimensional simulations are the first self-consistent problems (i.e., mutual interaction between particles and fields) in the set. The MAGIC code can be run in the one-dimensional mode in several ways. We suggest using a single cell in the transverse dimension bounded by periodic symmetry planes (see SYMMETRY command). The periodic symmetry model requires overlapping cells at each boundary; thus, four full-grid points (three cells) are needed in the transverse dimension. In the longitudinal direction, any number of cells can be used; however, the quality of the simulation will improve with careful resolution of any space-charge barrier which may result.

The particles for this simulation must be introduced using a PARTICLES command. We suggest starting the particles out a small distance (fraction of the first cell) from the cathode and with a commensurate velocity (i.e., one given by the Child-Langmuir equations). These are all required input data. For output, we suggest phase space plots (p_i vs.

x_1), range plots of fields (E_1 vs. x_1 and J_1 vs. x_1), and time histories of the same at selected locations.

The constant voltage for this simulation can be applied and maintained using the CIRCUIT command. Note that the abrupt application of a constant voltage and the subsequent breakdown will result in a transient. That is, oscillations will occur prior to reaching a steady state. This is, of course, physical. However, it has been shown† that the transient can be minimized if the voltage is initially given the time-dependence,

$$V(t) = V\left[\frac{4}{3}\left(\frac{t}{\tau}\right) - \frac{1}{3}\left(\frac{t}{\tau}\right)^4\right], \qquad 0 < t < \tau$$

where (2.37)

$$\tau = 3\left(\frac{md^2}{2eV}\right)^{1/2} .$$

The voltage is maintained constant at V after the period τ.

The simplest way to input this function is to use the numerical data option. The input data for this simulation is shown in Table 2.5.

2.5.3 Analytical Solution.

In one dimension, the continuity equation is

$$\partial_x J + \partial_t \rho = 0 . \qquad (2.38)$$

The steady-state assumption requires that

† M. Lampel and M. Tiefenback, "An Applied Voltage to Eliminate Current Transients in a One-Dimensional Diode," Appl. Phys. Lett. 43 (1), July 1983.

$$\partial_t \rho = 0 \quad , \tag{2.39}$$

and subsequently,

$$J = J^+ \ , \tag{2.40}$$

where J^+ is the current density at the cathode surface. The one-dimensional Poisson equation,

$$\partial_x^2 \phi = - \frac{\rho}{\varepsilon} \quad , \tag{2.41}$$

also applies. Here the density is given by

$$\rho = \frac{J}{v} \quad . \tag{2.42}$$

The velocity can be related to potential by the (nonrelativistic) expression,

$$v = \left(\frac{2e\phi}{m} \right)^{1/2} \quad . \tag{2.43}$$

Substitution of these results into the Poisson equation yields the result,

$$\partial_x^2 \phi = - \frac{J^+}{\varepsilon} \left(\frac{m}{2e} \right) \phi^{-1/2} \ . \tag{2.44}$$

This can be integrated by making use of the substitution,

$$\frac{d}{dx} \left(\frac{d\phi}{dx} \right)^2 = 2 \left(\frac{d\phi}{dx} \right) \left(\frac{d^2\phi}{dx^2} \right) \quad , \tag{2.45}$$

to obtain the familiar result†,

$$\phi = \left(\frac{3}{2} \right)^{4/3} \left(\frac{J^+}{\varepsilon} \right)^{2/3} \left(\frac{m}{2e} \right)^{1/3} x^{4/3} . \qquad (2.46)$$

Thus, the cathode current density is determined by anode potential and separation, or

$$J^+ = \frac{4}{9} \varepsilon \left(\frac{2e}{m} \right)^{1/2} \frac{V^{3/2}}{d^2} . \qquad (2.47)$$

Using the parameters in Equation (2.36), we obtain the analytical result,

$$J^+ = 8.20 \times 10^4 \ A/m^2 . \qquad (2.48)$$

Range plot results from the simulation are illustrated in Figures 2.6 and 2.7. The current density versus distance shown in Figure 2.6 appears to be stable at a value of

$$J^+ = 7.98 \times 10^4 \ A/m^2 . \qquad (2.49)$$

(The slight discrepancy at the origin is due to the way local charge conservation is handled by the field emission algorithm.) The electric field vs. distance is shown in Figure 2.7; this result exhibits the expected $x^{1/3}$ behavior. Finally, Figure 2.8 presents a plot of particle phase space. For this nonrelativistic simulation, the particle momentum should go as $x^{2/3}$ (i.e., the square root of potential).

† C. D. Child, Physical Review (Ser. I) 32, 492 (1911).
I. Langmuir, Physical Review 21, 419 (1923).

Table 2.5. Input data for Problem 2.5.

```
title *problem 2.5* /
comment *space-charge limiting (child-langmuir problem)* /
system 1 /
x1grid 1 42 2 0.0 40 1.875e-4 3.0e-2 /
x2grid 1  4 2 0.0  2 3.75e-3  7.5e-3 /
conductor k  1  2 2  2 3 /
conductor a -1 42 2 42 3 /
symmetry periodic  1 2 2 42 2 -1 2 3 42 3 /
fields 1 1 4000 5.0e-13 /
courant 0 0 /
particles emission null electrons 0.0 0.0 1 1 2 2 1
      1.0e6 1.1680316e-5 0.0 0.0 0.0 0.0 0.0 1 2 2 2 3 /
forces 0.0 0.5 1.0 1.0 /
poisson 2 a +1.0 k 0.0 1 0.0 1.0 1 /
circuit voltage 1 0.0 1 0 42 2 2 2 /
function voltage 0 10 0.0 0.0 6.0e-11 1.67e4 1.2e-10 3.32e4
                 1.8e-10 4.94e4 2.4e-10 6.46e4 3.0e-10 7.83e4
                 3.6e-10 8.95e4 4.2e-10 9.71e4 4.8e-10 1.00e5
                                               1.0     1.00e5 /
statistics 400 /
diagnose spacing 0 1 /
linprint 4000  1 2 2 42 2 1 1 /
linprint 4000 11 2 2 42 2 1 1 /
trajectory 800 1 1 0.0 3.0e-2 0.0 3.0e-2 /
phasespace 800 31 0 0.0 3.0e-2 0.0 3.75e-3  1.0e6 2.0e8
                               -2.0e8 2.0e8 -2.0e8 2.0e8 /
observe 1 0 twod 1 0.0 1.0 0.0 1.0 1  2 2  2 2
            twod 1 0.0 1.0 0.0 1.0 1 22 2 22 2
            twod 1 0.0 1.0 0.0 1.0 1 41 2 41 2 /
range 800 1  7 2 2 42 2 3 /
range 800 1  1 2 2 42 2 3 /
range 800 1 11 2 2 42 2 3 /
range 800 1 10 2 2 42 2 3 /
timeout -1 0 /
start /
stop /
```

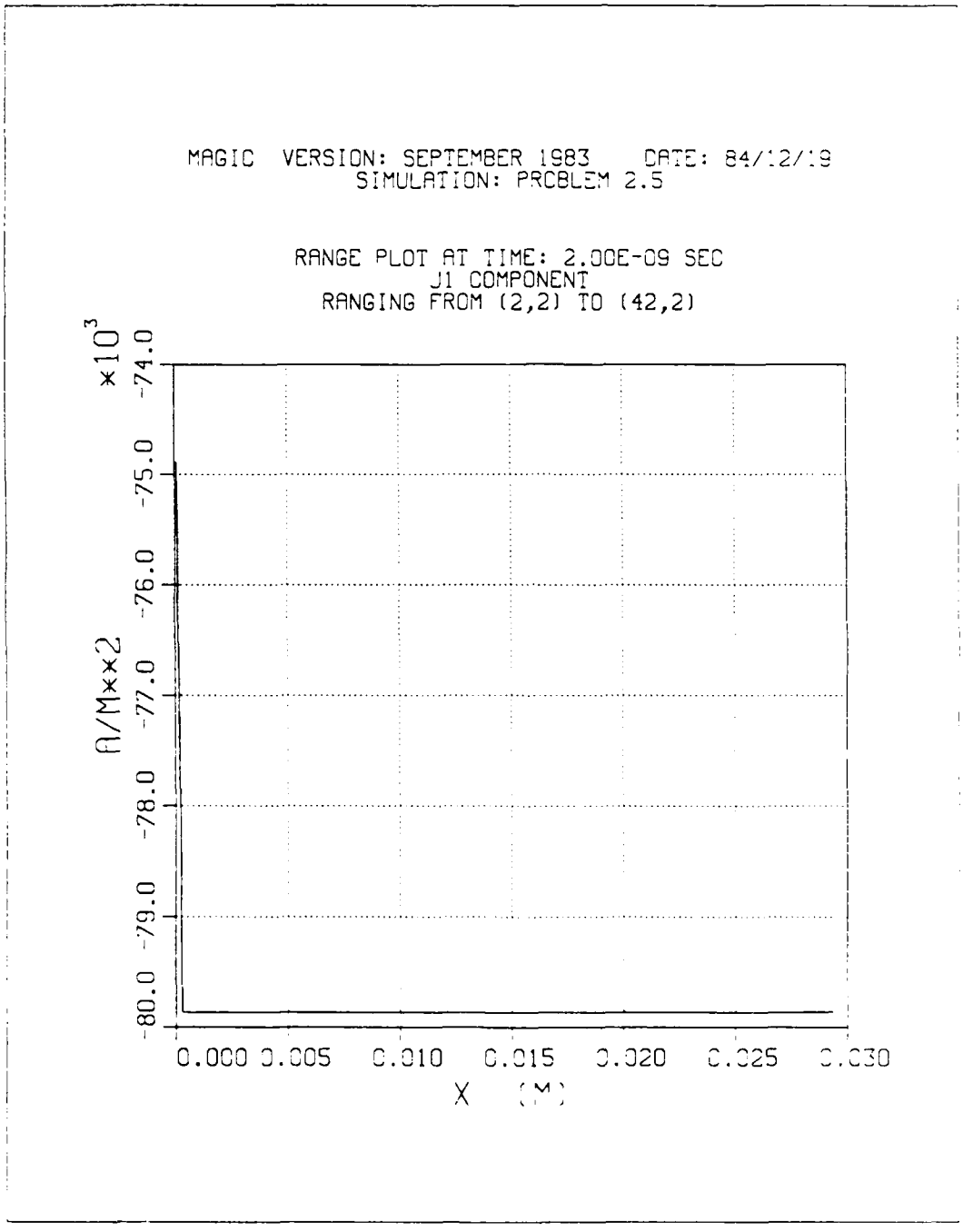

Figure 2.6. Current density vs. distance, Problem 2.5.

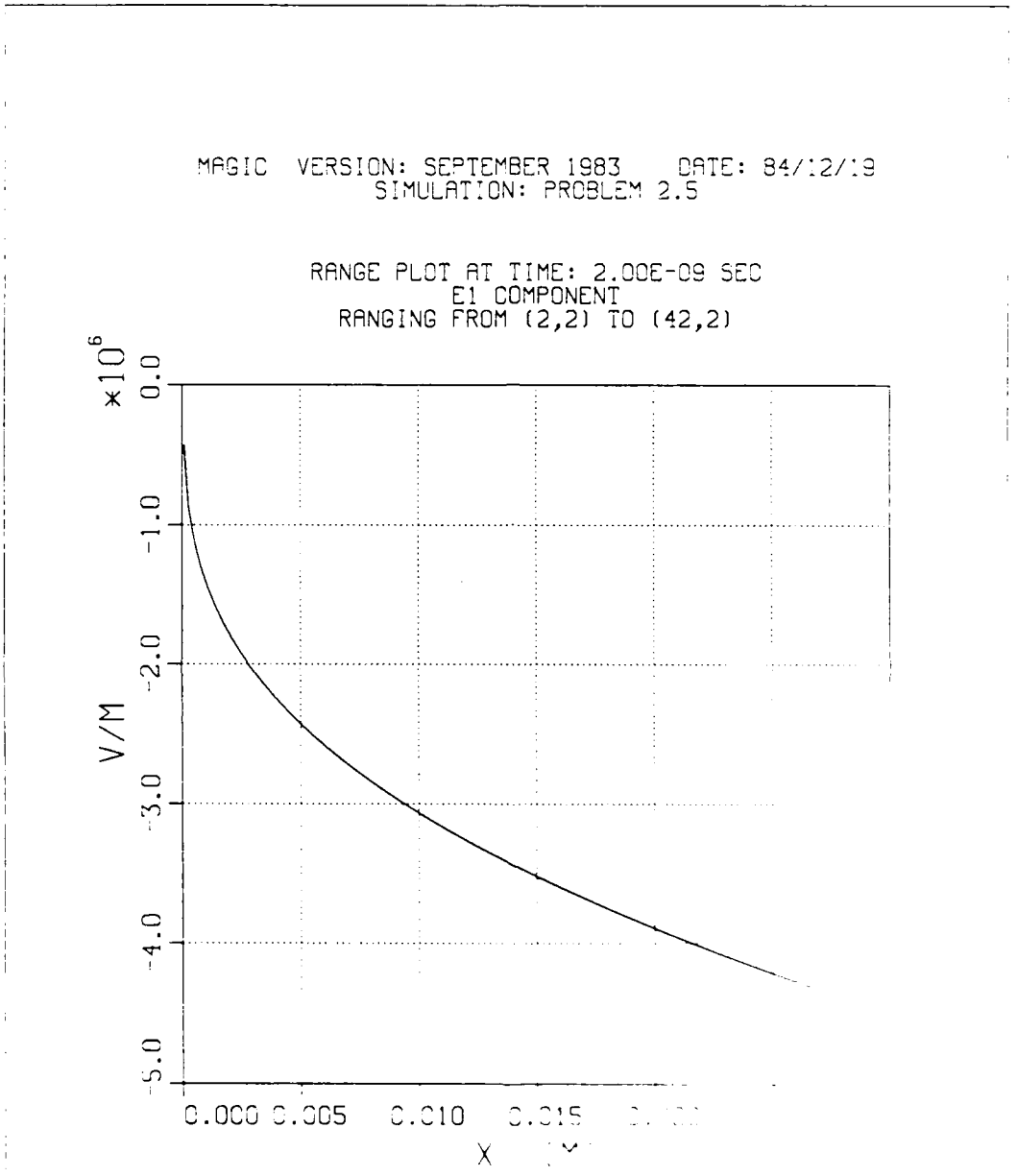

Figure 2.7. Electric [illegible]

AD-A191 110 PULSED POWER SIMULATION PROBLEMS IN MAGIC(U) MISSION 2/2
RESEARCH CORP ALEXANDRIA VA B COPLEN ET AL. 10 APR 87
MRC/WDC-R-124 DNA-TR-87-140 DNA001-84-C-0200

UNCLASSIFIED F/G 20/14 NL

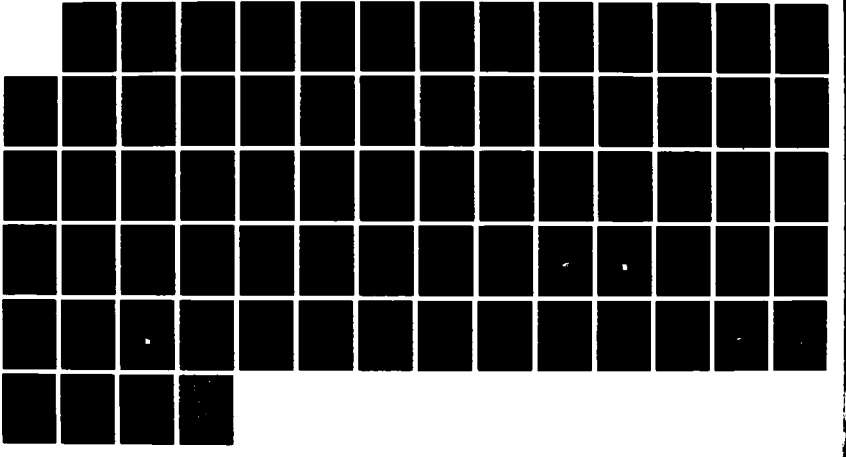

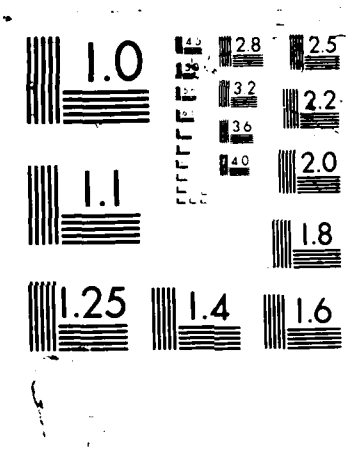
1.0
1.1
1.25
1.4
1.6
1.8
2.0
2.2
2.5
2.8
3.2
3.6
4.0

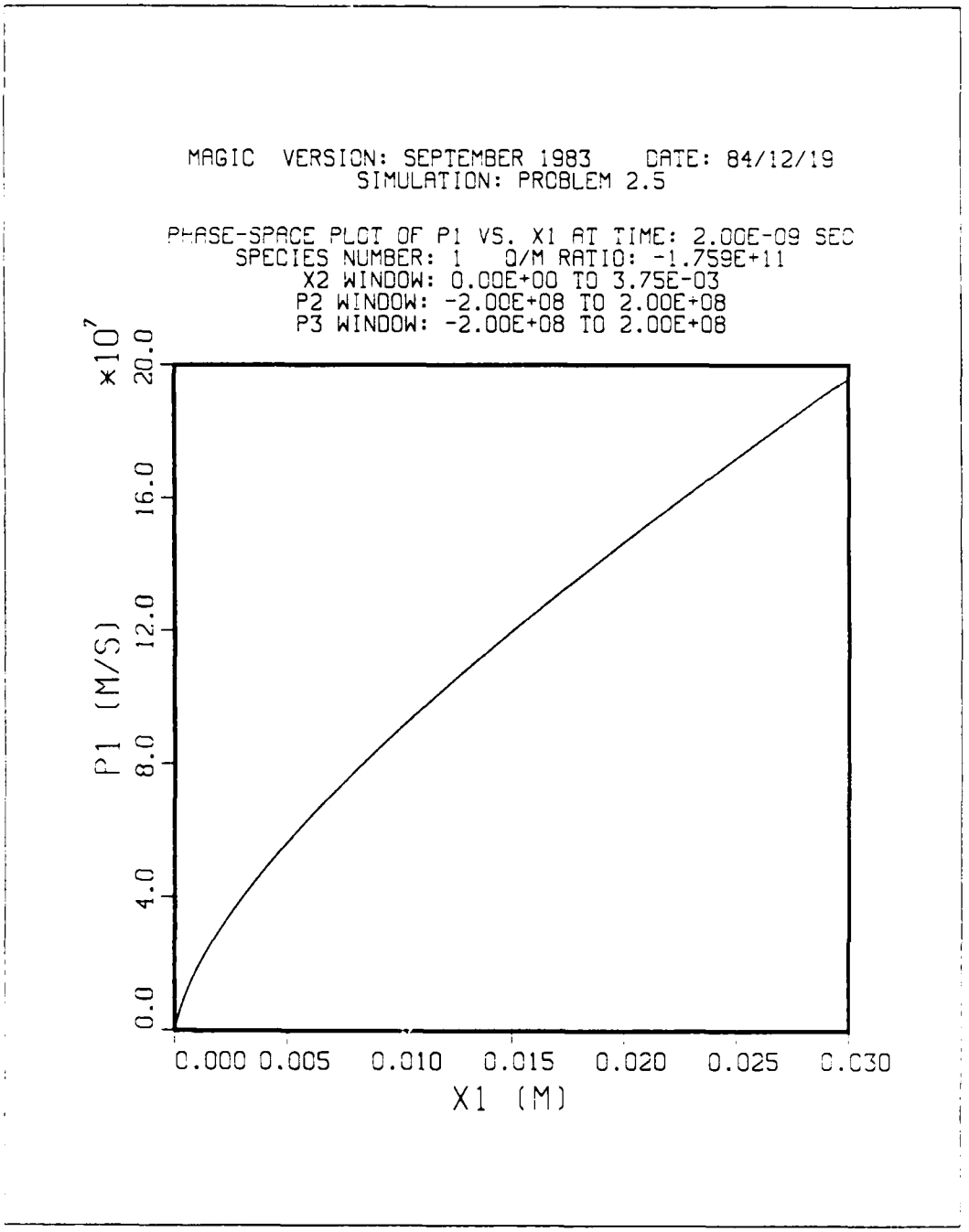

Figure 2.8. Particle phase space, Problem 2.5.

2.6 MAGNETIC INSULATION.

2.6.1 Problem Description.

By adding a magnetic field perpendicular to the plane described in Problem 2.5, a one-dimensional magnetic insulation simulation is created. For example, if x measures distance across a gap of width, d, and y measures distance along the conducting surfaces, then we add a constant magnetic field,

$$\overline{B} = \hat{z}B \quad , \tag{2.50}$$

where $B = 4.6 \times 10^{-2}$ T. This value of magnetic field was selected on the basis of reasonable hub thickness. Other parameters are maintained as in Problem 2.5, i.e.,

$$\begin{aligned} d &= 3 \times 10^{-2} m \\ V &= 1 \times 10^{5} V \quad . \end{aligned} \tag{2.51}$$

As with the Child-Langmuir physics, the perpendicular electric field, E_x, draws electrons out of the cathode. Now, however, the magnetic field tends to turn electrons in the y direction. This leads in turn to a y-component of current density, a y-component of electric field and a z-component of (self) magnetic field. Despite the presence of these nonvanishing and spatially dependent fields (E_x, E_y, B_z, J_x, J_y), the problem is still one-dimensional.

2.6.2 Suggested Approach.

The external magnetic field can be added using a BEXTERNAL command. (Note that the simulation automatically adds this field to the dynamic field from Maxwell's equations to compute particle forces.)

The time transient experienced in this problem is even more severe than that in Problem 2.5. Therefore, we recommend using a time-dependent voltage similar to that suggested in 2.5, but with a value of τ equal to some multiple (say 4) of the gyromagnetic period. Note that this period corresponds roughly to the particle lifetime (surface-to-surface), as shown in Problem 2.3. Although both results (stepped or transient voltage) are physical, the transient case corresponds more closely to what can be accomplished with actual devices. That is, a slowly increasing voltage tends to mask the violence of the boundary layer transient.

The input data for this simulation is shown in Table 2.6.

2.6.3 Analytical Solution.

A solution of this problem was first done by Sudan and Lovelace†. We consider that the problem is infinite and symmetrical in the y and z directions, so that all quantities will be unvarying in y and z. In the steady-state solution of the problem, we will have two regions, one near the cathode filled with space charge and one next to the anode which is a vacuum region. The regions will be separated by a surface at $x = x_t$.

The electron equations of motion are

$$\partial_t v_x = \frac{-e}{m} \left[E_x(x) + v_y B_z \right]$$
$$\partial_t v_y = \frac{e}{m} v_y B_z \ . \qquad (2.52)$$

† R. N. Sudan and R. V. Lovelace, Phys. Rev. Lett. 31, 1174, (1973).

Since we assume that $v_x = v_y = 0$ for electrons emerging from the cathode ($x = 0$) and that B_z is constant in space, we can integrate both sides of Equation (2.52) to obtain

$$v_y = x\omega_c \tag{2.53}$$

where $\omega_c = eB_o/m$ is the electron cyclotron frequency. We set $\phi = 0$ at the cathode and obtain through energy conservation the equation

$$\frac{m}{2}(v_x^2 + v_y^2) = e\phi(x) \ . \tag{2.54}$$

This requires that, at the turning point,

$$\frac{1}{2}\omega_c^2 x_t^2 = \frac{e}{m}\phi(x_t) \ . \tag{2.55}$$

We assume that there will be a flow of charge from the cathode in this problem that is balanced by an opposing return flow. Both flows will be separately conserved, except at the turning point. We therefore have by conservation of charge:

$$\partial_x J_x + \partial_y J_y = \partial_t \rho \ , \tag{2.56}$$

where J_x and J_y and the current density in the x and y direction respectively and ρ is the change density. Since we have steady-state conditions $\partial_t \rho = 0$ and also $\partial_y J_y = 0$, because all quantities must be constant in the y direction, $J_x = J_o = \rho v_x$ = constant. Because of both emitted and return flows, the density must be

$$\rho = \frac{2J_o}{v_x} \ . \tag{2.57}$$

We have both magnetic and electric fields in the problem. We approximate the magnetic fields as being constant in space, $B_z = B_o$. The electric fields are found via the electrostatic potential as determined from Poisson's equation:

$$\partial_x^2 \phi = - \frac{\rho}{\varepsilon_o} . \tag{2.58}$$

For the vacuum region, $\rho = 0$, so ϕ will be

$$\phi = V_o + f(d-x) , \tag{2.59}$$

where f is a constant to be determined as part of the solution of the problem. The potentials and derivatives for the two regions will be matched at x_t.

The cathode surface, at steady-state, is a space charge limited emitter, implying

$$\partial_x \phi(0) = 0 . \tag{2.60}$$

By Poisson's equation and conservation of charge we have

$$\partial_x^2 \phi = - 2J_o / \varepsilon_o v_x . \tag{2.61}$$

We can use energy conservation and the equations of motion to write

$$\partial_x^2 \phi = (m/2e)^{1/2} J_o / (\phi - \frac{q^2}{2} x^2)^{1/2} \tag{2.62}$$

where $q^2 = \frac{m}{e} \omega_c^2$.

We define

$$\psi = \phi - \frac{1}{2} q^2 x^2 \tag{2.63}$$

and write (using prime notation, $\partial_x \psi = \psi'$)

$$\psi'' + q^2 = \left(\frac{K}{\psi}\right)^{1/2} , \tag{2.64}$$

where $K = 2J_o(m/2e)^{1/2}$.

This can be integrated to obtain

$$\psi' = (4K\ \psi^{1/2} - 2q^2\ \psi)^{1/2} . \tag{2.65}$$

This equation gives us a condition on ψ' and thus ϕ' at the turning point. The variable ψ is actually $(m/2e)v_x^2$. Therefore, $\psi = 0$ at x_t so that

$$\phi'(x_t) = q^2 x_t . \tag{2.66}$$

Using the fact that ϕ and ϕ' must be continuous across the surface at x_t, we have then the condition for the turning point,

$$V_o = \frac{e}{mc^2} B_o^2 x_t (d - x_t/2) . \tag{2.67}$$

The steady-state field in the gap is then also the same as for parapotential flow,

$$\partial_x \phi = q^2 x_t . \tag{2.68}$$

For the parameters in Equation (2.51), we have

$$x_t = 1.18\times10^{-2} \text{ m}$$
$$E = 4.14\times10^{6} \text{ V/m} . \tag{2.69}$$

Results from the simulation are shown in Figures 2.9 through 2.12. The transverse current density J_y is shown in Figure 2.9. The normal electric field E_x as a function of distance is shown in Figure 2.10. From this figure, we estimate the turning distance and gap field to be

$$x_t = 1.2\times10^{-2} \text{ m}$$
$$E = 4.2\times10^{6} \text{ V/m} , \tag{2.70}$$

in reasonable agreement with the analytical results. Figure 2.11 illustrates the self-magnetic field (dynamic component only) vs. distance. The diamagnetic effect is confirmed small in comparison to the externally applied field, thus justifying the initial assumption. Finally, Figure 2.12 presents a particle phase-space (p_2 vs. x_1) plot. (This plot is composed of individual particle coordinates.) Note the extent to which this result agrees with Equation (2.53). Graphically taking the slope of this curve, we estimate ω_c from the simulation to be 8×10^{9} rad/sec vs. the analytical value of 8.07×10^{9} rad/sec.

Table 2.6. Input data for Problem 2.6.

```
title *problem 2.6i* /
comment *magnetic insulation boundary layer* /
system 1 /
x1grid 1 42 2 0.0 40 1.875e-4 3.0e-2 /
x2grid 1  4 2 0.0  2 3.75e-3  7.5e-3 /
conductor k  1  2 2  2 3 /
conductor a -1 42 2 42 3 /
symmetry periodic  1 2 2 42 2 -1 2 3 42 3 /
fields 1 1 12000 5.0e-13 /
courant 0 0 /
particles emission null electrons 0.0 0.0 1 1 2 2 1
        1.0e6 1.1680316e-5 0.0 0.0 0.0 0.0 0.0 1 2 2 2 3 /
forces 0.5 1.0 1.0 /
bexternal 0.0 0.0 4.6176342e-2 /
poisson 2 a +1.0 k 0.0 1 0.0 1.0 1 /
circuit voltage 1 0.0 1 0 42 2 2 2 /
function voltage 0 17 0.0 0.0 2.065e-10 8.896e3 4.13e-10 1.778e4
            6.195e-10 2.664e4 8.26e-10 3.542e4 1.0325e-09 4.41e4
            1.239e-09 5.25e4 1.4455e-09 6.069e4 1.652e-09 6.85e4
            1.8585e-09 7.57e4 2.065e-09 8.24e4 2.2715e-09 8.82e4
            2.478e-09 9.31e4 2.6845e-09 9.68e4 2.891e-09 9.92e4
                                    3.0975e-09 1.00e5 1.0 1.00e5 /
statistics 400 /
diagnose 6 0 1
         3 4000 4001
         4 4000 4001
         5 4000 4001 /
linprint 4000  1 2 2 42 2 1 1 /
linprint 4000 11 2 2 42 2 1 1 /
trajectory 800 1 1 0.0 3.0e-2 0.0 3.0e-2 /
phasespace 800 31 0 0.0 3.0e-2 -1.0 1.0  -1.0e8 1.0e8
                               -9.0e9 9.0e9 -9.0e9 9.0e9 /
phasespace 800 41 0 0.0 3.0e-2 -1.0 1.0  -9.0e9 9.0e9
                               -1.0e8 1.0e8 -9.0e9 9.0e9 /
observe 1   twod 1 0.0 1.0 1  2 2  2 2
            twod 1 0.0 1.0 1 22 2 22 2
            twod 1 0.0 1.0 1 41 2 41 2
            twod 1 0.0 1.0 6  2 2  2 2
            twod 1 0.0 1.0 6 22 2 22 2
```

Table 2.6. Input data for Problem 2.6. (continued).

```
            twod 1 0.0 1.0 6 41 2 41 2
            twod 1 0.0 1.0 8  3 2  3 2
            twod 1 0.0 1.0 8 22 2 22 2
            twod 1 0.0 1.0 8 41 2 41 2
            twod 1 0.0 1.0 7  2 2  2 2
            twod 1 0.0 1.0 7 22 2 22 2
            twod 1 0.0 1.0 7 41 2 41 2
            twod 1 0.0 1.0 10 2 2  2 2
            twod 1 0.0 1.0 10 22 2 22 2
            twod 1 0.0 1.0 10 41 2 41 2 /
range 800 1  7 2 2 42 2 3 /
range 800 1  8 2 2 42 2 3 /
range 800 1  8 2 3 42 3 3 /
range 800 1  1 2 2 42 2 3 /
range 800 1  1 2 3 42 3 3 /
range 800 1  2 2 2 42 2 3 /
range 800 1  2 2 3 42 3 3 /
range 800 1  6 2 2 41 2 3 /
range 800 1  6 2 3 41 3 3 /
range 800 1 11 2 2 42 2 3 /
timeout 60 1 /
start /
stop /
```

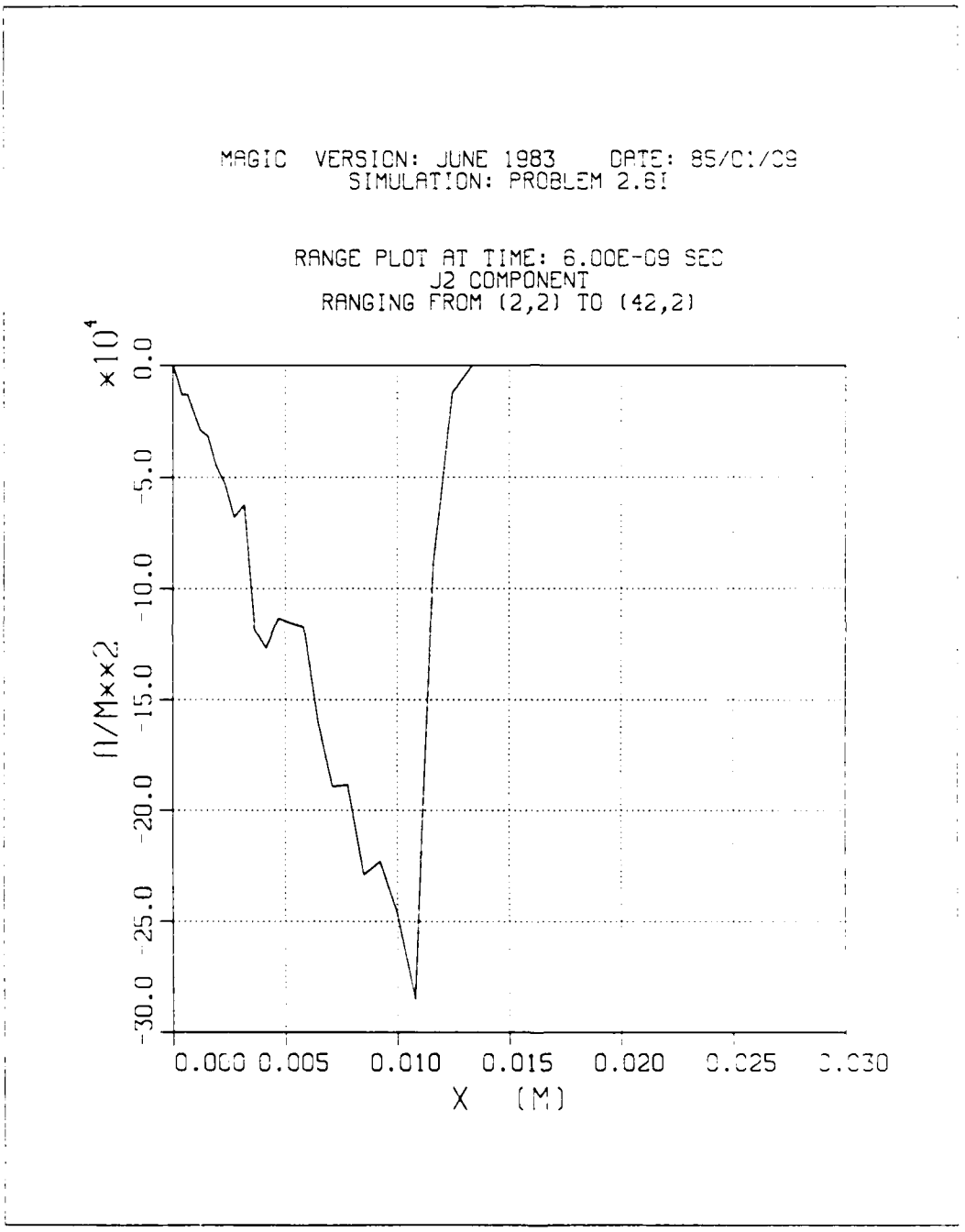

Figure 2.9. Current density vs. distance, Problem 2.6.

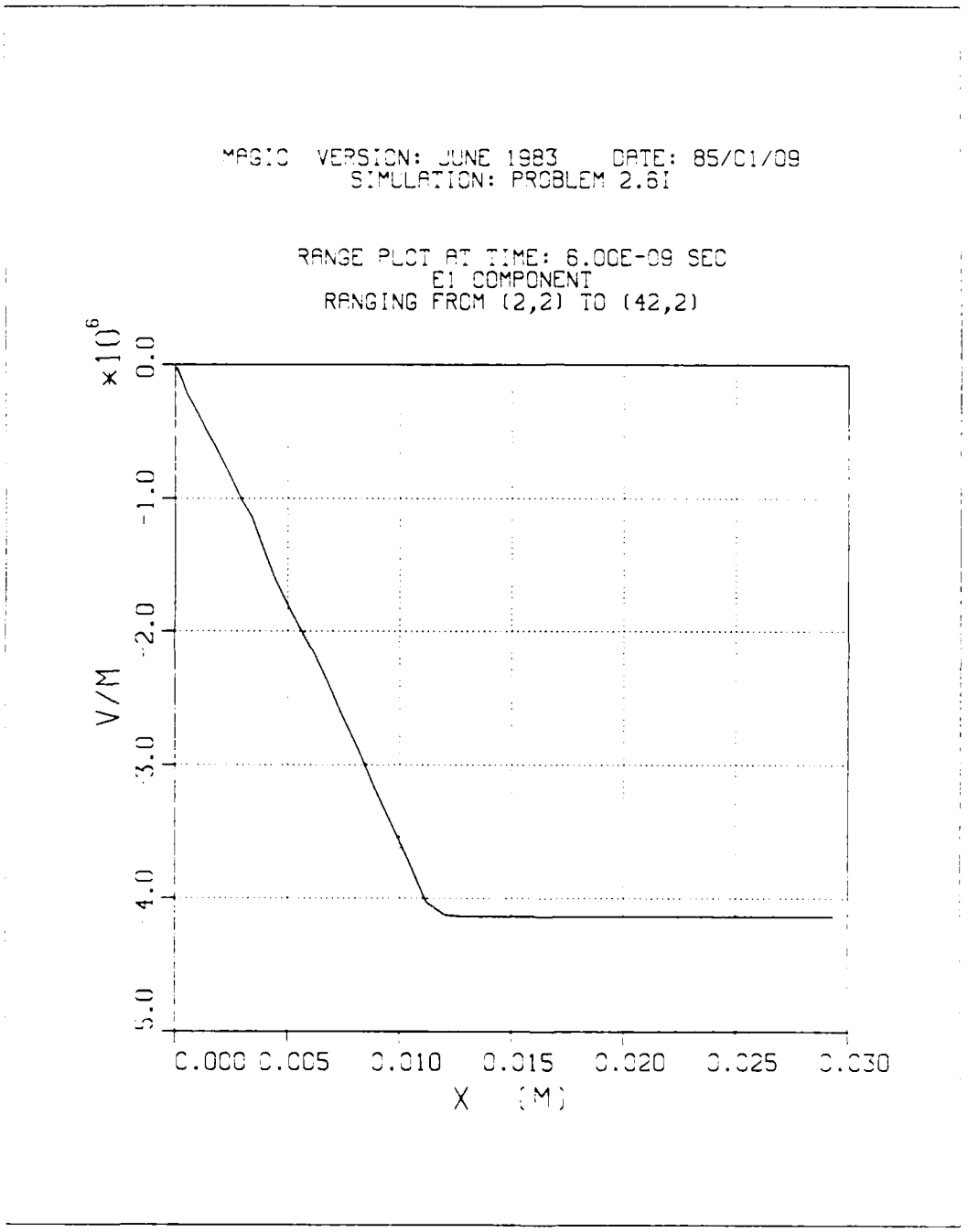

Figure 2.10. Electric field vs. distance, Problem 2.6.

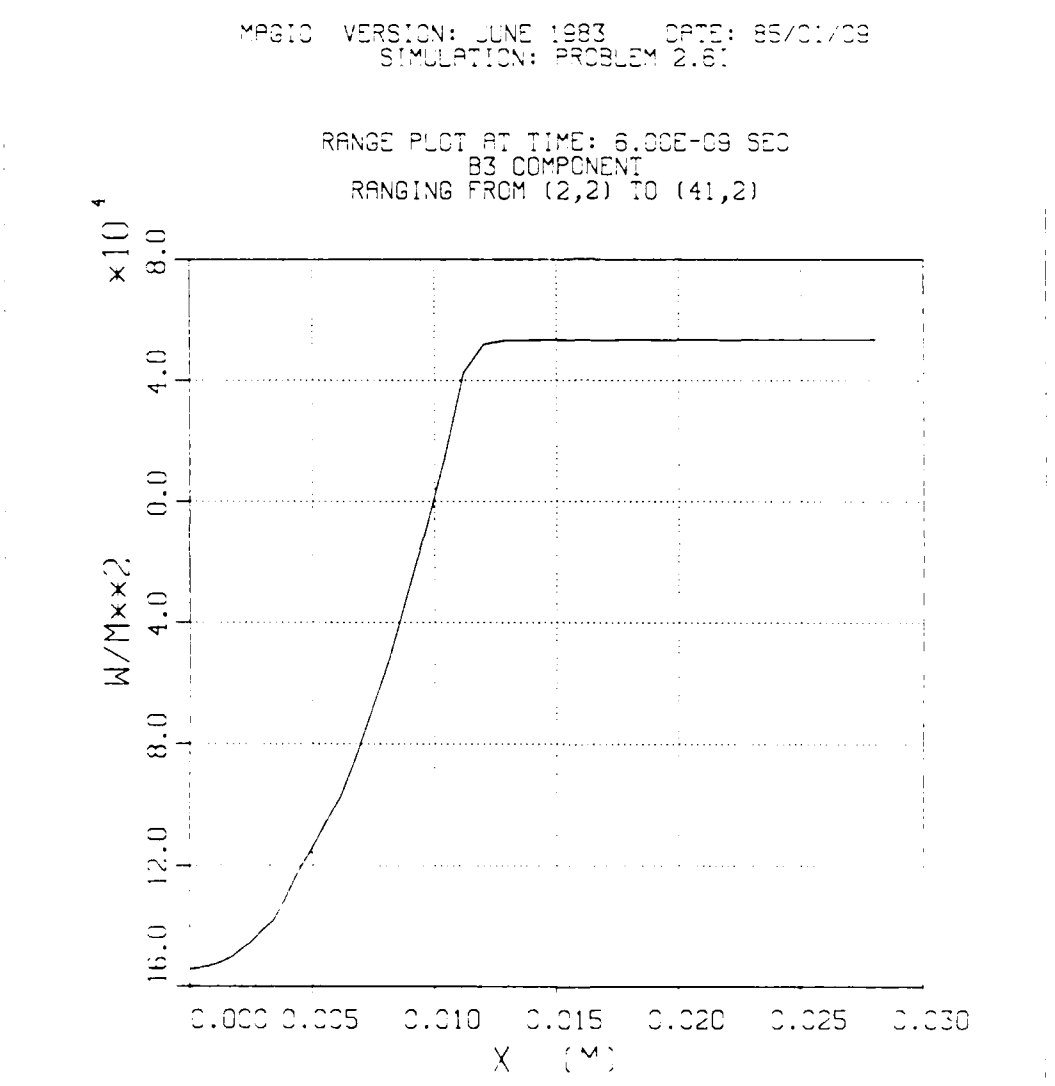

Figure 2.11. Magnetic field vs. distance, Problem 2.6.

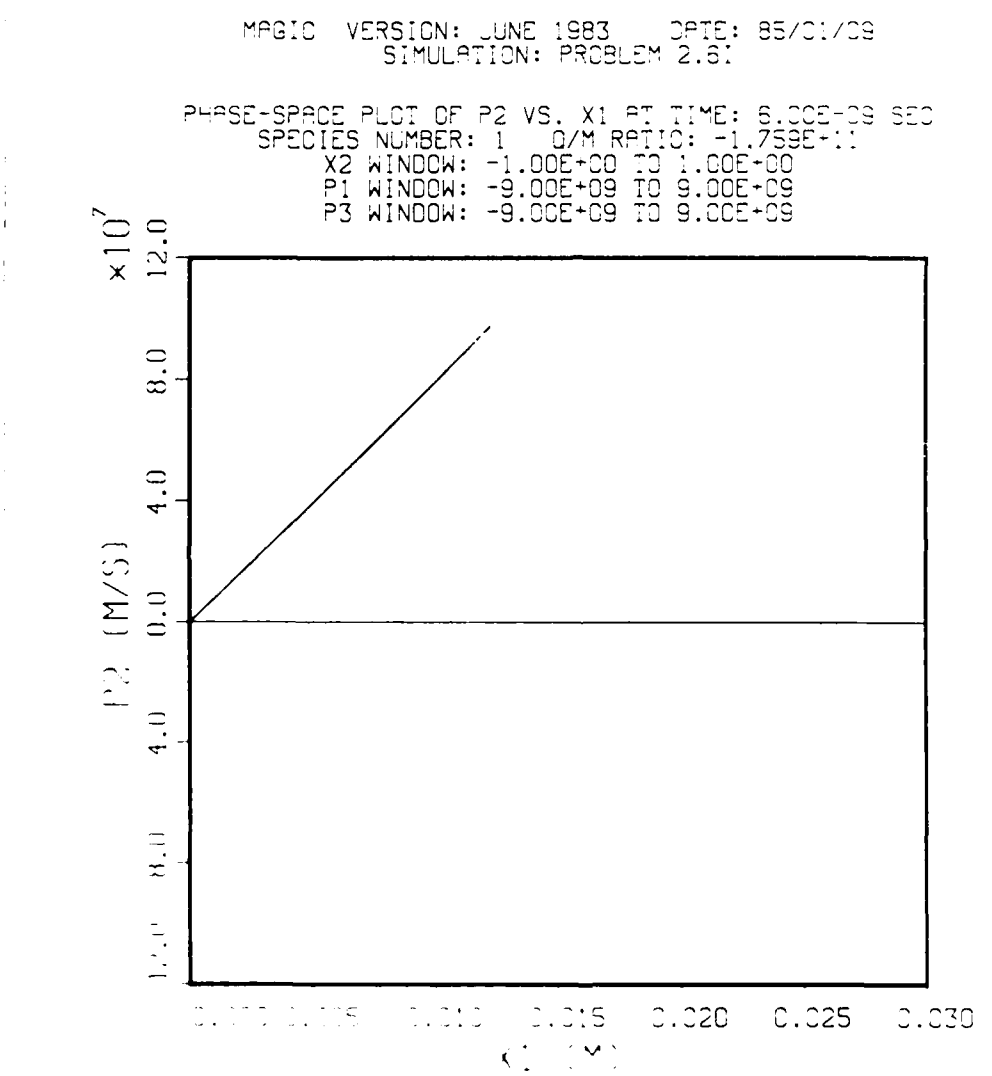

Figure 2.12. Particle phase space, Problem 2.6.

SECTION 3
PULSED POWER TRANSPORT

This section presents problems involving pulsed power transport (e.g., diode) applications. The objective is to combine previously introduced simulation concepts in realistic applications. However, this objective must be tempered by economic reality. Realistic applications will often require expensive simulations, whereas the simulations presented here must be sufficiently inexpensive to allow use as a learning tool. Thus, we have established a maximum cost of about five minutes of Cray CPU time per problem, and have compromised simulation parameters to meet this restriction. The resulting problems may lack geometric and temporal realism; however, they introduce the important simulation concepts and are, at the same time, affordable.

3.1 COAXIAL LINE WITH FIELD EMISSION.

3.1.1 Problem Description.

The first problem involves a uniform section of coaxial transmission line, as previously illustrated in Figure 1.1. For convenience, the dimensions of Problem 1.1,

$$\begin{aligned} r_o &= 0.20\text{m} \\ r_i &= 0.10\text{m} \\ L &= 0.60\text{m} , \end{aligned} \tag{3.1}$$

are duplicated exactly. Whereas Problem 1.1 simulated a cold-test, here we wish to cause field emission of electrons to occur on the cathode. Therefore, the incident voltage pulse is semi-infinite with a 4 MV peak and a rise time of 1 nsec, or

$$\phi(t) = \begin{cases} \phi_p^+\left(\frac{t}{\tau}\right) , & 0 < t < \tau \\ \phi_p^+ , & \tau \leq t < \infty . \end{cases} \tag{3.2}$$

Plasma formation will be allowed on the cathode at a breakdown field of 2.5×10^7 V/m.

We wish to measure the voltage and magnetic field (current) at the inlet, midpoint, and outlet as a function of time, the radial electric field and axial current density as a function of radius, and the particle trajectories at selected times during the simulation. The primary objective is to observe the following: (1) field emission at the cathode and electron leakage to the anode as the incident wave front propagates down the line, (2) magnetic self-insulation behind the incident wave front, and (3) the effect of the space-charge boundary layer on the impedance of the line.

3.1.2 Suggested Approach.

Resolution of the space-charge barrier in field emission typically requires modification to the spatial grid. In Problem 1.1, it was possible to use a uniform spatial grid in both dimensions. However, the particle simulations of Problems 2.5 and 2.6 show that non-uniform spacing normal to an emitting surface produces more accurate results due to better resolution of gradients. In MAGIC, non-uniform regions can be defined over portions of the grid and matched to other non-uniform regions or to uniform regions. It is important to make sure that when matching regions, the cells bordering an adjacent region should have approximately the same size. Within a region, a 20% cell-to-cell variation is generally acceptable. Also, the cell aspect ratio should not exceed five. In this case, we have used a spacing of 0.002 m at the cathode, increasing linearly to 0.008 m at the anode.

All boundary conditions are the same as in Problem 1.4. However, the implicit (time-biased) field algorithm is recommended to stabilize the representation of field emission. Two-dimensional particle kinematics is sufficient for this simulation (and all others in this set), since the initial distribution is two-dimensional and the TM mode cannot induce a three-dimensional component.

Finally, electron field emission must be specified along the cathode surface. In MAGIC, field emission must be enabled for each intended (conformal) surface and species using the PARTICLES command. Note that field emission can occur (depending on the dynamics) only on surfaces which have been so enabled. Also, each command specifies only one particle species (e.g., electrons). Thus, if emission can occur at one surface for more than one species, each must be enabled separately. (A common example involves electron beam emission and ion field emission from the same surface.) In this case, we also recommend leaving a five

cell zone at the inlet in which no emission occurs to allow the TEM waveform to develop.

This input data for this simulation is shown in Table 3.1.

3.1.3 Analytical Solution.

The space-charge boundary layer can be considered as a region of impedance (Z_2) different from that of the inlet region (Z_1). Then the steady-state relations developed previously in Equation (1.15) for an impedance mismatch are valid. The voltage equation and the measured simulation voltage can then be used to estimate the boundary layer region impedance,

$$Z_2 = Z_1 \frac{\phi}{2\phi^+ - \phi} \quad . \tag{3.3}$$

From the inlet voltage shown in Figure 3.1, we estimate the final voltage to be $\phi \approx 3.25$ MV. Then Equation (3.3) yields

$$Z_2 = 28.5\ \Omega \quad . \tag{3.4}$$

Figures 3.2 and 3.3 illustrate the progression of the pulse down the line.

The same process can be repeated using the current equation. In this case, the magnetic field in the gap (at the anode) should be used to compute the total current, or

$$I_0 = \frac{2\pi r_0}{\mu_0} B_\theta(r_0) \quad . \tag{3.5}$$

If the magnetic field at the cathode is used, then the current contribution due to the boundary layer must be included, yielding

$$I_i = \frac{2\pi r_i}{\mu_0} B_\theta(r_i) + \int_{r_i}^{r_0} dr\, 2\pi r\, J_z(r) \ . \qquad (3.6)$$

In principle, the two currents (I_i and I_0) should be identical, and either can be used in Equation (1.15) to estimate the impedance.

The impedance can also be estimated more crudely by measuring the hub thickness (or effective gap) and using the conventional impedance equations. From the particle trajectory plot shown in Figure 3.4, we estimate the effective cathode radius (near outlet) to be $r \approx 0.15$ m. Then Equation (1.9) yields

$$Z_2 \approx 17.3\ \Omega \ . \qquad (3.7)$$

The problem with this commonly used method is that it ignores the boundary layer dynamics.

Table 3.1. Input data for Problem 3.1.

```
title *problem 3.1* /
comment *base problem: 41.6 ohm coaxial transmission line.* /
system 2 /
x1grid 1 62 2 0.0 60 0.01 0.6 /
x2grid 1 22 2 0.1 20 0.002 0.1 /
fields 1 3 800 6.25e-12 0.5 0.5 0.0
       4 1.0 0.29912 0.15022 0.11111 /
courant 0 0 /
conductor cathode 1 2  2 62  2 /
conductor anode  -1 2 22 62 22 /
particles emission null electrons 0 0 6 1 1 2 1
          1.0e+7 6.25e-5  2.5e7 0.0 0.0 0.0 0.0 1 7 2 62 2 /
kinematics 1 0 0 0 0 /
currents 64 1.0 /
forces 0 0.5 1.0 1.0 /
voltage incident radial 1 twod 0 1.0 1 2 2 2 22 2 /
function incident 0 3 0.0 0.0 1.0e-9 4.0e6 1.0 4.0e6 /
function radial 5  -1 1 /
lookback 1 1 -1 62 2 62 22 /
diagnose spacing 0 1 courant 0 1 /
statistics 200 /
trajectory 200 1 1 0.0 0.6 -0.15 0.45 /
observe 1 1 twod 1 0.0 1.0 0.0 1.0 2  2  2  2 22
            twod 1 0.0 1.0 0.0 1.0 2 32  2 32 22
            twod 1 0.0 1.0 0.0 1.0 2 62  2 62 22
            twod 1 0.0 1.0 0.0 1.0 6  2  2  2  2
            twod 1 0.0 1.0 0.0 1.0 6 32  2 32  2
            twod 1 0.0 1.0 0.0 1.0 6 61  2 61  2
            twod 1 0.0 1.0 0.0 1.0 6  2 21  2 21
            twod 1 0.0 1.0 0.0 1.0 6 32 21 32 21
            twod 1 0.0 1.0 0.0 1.0 6 61 21 61 21 /
range 200 1 2  2 2  2 22 1
          1 2 32 2 32 22 1
          1 2 62 2 62 22 1
          1 6  2 2  2 22 1
          1 6 32 2 32 22 1
          1 6 61 2 61 22 1 /
display 0 0.0 0.6 -0.15 0.45 /
output 0 /
timeout 60 1 /
start /
stop /
```

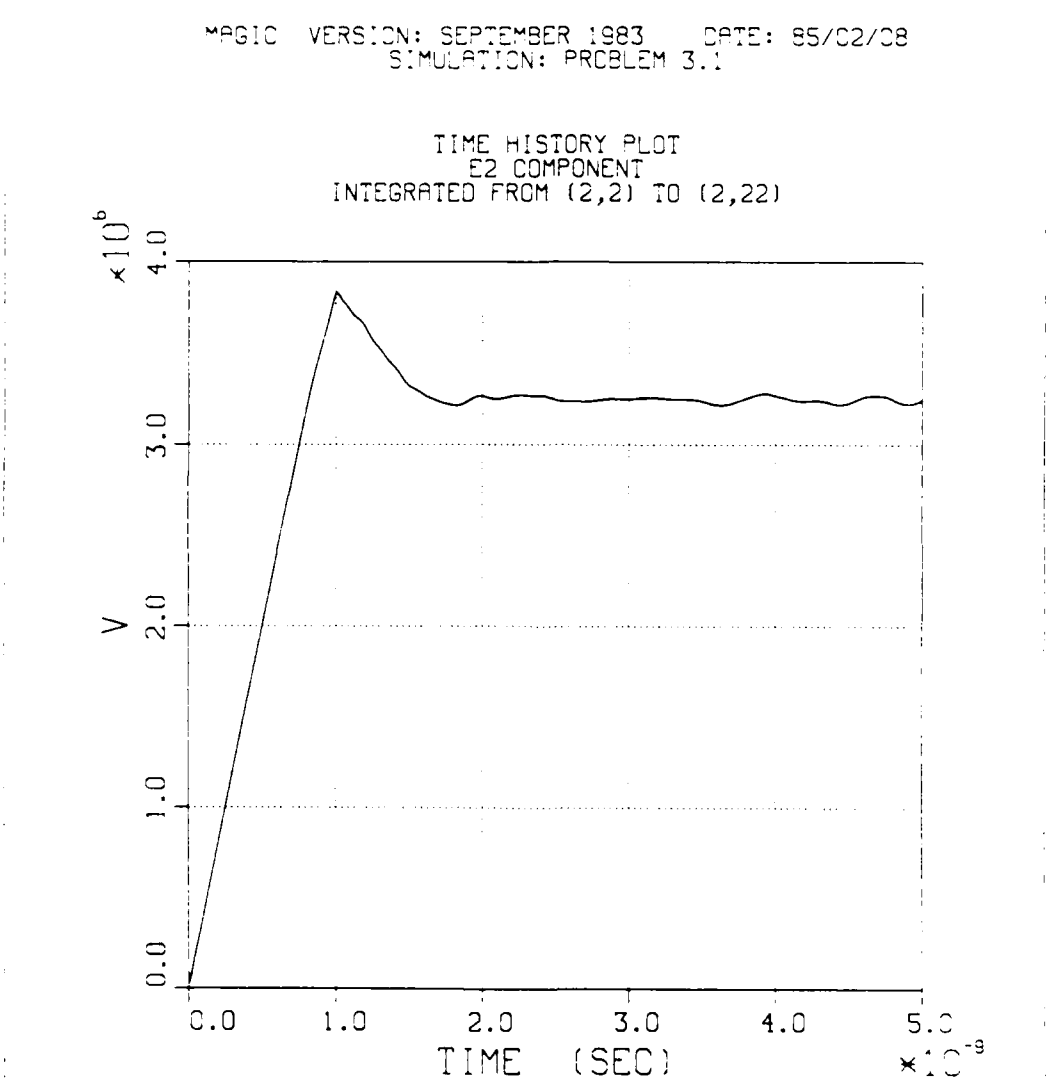

Figure 3.1. Inlet voltage vs. time, Problem 3.1.

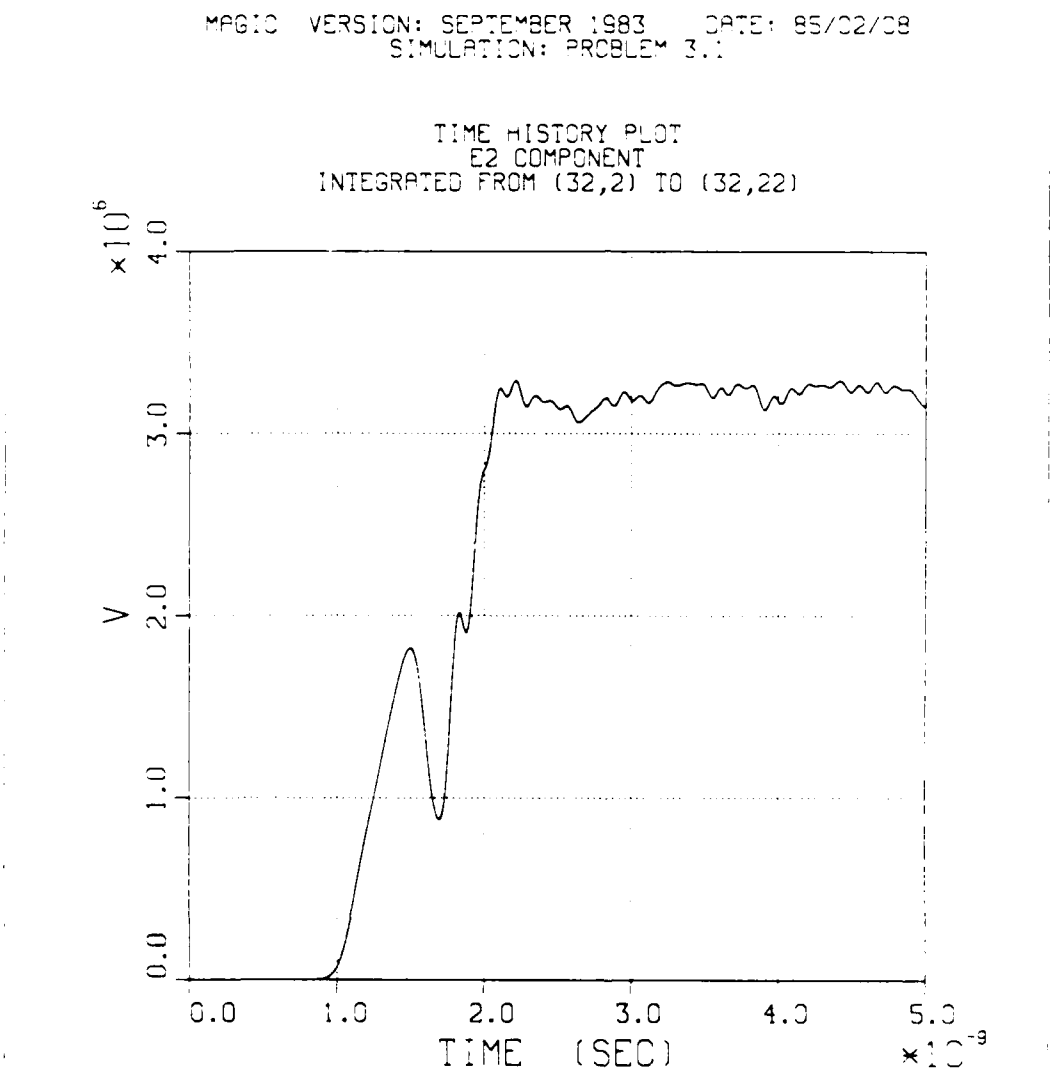

Figure 3.2. Midpoint voltage vs. time, Problem 3.1.

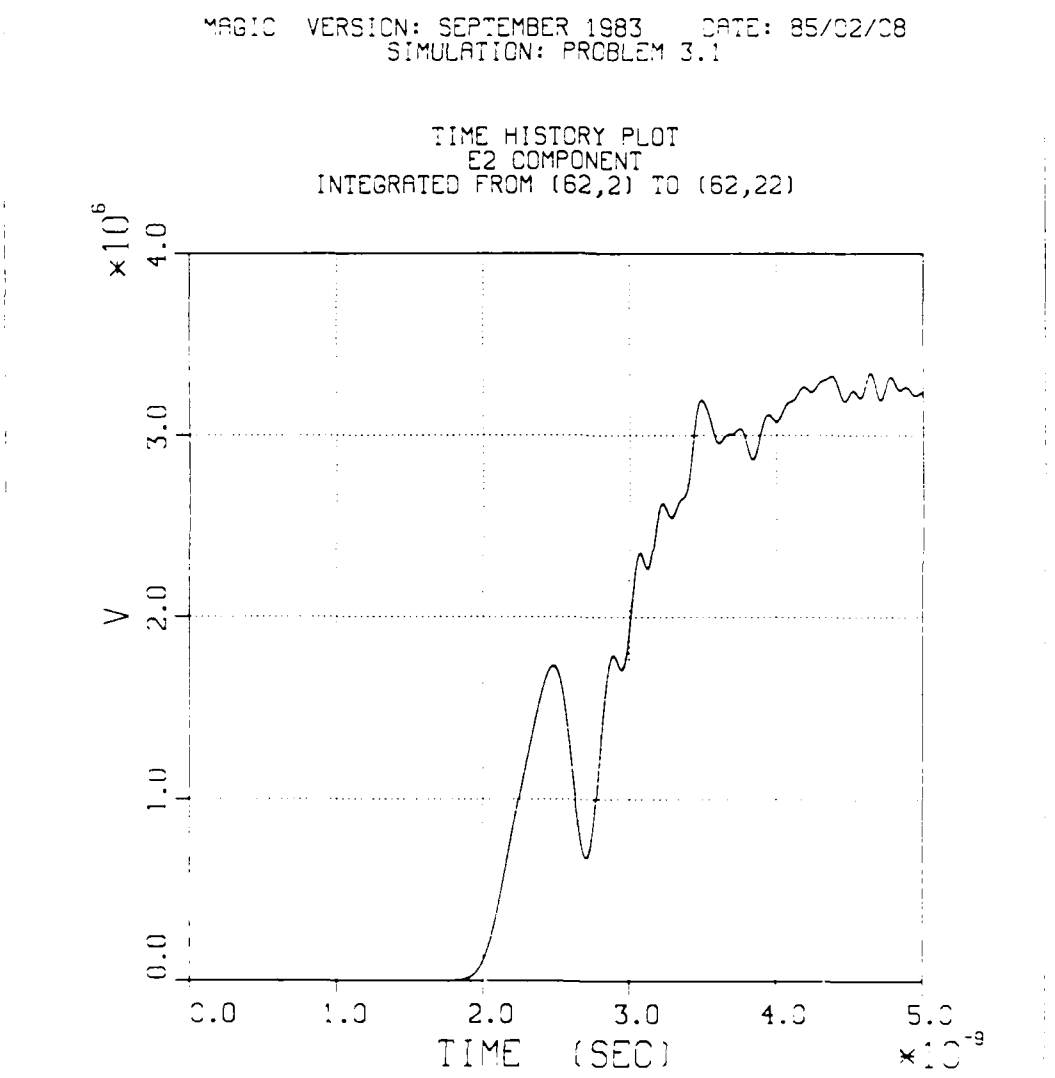

Figure 3.3. Outlet voltage vs. time, Problem 3.1.

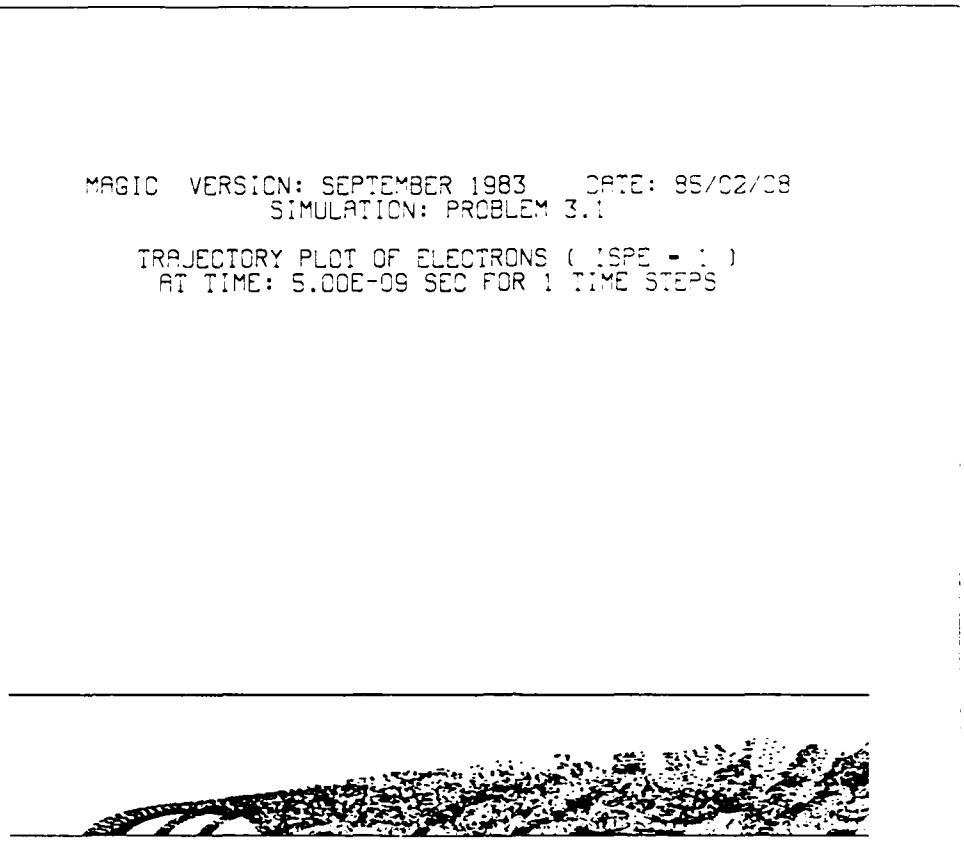

Figure 3.4. Trajectory plot, Problem 3.1.

3.2 COAXIAL LINE WITH SHORT.

3.2.1 Problem Description.

Problem 3.2 uses the coaxial transmission line of Problem 3.1, but with a short across the outlet. Repeat the measurements defined above.

3.2.2 Suggested Approach.

Replace the LOOKBACK command at the outlet with a CONDUCTOR command, which will short the cathode and anode. Input data for this simulation is shown in Table 3.2.

3.2.3 Analytical Solution.

Problem 3.2 is similar to the classical three-region impedance problem, illustrated in Figure 3.5. In this case, Z_1 represents the inlet (plasma-free) region, Z_2 represents the boundary layer (plasma) region, and $Z_3(=0)$ represents the short. The present analysis is complicated by the fact that the boundary layer effect is transient; that is, the value of Z_2 changes during the period in which it has an effect. This is in contrast with Problem 3.1, in which the boundary layer achieves a non-trivial ($Z_2 \neq Z_1$) steady state. The following derivation assumes a constant value of Z_2 as well as a steady-state pulse.

From our previous derivation for a single mismatch, we obtained the scattered wave solution (ϕ^-) for an incident wave (ϕ^+) from the left-hand side, or

$$\phi^- = a\phi^+ \quad , \tag{3.8}$$

where the scattering coefficient is

$$a = \frac{Z_2 - Z_1}{Z_1 + Z_2} \quad . \tag{3.9}$$

If the wave is incident from the right-hand side, then the solution is

$$\phi^- = -a\phi^+ \quad . \tag{3.10}$$

Figure 3.5 exhibits two mismatches (Z_1,Z_2 and Z_2,Z_3), with scattering coefficients labeled a and b, respectively. Thus, multiple scatterings occur, as waves are trapped in region 2 between the mismatches. The solution is given by the infinite series,

$$\begin{aligned} \phi/\phi^+ = {} & (1 + a) + (1 + a)b(1 - a) \\ & + (1 + a)b(1 - a)(-ab) + \ldots \quad , \end{aligned} \tag{3.11}$$

where the terms represent contributions at increasing times, $n\delta t$, where δt is the transit time in region 2 (between a and b). The series may be summed to yield

$$\phi = \phi^+ \frac{2Z_3}{Z_1 + Z_3} \quad , \quad t \to \infty \quad , \tag{3.12}$$

which result should be compared with Equation (1.15). In other words, the steady-state response is independent of the value of Z_2. In some cases, the transient response may be highly dependent upon Z_2, since the terms in Equation (3.11) add sequentially during the transient.

For this simulation, the transient response is illustrated in the voltage plots of Figures 3.6 and 3.7. The inlet voltage in Figure 3.6 closely resembles the previous result in Figure 3.1. (The scattered wave from the short is just beginning to reach the inlet.) The effect of the short is clear in Figure 3.7, which shows the voltage at midpoint. (This result should be compared with that of Figure 3.2.)

One important point is that impedance effects due to plasma can be strongly influenced by effects in other regions. This is illustrated in the electron trajectory plots in Figures 3.8, 3.9, and 3.10, which represent different points of time (2.50, 3.75, and 5.00 nsec) in the simulation. During the transient, the impedance in this region (Z_2) will change from 41.6 ohms to a very low value at the leading edge and then from approximately 28.5 ohms to a final value of 41.6 ohms.

It is also useful to compare the responses of Problems 3.2 and 1.3 (from the earlier set). This illustrates the effect of the plasma upon propagation velocity.

Table 3.2. Input data for Problem 3.2.

```
title *problem 3.2* /
comment *problem3.2 duplicates 3.1,
    but with a short at the outlet.* /
system 2 /
x1grid 1 62 2 0.0 60 0.01 0.6 /
x2grid 1 22 2 0.1 20 0.002 0.1 /
fields 1 3 800 6.25e-12 0.5 0.5 0.0
       4 1.0 0.29912 0.15022 0.11111 /
courant 0 0 /
conductor cathode 1 2  2 62  2 /
conductor anode  -1 2 22 62 22 /
conductor short  -1 62 2 62 22 /
particles emission null electrons 0 0 6 1 1 2 1
          1.0e+7 6.25e-5 2.5e7 0.0 0.0 0.0 0.0 1 7 2 62 2 /
kinematics 1 0 0 0 0 /
currents 64 1.0 /
forces 0 0.5 1.0 1.0 /
voltage incident radial 1 twod 0 1.0 1 2 2 2 22 2 /
function incident 0 3 0.0 0.0 1.0e-9 4.0e6 1.0 4.0e6 /
function radial 5  -1 1 /
z lookback 1 1 -1 62 2 62 22 /
diagnose spacing 0 1 courant 0 1 /
statistics 200 /
trajectory 200 1 1 0.0 0.6 -0.15 0.45 /
observe 1 1 twod 1 0.0 1.0 0.0 1.0 2  2  2  2 22
            twod 1 0.0 1.0 0.0 1.0 2 32  2 32 22
            twod 1 0.0 1.0 0.0 1.0 2 62  2 62 22
            twod 1 0.0 1.0 0.0 1.0 6  2  2  2  2
            twod 1 0.0 1.0 0.0 1.0 6 32  2 32  2
            twod 1 0.0 1.0 0.0 1.0 6 61  2 61  2
            twod 1 0.0 1.0 0.0 1.0 6  2 21  2 21
            twod 1 0.0 1.0 0.0 1.0 6 32 21 32 21
            twod 1 0.0 1.0 0.0 1.0 6 61 21 61 21 /
range 200 1 2  2 2  2 22 1
          1 2 32 2 32 22 1
          1 2 62 2 62 22 1
          1 6  2 2  2 22 1
          1 6 32 2 32 22 1
          1 6 61 2 61 22 1 /
display 0 0.0 0.6 -0.15 0.45 /
output 0 /
timeout 60 1 /
start /
stop /
```

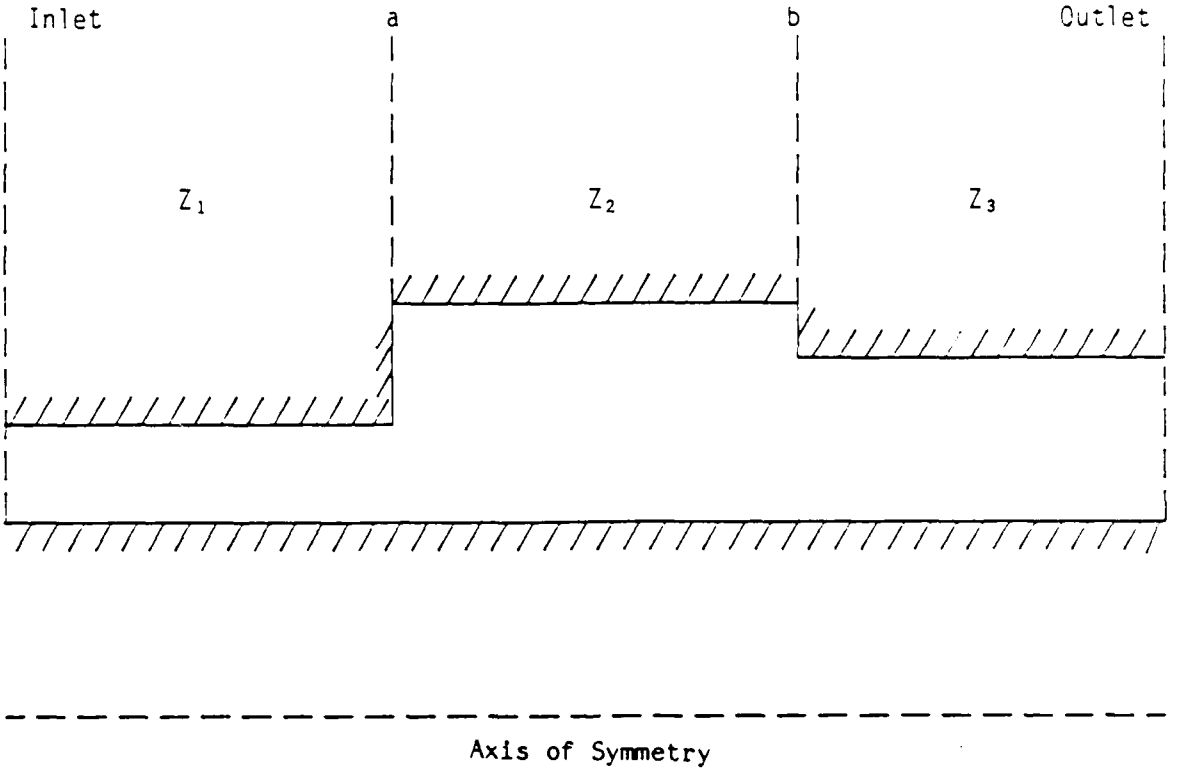

Figure 3.5. Three-region impedance geometry.

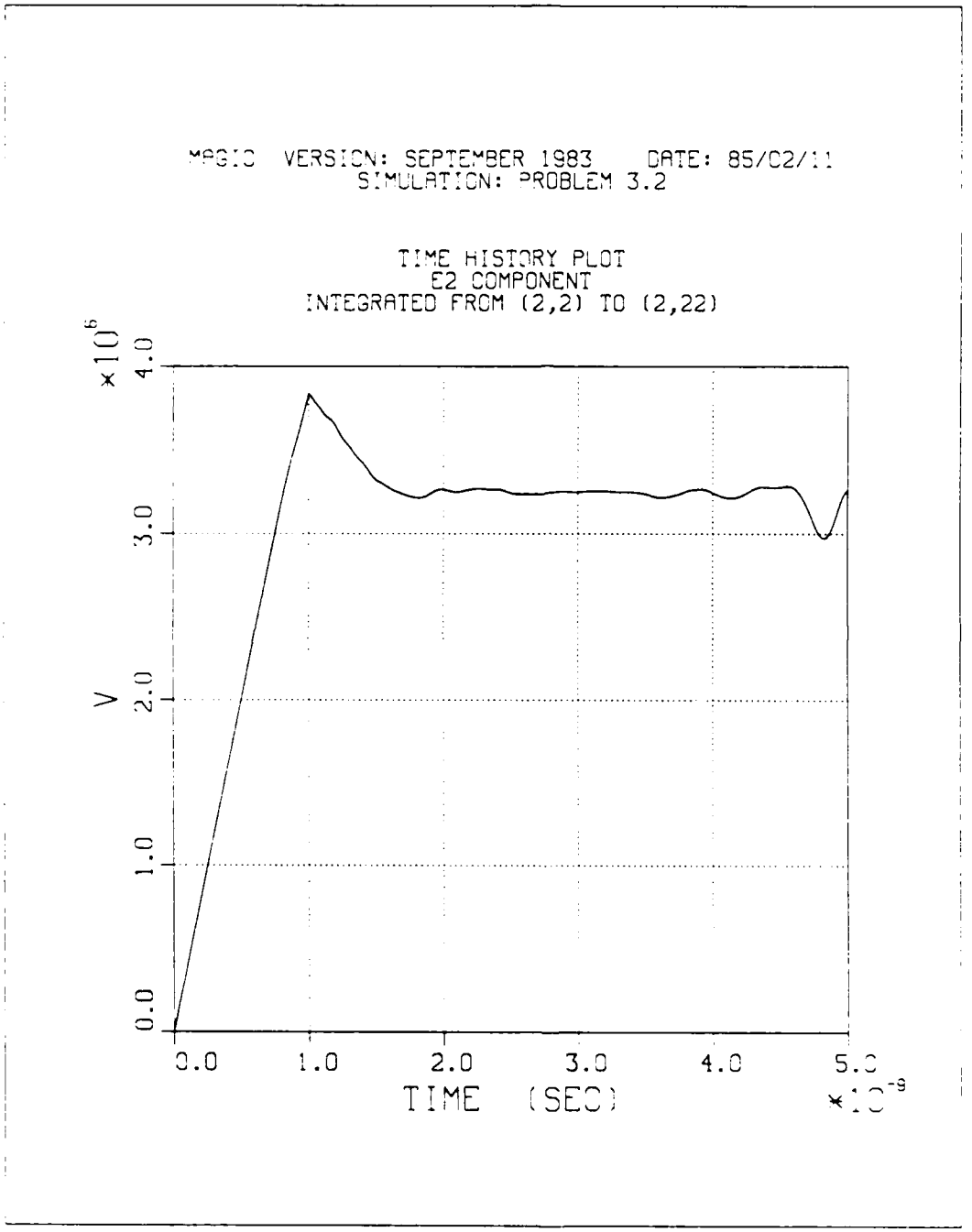

Figure 3.6. Inlet voltage vs. time, Problem 3.2.

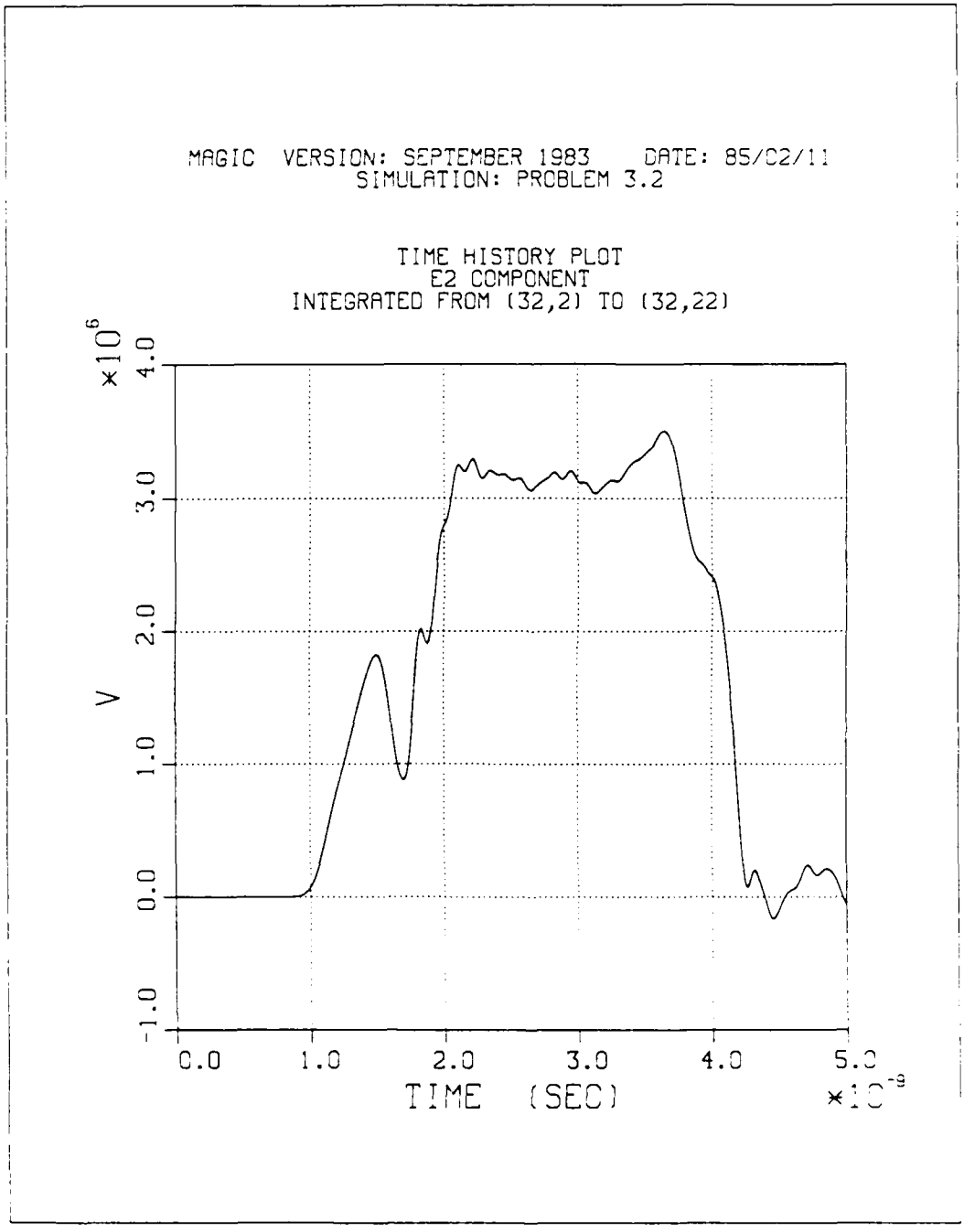

Figure 3.7. Midpoint voltage vs. time, Problem 3.2.

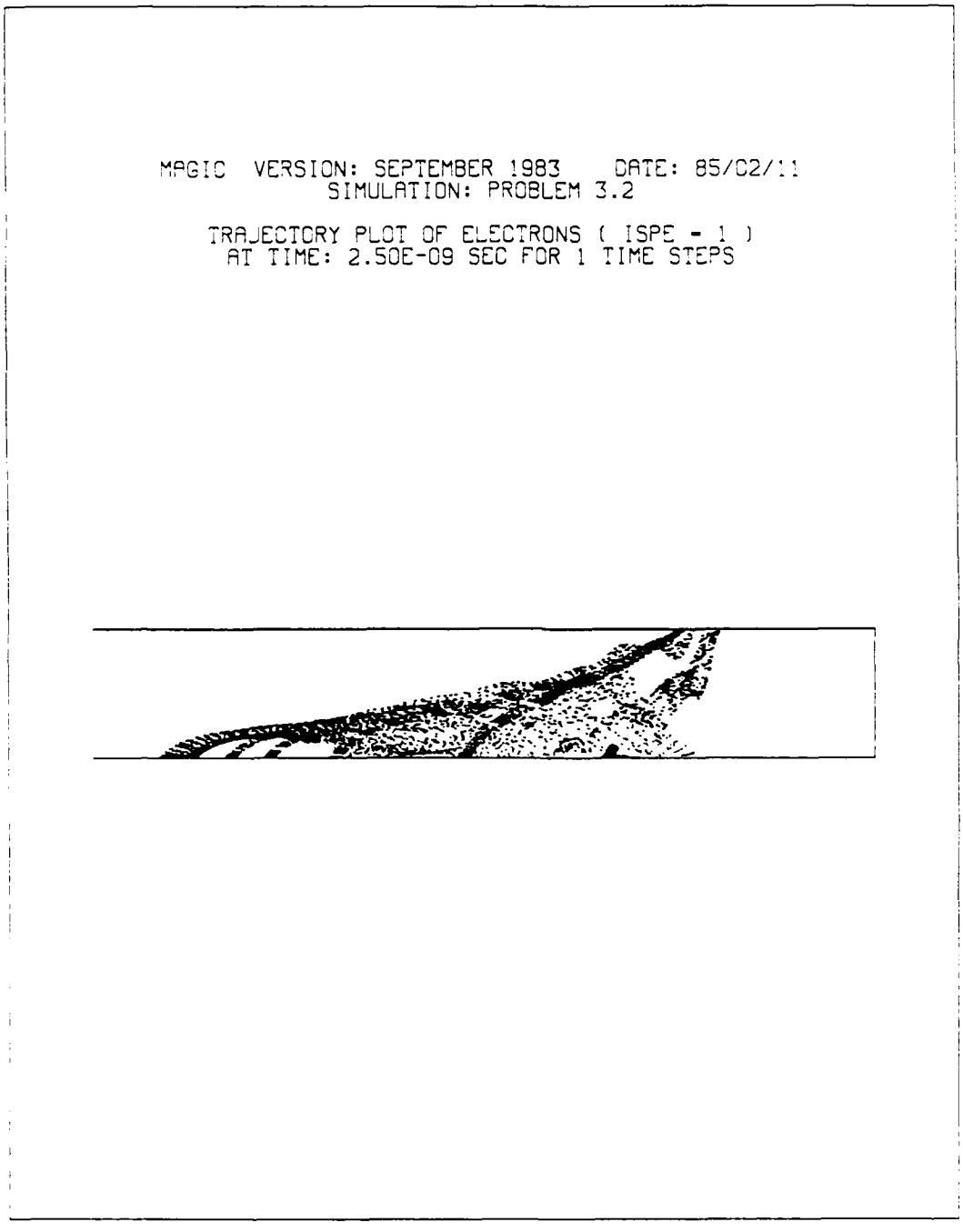

Figure 3.8. Trajectory plot at 2.5 nsec, Problem 3.2.

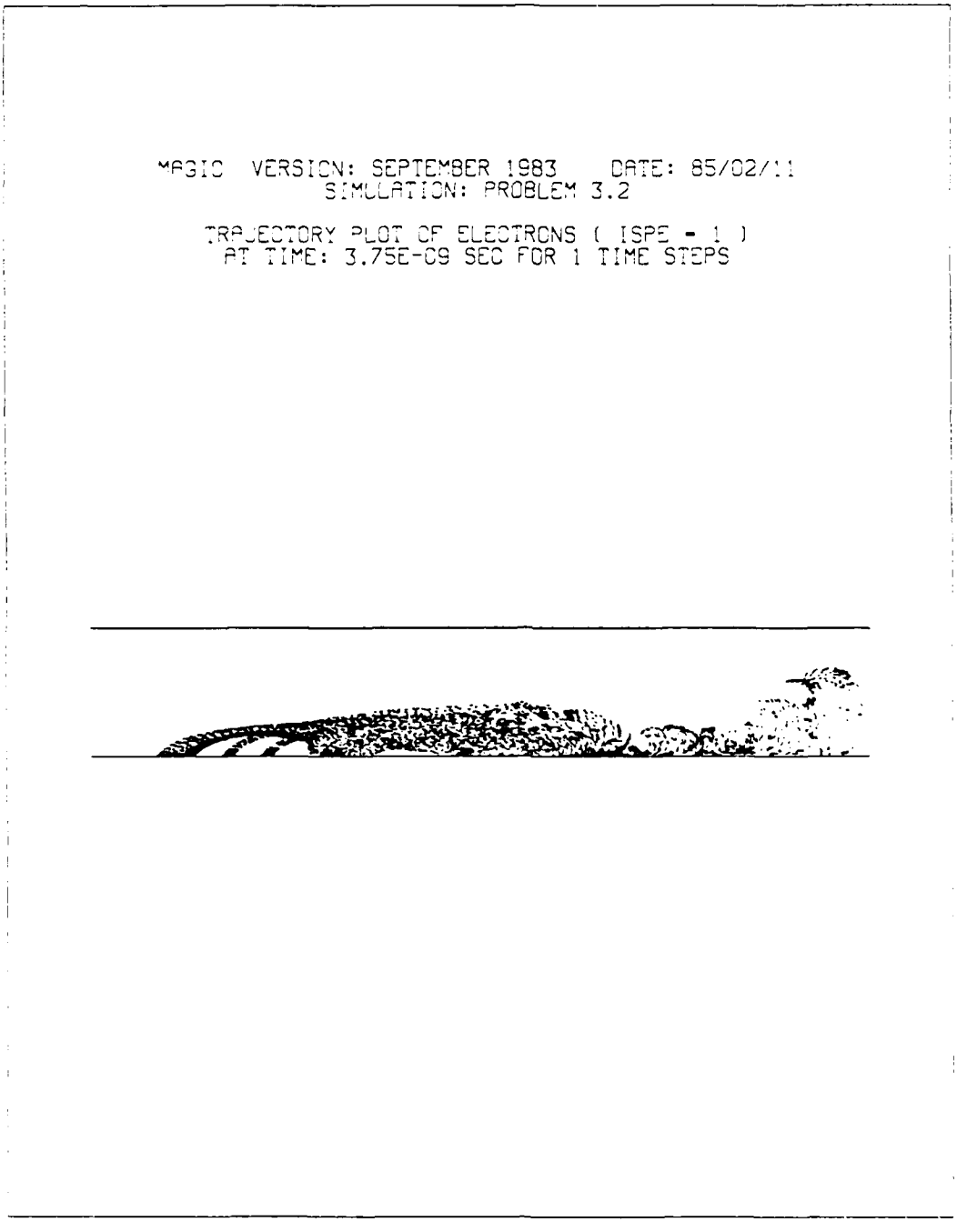

Figure 3.9. Trajectory plot at 3.75 nsec, Problem 3.2.

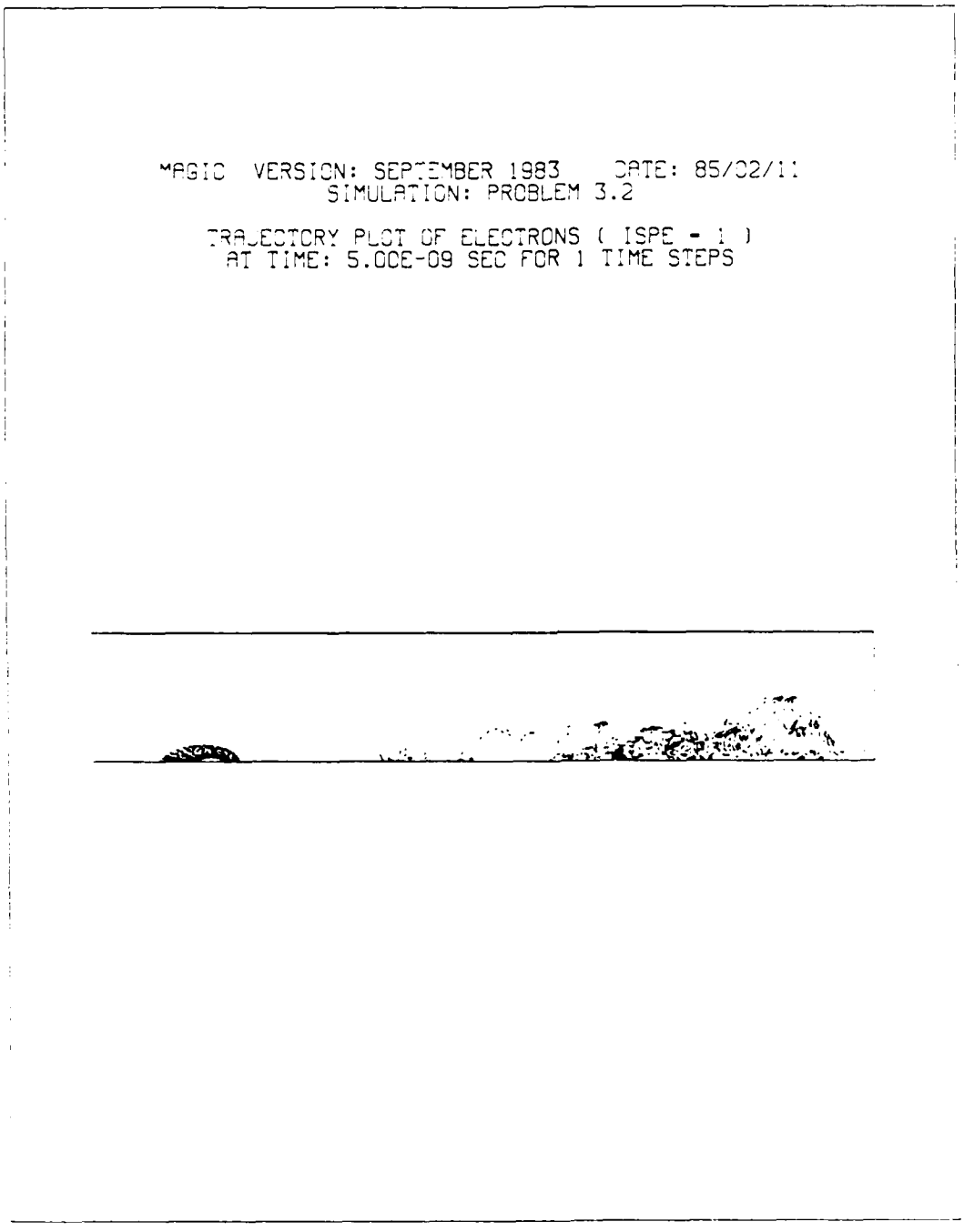

Figure 3.10. Trajectory plot at 5.0 nsec, Problem 3.2.

3.3 COAXIAL LINE WITH GEOMETRIC MISMATCH.

3.3.1 Problem Description.

The previous problem illustrated the effect of a short ($Z = 0$) on the boundary layer dynamics. Here, we consider a geometric modification of Problem 3.1 in which the cathode radius (r_i) is reduced to 0.05 m at a distance 0.2 m from the outlet. In effect, this doubles the (cold-test) impedance of the outlet region.

3.3.2 Suggested Approach.

Non-uniform spacing is now suggested for the axial grid as well as the radial. If the spacing is made symmetric about the mismatch, then a cell aspect of unity is attained at the corner of the shoulder. We suggest limiting the field emission to the low impedance surface (inlet region) of the line. This input data for this simulation is shown in Table 3.3.

3.3.3 Analytical Solution.

Results developed for Problem 3.2 are applicable. The inlet voltage is shown in Figure 3.11. From our measurement of the voltage (ϕ = 3.25 MV) and Equation (3.12), we estimate the outlet impedance to be

$$Z_3 = 28.4\ \Omega\ , \tag{3.13}$$

almost the same as that for Z_2 in Problem 3.1. In other words, the outlet region impedance is dominated by field emission from the inlet region.

Figure 3.12 presents an electron trajectory plot at the end of the simulation.

Table 3.3. Input data for Problem 3.3

```
title *problem 3.3* /
comment *in problem 3.3 an impedance mismatch is introduced
         20 cells from the outlet.* /
system 2 /
x1grid 1 62 2 0.0 60 0.01 0.6 /
x2grid 1 32 2 0.05 10 0.008 0.05 20 0.002 0.1 /
fields 1 3 800 6.25e-12 0.5 0.5 0.0
       4 1.0 0.29912 0.15022 0.11111 /
courant 0 0 /
conductor cathode 1 2 12 42 12 42  2 62  2 /
conductor anode  -1 2 32 62 32 /
particles emission null electrons 0 0 6 1 1 2 1
          1.0e+7 6.25e-5 2.5e7 0.0 0.0 0.0 0.0 1 7 12 42 12 /
kinematics 1 0 0 0 0 /
currents 64 1.0 /
forces 0 0.5 1.0 1.0 /
voltage incident radial 1 twod 0 1.0 1 2 12 2 32 2 /
function incident 0 3 0.0 0.0 1.0e-9 4.0e6 1.0 4.0e6 /
function radial 5  -1 1 /
lookback 1 1 -1 62 2 62 32 /
diagnose spacing 0 1 courant 0 1 /
statistics 200 /
trajectory 200 1 1 0.0 0.6 -0.15 0.45 /
observe 1 1 twod 1 0.0 1.0 0.0 1.0 2  2 12  2 32
            twod 1 0.0 1.0 0.0 1.0 2 32 12 32 32
            twod 1 0.0 1.0 0.0 1.0 2 42 12 42 32
            twod 1 0.0 1.0 0.0 1.0 2 62  2 62 32
            twod 1 0.0 1.0 0.0 1.0 6  2 12  2 12
            twod 1 0.0 1.0 0.0 1.0 6 32 12 32 12
            twod 1 0.0 1.0 0.0 1.0 6 42 12 42 12
            twod 1 0.0 1.0 0.0 1.0 6 61  2 61  2
            twod 1 0.0 1.0 0.0 1.0 6  2 31  2 31
            twod 1 0.0 1.0 0.0 1.0 6 32 31 32 31
            twod 1 0.0 1.0 0.0 1.0 6 42 31 42 31
            twod 1 0.0 1.0 0.0 1.0 6 61 31 61 31 /
range 200 1 2  2 12  2 32 1
          1 2 32 12 32 32 1
          1 2 42 12 42 32 1
          1 2 62  2 62 32 1
          1 6  2 12  2 32 1
```

Table 3.3. Input data for Problem 3.3 (continued).

```
          1 6 32 12 32 32 1
          1 6 42 12 42 32 1
          1 6 61  2 61 32 1 /
display 0 0.0 0.6 -0.15 0.45 /
output 0 /
timeout 60 1 /
start /
stop /
```

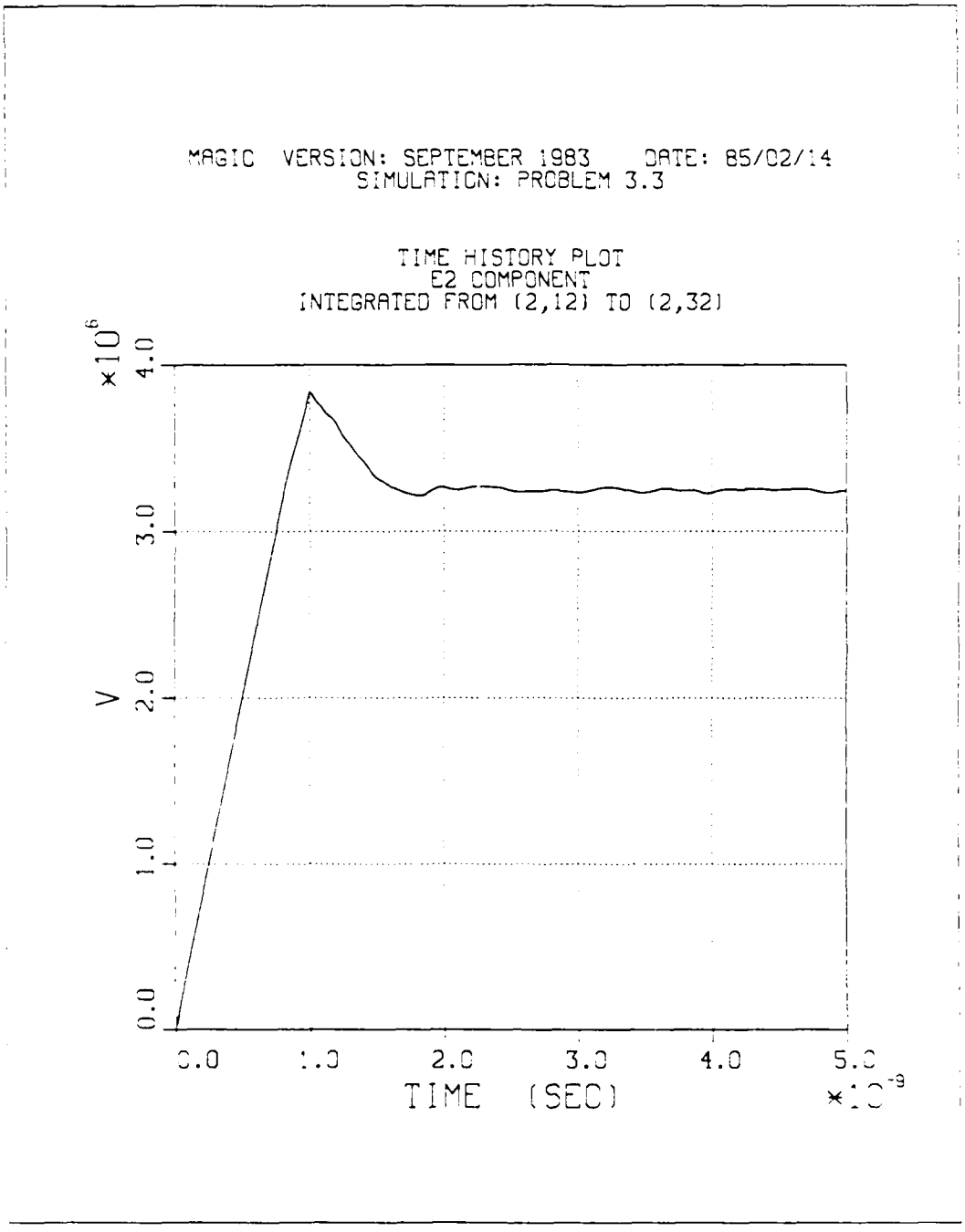

Figure 3.11. Inlet voltage vs. time, Problem 3.3.

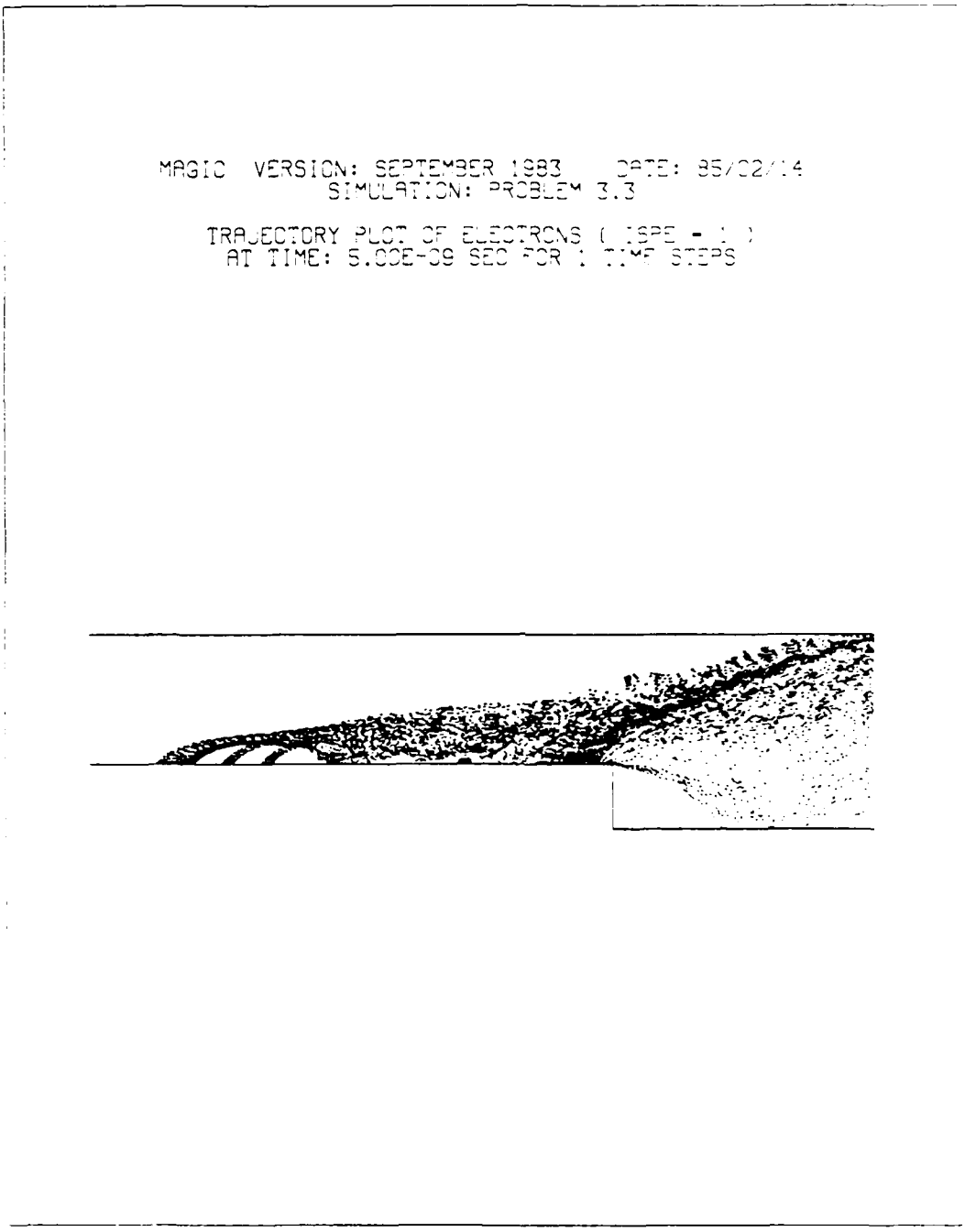

Figure 3.12. Trajectory plot, Problem 3.3.

3.4 COLD-TEST OF DIODE.

3.4.1 Problem Description.

Based on the coaxial line dimensions in Problem 3.3, we have created a diode by reducing both anode and cathode radii in the outlet region until they extend to the axis. The geometry and dimensions are shown in Figure 3.13. No emission surfaces are specified in this problem, so cold-test results are expected.

3.4.2 Suggested Approach.

The spatial grid can be decreased by 0.2 m in the axial coordinate, but it needs to be increased by 0.1 m in the radial coordinate. Because the problem involves cold-test (no particles), a relatively coarse spacing could be used. However, three subsequent simulations (Problems 3.5, 3.6, and 3.8) will require particles for the same geometry. Therefore, non-uniform spacing similar to that used in Problem 3.3 is recommended so that the electromagnetic model will be identical for all diode simulations.

Since this simulation extends down to zero radius, it will be necessary to use the SYMMETRY command to specify an axial symmetry boundary condition. (All symmetry boundary conditions in MAGIC (axial, mirror, and periodic) must be specified explicitly by the user. They are not supplied automatically by the code.) Note that the boundary need not extend as far as is shown in Figure 3.13, but it must cover the non-conducting section on axis. Time histories and range plots should be placed at the inlet, the first impedance mismatch, and the axis of symmetry.

Input data for this simulation is shown in Table 3.4.

3.4.3 Analytical Solution.

The analytical value for the impedance in the cylindrical region between cathode and anode is

$$Z = \frac{1}{2\pi} \left(\frac{\mu_0}{\varepsilon_0} \right)^{1/2} \frac{d}{r} \quad , \tag{3.14}$$

where d represents the gap between conductors and r is the radius. Once again, the analytical solution discussed in Problem 3.2 is applicable. In this case, the impedance Z_2 is variable according to Equation (3.14), and we can envision a third region of infinite impedance ($Z_3 = \infty$) at the axis. Thus, the series solution developed in Problem 3.2 is applicable for the transient response. This will be most apparent in the measurement of inlet voltage versus time shown in Figure 3.14, where several of the multiple scatterings described in Equation (3.11) can be observed. Finally, according to Equation (3.12), the final steady-state voltage should be exactly twice the incident voltage, as confirmed in Figures 3.15 and 3.16.

Table 3.4. Input data for Problem 3.4.

```
title *problem 3.4* /
comment *problem 3.4 is a cold test of a diode.* /
system 2 /
x1grid 1 67 2 0.0 25 0.008 0.2 20 0.008 0.1
                                20 0.002 0.1  /
x2grid 1 42 2 0.0 20 0.008 0.1 20 0.002 0.1 /
fields 1 3 800 6.25e-12 0.5 0.5 0.0
       4 1.0 0.29912 0.15022 0.11111 /
courant 0 0 /
conductor cathode 1 2 22 47 22 47  2 /
conductor anode  -1 2 42 67 42 67  2/
symmetry axial 1 2  2 67  2 /
z particles emission null electrons 0 0 6 1 1 2 1
            1.0e+7 6.25e-5 2.5e7 0.0 0.0 0.0 0.0 1 7 22 47 22 /
kinematics 1 0 0 0 0 /
currents 64 1.0 /
forces 0 0.5 1.0 1.0 /
voltage incident radial 1 twod 0 1.0 1 2 22 2 42 2 /
function incident 0 3 0.0 0.0 1.0e-9 4.0e6 1.0 4.0e6 /
function radial 5  -1 1 /
diagnose spacing 0 1 courant 0 1 /
statistics 200 /
trajectory 200 1 1 0.0 0.6 -0.15 0.45 /
observe 1 1 twod 1 0.0 1.0 0.0 1.0 2  2 22  2 42
            twod 1 0.0 1.0 0.0 1.0 2 47 22 47 42
            twod 1 0.0 1.0 0.0 1.0 1 47  2 67  2 /
range 200 1 2  2 22  2 42 1
          1 2 47 22 47 42 1
          1 1 47  2 67  2 1 /
display 0 0.0 0.6 -0.15 0.45 /
output 0 /
timeout 60 1 /
start /
stop /
```

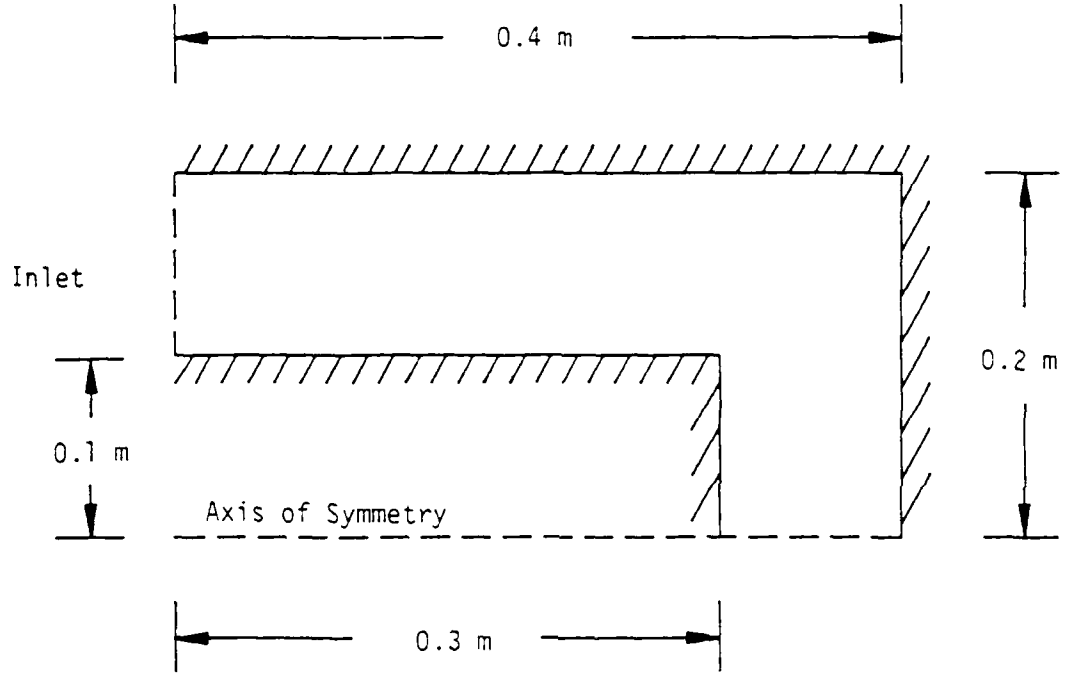

Figure 3.13. Diode geometry.

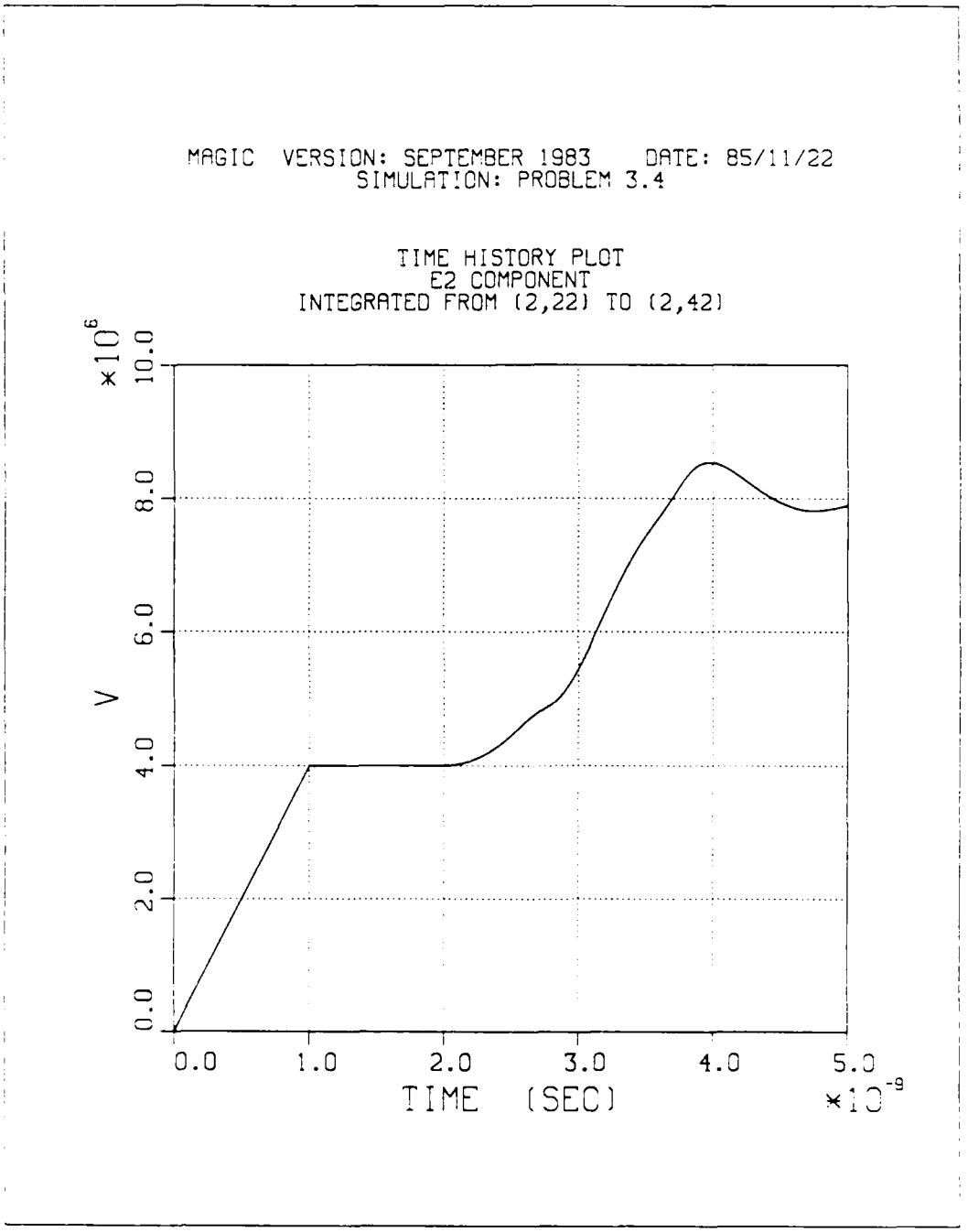

Figure 3.14. Inlet voltage vs. time, Problem 3.4.

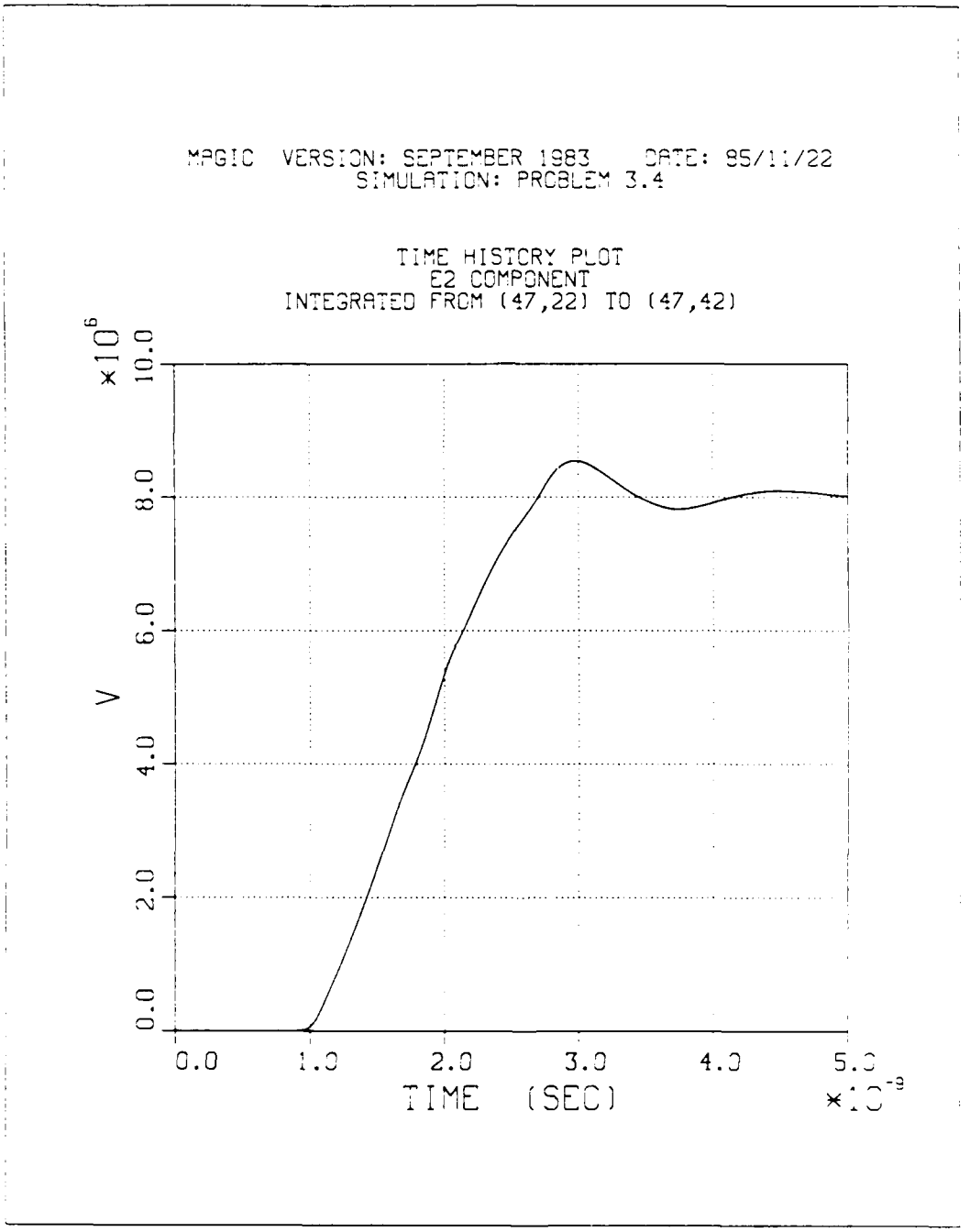

Figure 3.15. Midpoint voltage vs. time, Problem 3.4.

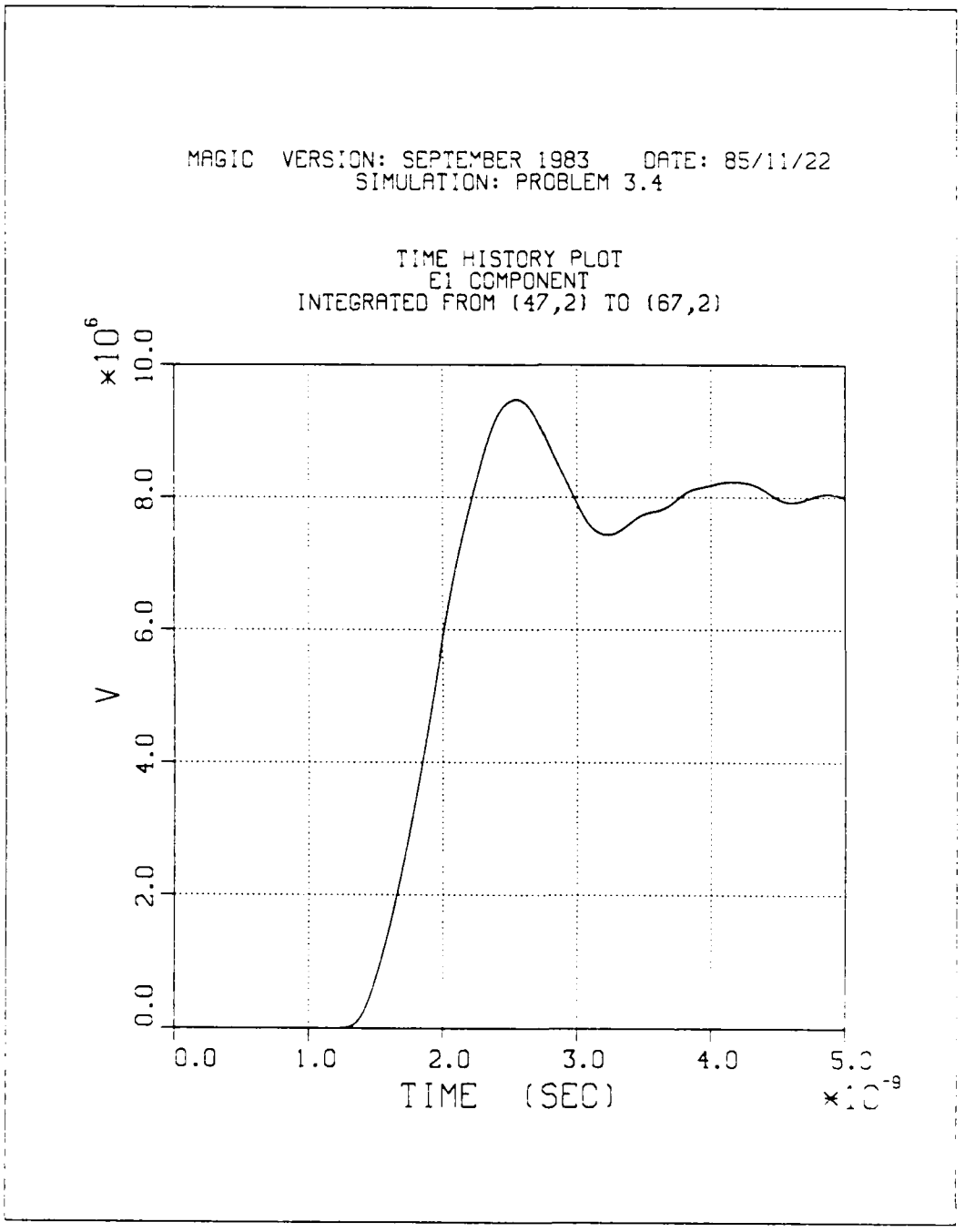

Figure 3.16. Axis voltage vs. time, Problem 3.4.

3.5 DIODE WITH CATHODE FIELD EMISSION.

3.5.1 Problem Description.

Problem 3.5 is the same as Problem 3.4, except that electron field emission is enabled everywhere on the cathode (two separate, conformal surfaces). The field emission and incident pulse parameters are the same as those specified in Problem 3.1.

3.5.2 Suggested Approach.

The electromagnetic model can be taken over directly from Problem 3.4, assuming that a sufficiently fine spatial grid has been used. The emitting surfaces should run from near the inlet (five cells from the inlet boundary) to the corner of the cathode, and from there to the axis. The input data for this simulation is shown in Table 3.5.

3.5.3 Analytical Solution.

At early time, the transient response will be dominated by plasma effects in the coaxial section. These results must agree with those from Problem 3.1; i.e., the voltage is initially reduced from the incident wave value. This effect is illustrated in the inlet voltage shown in Figure 3.17.

In cold-test (Problem 3.4), the diode presented an infinite impedance. In the present case, the electrons will continue to flow across the diode, since the magnetic field on axis must vanish (by symmetry) and self-insulation cannot occur. Thus, the diode impedance will be reduced. An estimate of the impedance can be obtained by assuming Child-Langmuir physics to be applicable. We let the effective emission area be

$$A = \pi R^2 \quad , \tag{3.15}$$

where

$$R = 1/2(r_i + r_o) \quad .$$

Then, from Equation (2.47), the total current is given by

$$I = \pi R^2 \frac{4}{9} \varepsilon_0 \left(\frac{2e}{m} \right)^{1/2} \frac{V^{3/2}}{d^2} \quad . \tag{3.16}$$

Therefore, the effective impedance must be approximately given by

$$Z = \frac{(d/R)^2}{\pi \frac{4}{9} \varepsilon_0 \left(\frac{2e}{m} \right)^{1/2} (\phi^+)^{1/2}} \quad , \tag{3.17}$$

where we have used $V \approx \phi^+$. Using this method, we estimate the impedance Z to be 30 Ω. This estimate can be compared with the value of 28 Ω obtained from the simulation using the expression,

$$Z_3 = Z_1 \frac{\phi}{2\phi^+ - \phi} \quad , \tag{3.18}$$

where ϕ = 3.2 MV is estimated from the simulation. This is good agreement; however, there is strong sensitivity to the choice of radius, R.

Electron trajectory plots at two times during the simulation (2.5 and 5.0 nsec) are shown in Figures 3.18 and 3.19.

Table 3.5. Input data for Problem 3.5.

```
title *problem 3.5* /
comment *problem 3.5 is the same diode as problem 3.4,
         but with particles.* /
system 2 /
x1grid 1 67 2 0.0 25 0.008 0.2 20 0.008 0.1
                                20 0.002 0.1  /
x2grid 1 42 2 0.0 20 0.008 0.1 20 0.002 0.1 /
fields 1 3 800 6.25e-12 0.5 0.5 0.0
       4 1.0 0.29912 0.15022 0.11111 /
courant 0 0 /
conductor cathode 1 2 22 47 22 47  2 /
conductor anode  -1 2 42 67 42 67  2/
symmetry axial 1 2  2 67  2 /
particles emission null electrons 0 0 6 1 1 2 1
          1.0e+7 6.25e-5 2.5e7 0.0 0.0 0.0 0.0 1  7 22 47 22 /
particles emission null electrons 0 0 6 1 1 2 1
          1.0e+7 6.25e-5 2.5e7 0.0 0.0 0.0 0.0 1 47 22 47  2 /
kinematics 1 0 0 0 0 /
currents 64 1.0 /
forces 0 0.5 1.0 1.0 /
voltage incident radial 1 twod 0 1.0 1 2 22 2 42 2 /
function incident 0 3 0.0 0.0 1.0e-9 4.0e6 1.0 4.0e6 /
function radial 5  -1 1 /
diagnose spacing 0 1 courant 0 1 /
statistics 200 /
trajectory 200 1 1 0.0 0.6 -0.15 0.45 /
observe 1 1 twod 1 0.0 1.0 0.0 1.0 2  2 22  2 42
            twod 1 0.0 1.0 0.0 1.0 2 47 22 47 42
            twod 1 0.0 1.0 0.0 1.0 1 47  2 67  2 /
range 200 1 2  2 22  2 42 1
          1 2 47 22 47 42 1
          1 1 47  2 67  2 1 /
display 0 0.0 0.6 -0.15 0.45 /
output 0 /
timeout 60 1 /
start /
stop /
```

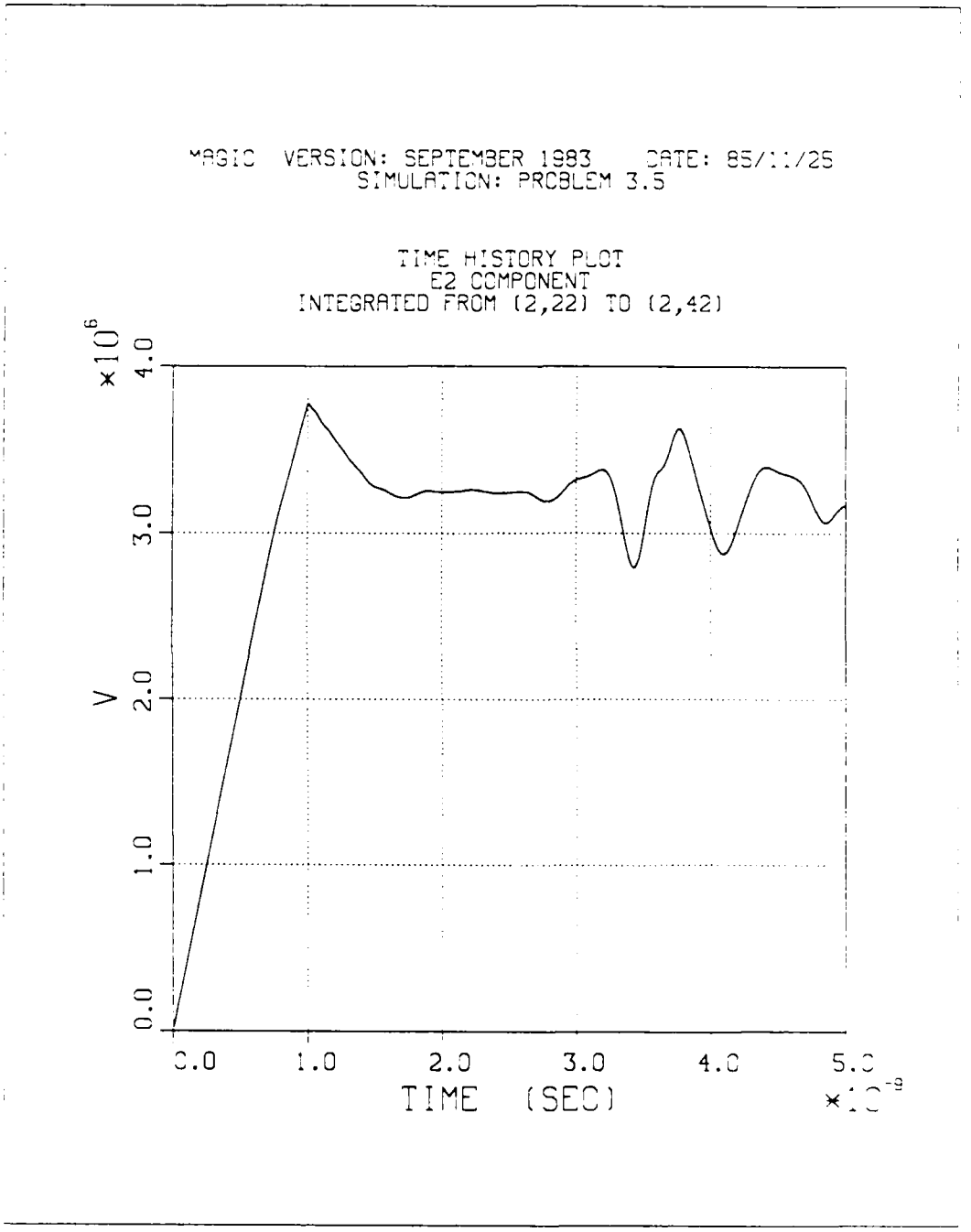

Figure 3.17. Inlet voltage vs. time, Problem 3.5.

MAGIC VERSION: SEPTEMBER 1983 DATE: 85/11/25
SIMULATION: PROBLEM 3.5

TRAJECTORY PLOT OF ELECTRONS (ISPE = 1)
AT TIME: 2.50E-09 SEC FOR 1 TIME STEPS

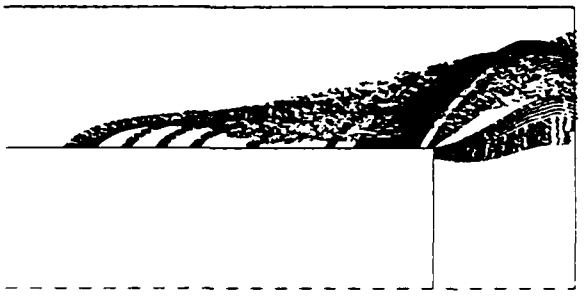

Figure 3.18. Trajectory plot at 2.5 nsec, Problem 3.5.

MAGIC VERSION: SEPTEMBER 1983 DATE: 85/11/25
SIMULATION: PROBLEM 3.5

TRAJECTORY PLOT OF ELECTRONS (ISPE = 1)
AT TIME: 5.00E-09 SEC FOR 1 TIME STEPS

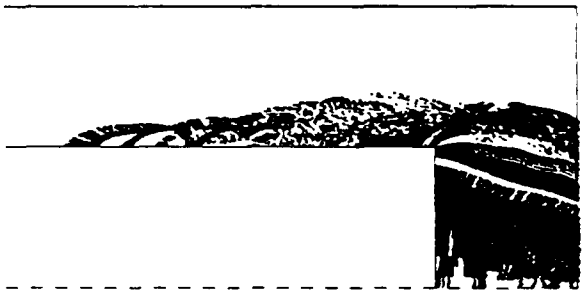

Figure 3.19. Trajectory plot at 5.0 nsec, Problem 3.5.

3.6 DIODE WITH ANODE FIELD EMISSION.

3.6.1 Problem Description.

Problem 3.6 is a duplication of Problem 3.5, with the addition of ion field emission from the radial portion of the anode. The same measurements used in the preceding simulations should be made, in addition to trajectory plots of both species (electrons and ions).

3.6.2 Suggested Approach.

Including ions in a diode simulation can cause problems due to their relative duration. Since the relative velocities go approximately as the square root of the mass ratio, ion particles can remain in a simulation much longer than electron particles. Thus, if ions and electrons are treated equivalently, the resulting large number of ion particles can render a simulation prohibitively expensive. This problem has four common remedies:

(1) use ions only when they impact physics,
(2) increase the charge-to-mass ratio to increase ion velocities artifically,
(3) reduce the number of ions created per cell, and
(4) reduce the ion creation frequency (time step multiple).

All of the above may be accomplished using options in the PARTICLES command. Input data for this simulation is shown in Table 3.6.

3.6.3 Analytical Solution.

At late time, when many ions have had time to cross the gap, a steady state with space-charge-limited flow from both anode and cathode can occur. The cathode will emit electrons and the anode will emit ions as if they are both covered with dense plasma.

The presence of ions in the gap will allow higher electron current densities and thus lower the effective impedance. The effective current is

$$I = \pi R^2 (J_e + J_i) \ , \tag{3.19}$$

where J_i and J_e are the steady-state electron and ion currents in the gap. The derivation which follows is based on a treatment given by Miller.† The current densities are

$$J_e = -en_e v_e$$

and

$$J_i = +en_i v_i \ , \tag{3.20}$$

where n_e and n_i are the electron and ion densities respectively, e is the electron charge, and v_e and v_i are the electron and ion velocities. We assume all particles enter the gap with zero velocity, so that the energies are given by

$$1/2\ m_e v_e^2 = e\phi$$

and

$$1/2\ m_i v_i^2 = e(\phi_o - \phi) \ , \tag{3.21}$$

where m_I and m_e are the electron and ion masses, respectively, and ϕ is the potential. The ions are (in this problem) assumed to be singly charged, ϕ_o is the potential at the anode, and both anode and cathode are assumed to behave as high-density plasmas, so that

$$\partial_x \phi = 0 \ , \tag{3.22}$$

at both anode and cathode surfaces. In a manner similar to that used for pure electron flow, we write Poisson's equation,

† R. B. Miller, An Introduction to the Physics of Intense Charged Particle Beams Plenum Publishing, New York, (1982) p. 55.

$$\partial_x^2 \phi = e(n_e - n_i)/\varepsilon_0 \ , \tag{3.23}$$

where x is the distance from the cathode. Assuming steady-state flow for both species, we write

$$\partial_x^2 \phi = \frac{J_e}{\varepsilon_0} \left(\frac{m_e}{2e} \right)^{1/2} \left(\phi^{-1/2} - \alpha(\phi_o - \phi)^{-1/2} \right) \ ,$$

where $\tag{3.24}$

$$\alpha = \frac{J_i}{J_e} \left(\frac{m_i}{m_e} \right)^{1/2} \ .$$

This equation can be simplified mathematically by substitution and a step of integration to obtain

$$(\partial_y \psi)^2 = \left(\frac{16}{9} \right) \left(\frac{J_e}{J_o} \right) [\psi^{1/2} + \alpha(1-\psi)^{1/2}] - \beta \ , \tag{3.25}$$

where $\psi = \phi/\phi_o$, $y = x/d$ (where d is the gap separation), and J_o is the electron current density for such a gap in the absence of ion flow.

The conditions of Equation (3.22) at both anode and cathode require

$$\alpha = 1$$

and $\tag{3.26}$

$$\beta = \frac{16}{9} \left(\frac{J_e}{J_o} \right) .$$

A second (numerical) integration of Equation (3.25) solves for J_e/J_o to yield

$$J_e = 1.86\ J_o \ , \tag{3.27}$$

and by Equations (3.24) and (3.26),

$$J_i = 1.86\ J_o \left(\frac{m_e}{m_i} \right)^{1/2} \ . \tag{3.28}$$

where J_o is the current density of electrons without ion flow,

$$J_o = \frac{4}{9} \varepsilon_0 \left(\frac{2e}{m} \right)^{1/2} \frac{\phi^{+3/2}}{d^2} \ . \tag{3.29}$$

Thus, the effective impedance must be approximately given by

$$Z = \frac{\phi^+}{1.86\ J_o \pi R^2 \left(1 + \left(\frac{m_e}{m_i} \right)^{1/2} \right)} \ ,$$

or

$$Z = \frac{Z_o}{1.86 \left(1 + \left(\frac{m_e}{m_i} \right)^{1/2} \right)} \ , \tag{3.30}$$

where Z_o is the impedance for electron only space-charge-limited flow. Therefore, the impedance is roughly one-half the value without ion flow. This is a steady-state value which, for realistic ratios of m_i/m_e, will not occur until late in time. The initial states of the gap will resemble the case with no ions; however, as the gap approaches steady-state ion flow, the impedance will fall to the final value.

Trajectory plots for electrons and ions at the end of the simulation are shown in Figures 3.20 and 3.21, respectively. Since the motion of the ions is thus limited, there is not much hope of observing the effect of Equation (3.30) without running longer in time.

Table 3.6. Input data for Problem 3.6.

```
title *problem 3.6* /
comment *problem 3.6 is the same diode as problem 3.5,
         but with two species of particles.* /
system 2 /
x1grid 1 67 2 0.0 25 0.008 0.2 20 0.008 0.1
                                10 0.002 0.05 10 0.008 0.05 /
x2grid 1 42 2 0.0 20 0.008 0.1 10 0.002 0.05 10 0.008 0.05 /
fields 1 3 800 6.25e-12 0.5 0.5 0.0
       4 1.0 0.29912 0.15022 0.11111 /
courant 0 0 /
conductor cathode 1 2 22 47 22 47  2 /
conductor anode  -1 2 42 67 42 67  2 /
symmetry axial 1 2  2 67  2 /
particles emission null electrons 0 0 6 1 1 2 1
          1.0e+7 6.25e-5 2.5e7 0.0 0.0 0.0 0.0 1  7 22 47 22 /
particles emission null electrons 0 0 6 1 1 2 1
          1.0e+7 6.25e-5 2.5e7 0.0 0.0 0.0 0.0 1 47 22 47  2 /
particles emission null ions 1 1 1 1 1 2 1
          1.0e+7 6.25e-5 2.5e7 0.0 0.0 0.0 0.0  -1 67 42 67  2 /
kinematics 1 0 0 0 0 /
currents 64 1.0 /
forces 0 0.5 1.0 1.0 /
voltage incident radial 1 twod 0 1.0 1 2 22 2 42 2 /
function incident 0 3 0.0 0.0 1.0e-9 4.0e6 1.0 4.0e6 /
function radial 5  -1 1 /
diagnose spacing 0 1 courant 0 1 /
statistics 200 /
trajectory 200 1 1 0.0 0.6 -0.15 0.45 /
observe 1 1 twod 1 0.0 1.0 0.0 1.0 2  2 22  2 42
            twod 1 0.0 1.0 0.0 1.0 2 47 22 47 42
            twod 1 0.0 1.0 0.0 1.0 1 47  2 67  2 /
range 200 1 2  2 22  2 42 1
          1 2 47 22 47 42 1
          1 1 47  2 67  2 1 /
display 0 0.0 0.6 -0.15 0.45 /
output 0 /
timeout 60 1 /
start /
stop /
```

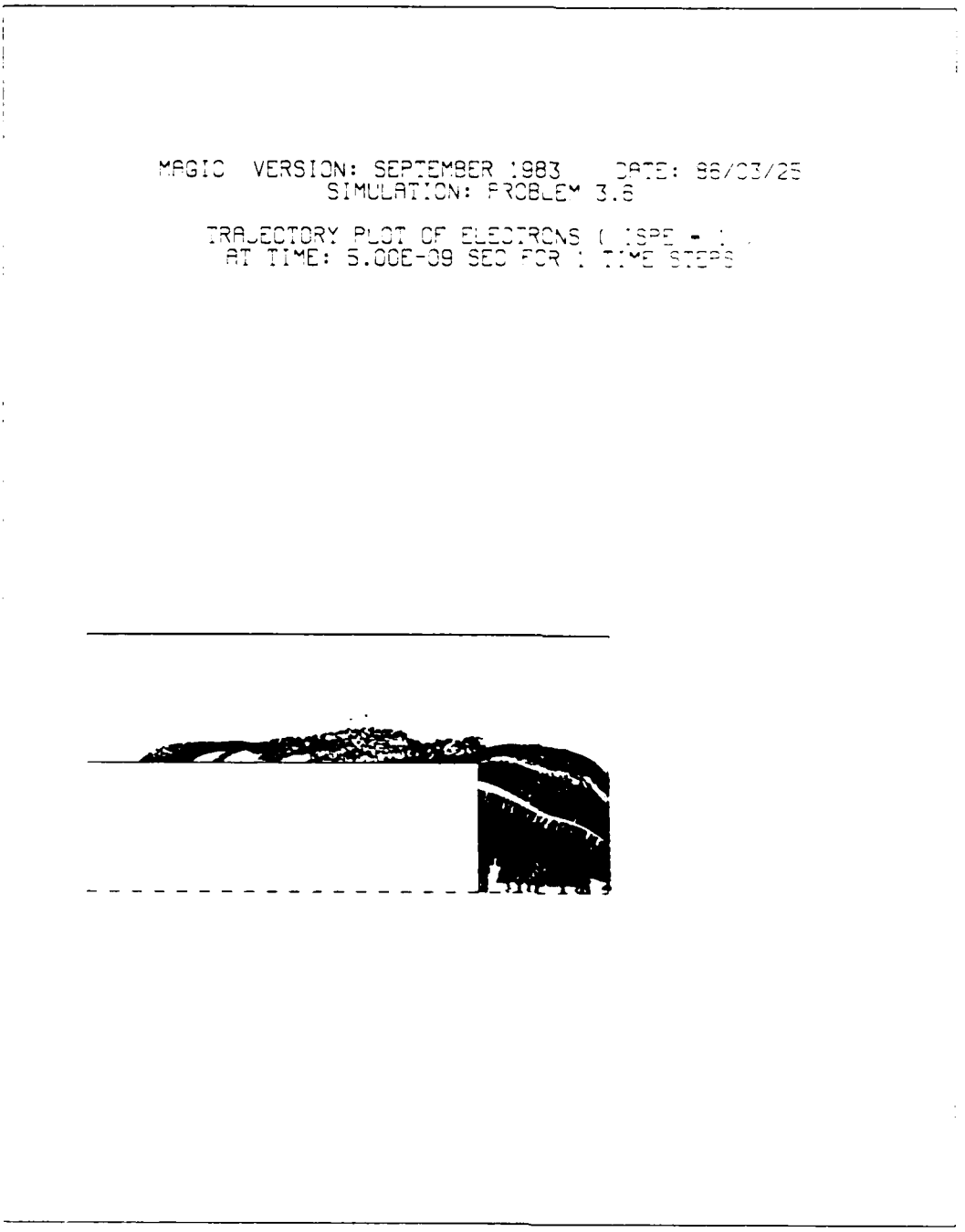

Figure 3.20. Electron trajectory plot, Problem 3.6.

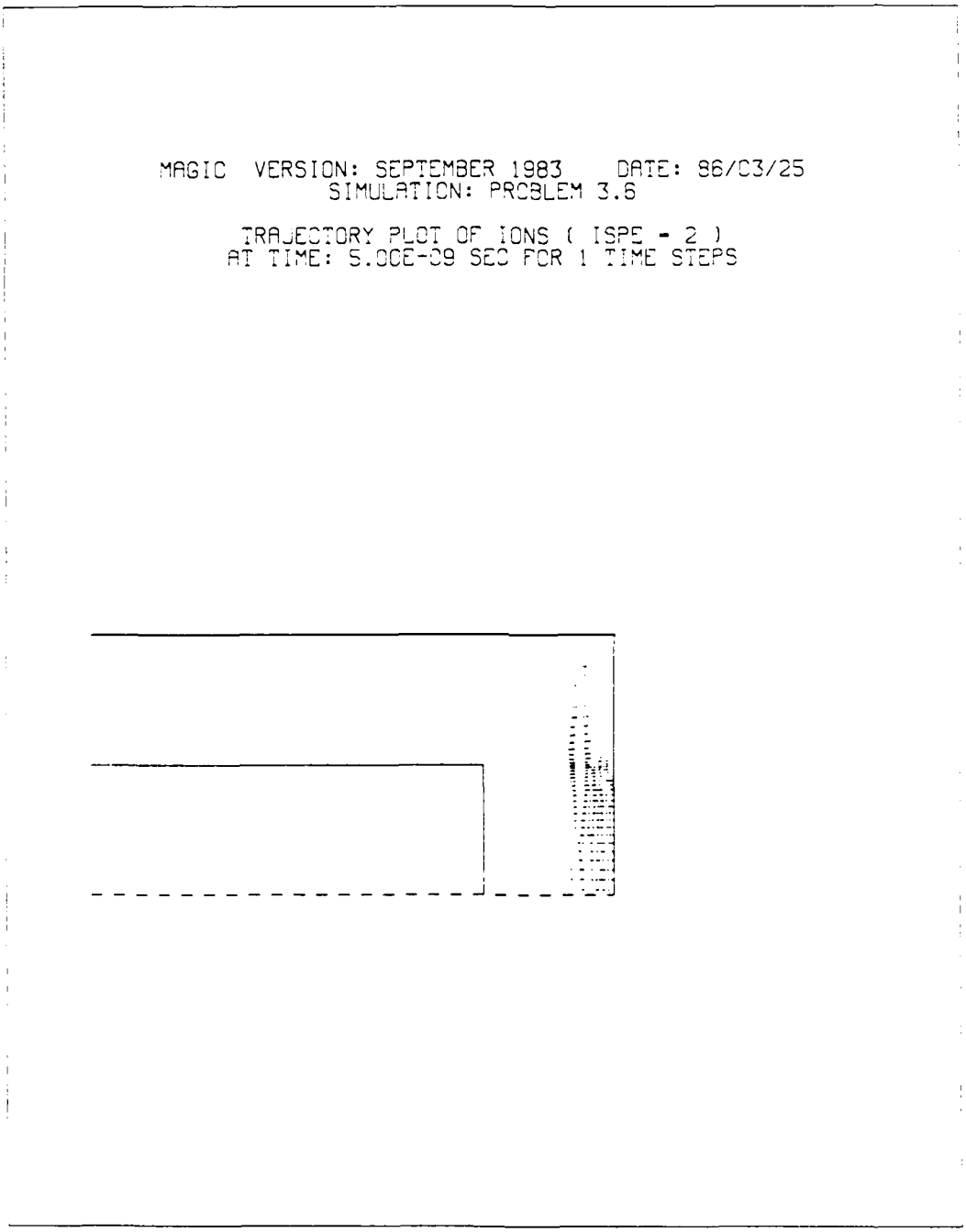

Figure 3.21. Ion trajectory plot, Problem 3.6.

3.7 COLD-TEST OF SHORTED DIODE.

3.7.1 Problem Description.

In this simulation, a short is to be placed between anode and cathode two cells above the axis of symmetry, and the field emission is to be deleted. Measurements consisting of range plots and time histories taken at the inlet, the mismatch, and near the short, should be made.

3.7.2 Suggested Approach.

Maintaining the previous electromagnetic model, simply delete the axial symmetry boundary condition and insert a conductor. The input data is shown in Table 3.7.

3.7.3 Analytical Solution.

The results derived for Problem 3.2 are clearly applicable here. The multiple reflections described in Equation (8) are particularly pronounced due to the disparity in impedances, i.e., $Z_2 \to \infty$ and $Z_3 = 0$. Voltage plots at inlet, midpoint, and near axis are shown in Figures 3.22, 3.23, and 3.24, respectively.

Table 3.7. Input data for Problem 3.7.

```
title *problem 3.7* /
comment *problem 3.7 is a cold test of problem 3.6
         with a short* /
system 2 /
x1grid 1 67 2 0.0 25 0.008 0.2 20 0.008 0.1
                                20 0.002 0.1  /
x2grid 1 42 2 0.0 20 0.008 0.1 20 0.002 0.1 /
fields 1 3 800 6.25e-12 0.5 0.5 0.0
       4 1.0 0.29912 0.15022 0.11111 /
courant 0 0 /
conductor cathode 1 2 22 47 22 47  4 /
conductor short 1 47  4 67  4 /
conductor anode  -1 2 42 67 42 67  4/
symmetry axial 1 2  2 67  2 /
z particles emission null electrons 0 0 6 1 1 2 1
           1.0e+7 6.25e-5 2.5e7 0.0 0.0 0.0 0.0 1  7 22 47 22 /
z particles emission null electrons 0 0 6 1 1 2 1
           1.0e+7 6.25e-5 2.5e7 0.0 0.0 0.0 0.0 1 47 22 47  4 /
kinematics 1 0 0 0 0 /
currents 64 1.0 /
forces 0 0.5 1.0 1.0 /
voltage incident radial 1 twod 0 1.0 1 2 22 2 42 2 /
function incident 0 3 0.0 0.0 1.0e-9 4.0e6 1.0 4.0e6 /
function radial 5  -1 1 /
diagnose spacing 0 1 courant 0 1 /
statistics 200 /
trajectory 200 1 1 0.0 0.6 -0.15 0.45 /
observe 1 1 twod 1 0.0 1.0 0.0 1.0 2  2 22  2 42
            twod 1 0.0 1.0 0.0 1.0 2 47 22 47 42
            twod 1 0.0 1.0 0.0 1.0 1 47  5 67  5 /
range 200 1 2  2 22  2 42 1
          1 2 47 22 47 42 1
          1 1 47  5 67  5 1 /
display 0 0.0 0.6 -0.15 0.45 /
output 0 /
timeout 60 1 /
start /
stop /
```

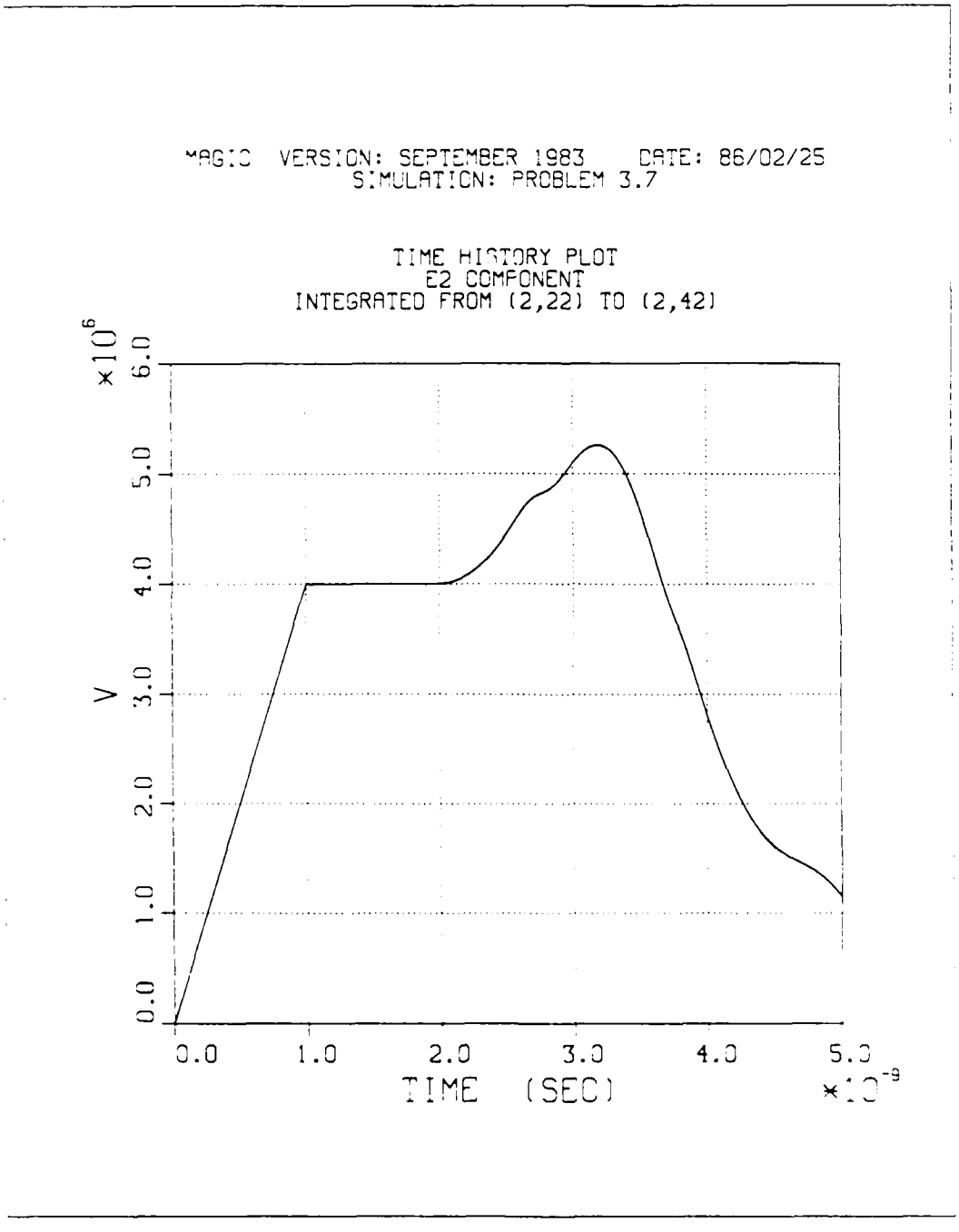

Figure 3.22. Inlet voltage vs. time, Problem 3.7.

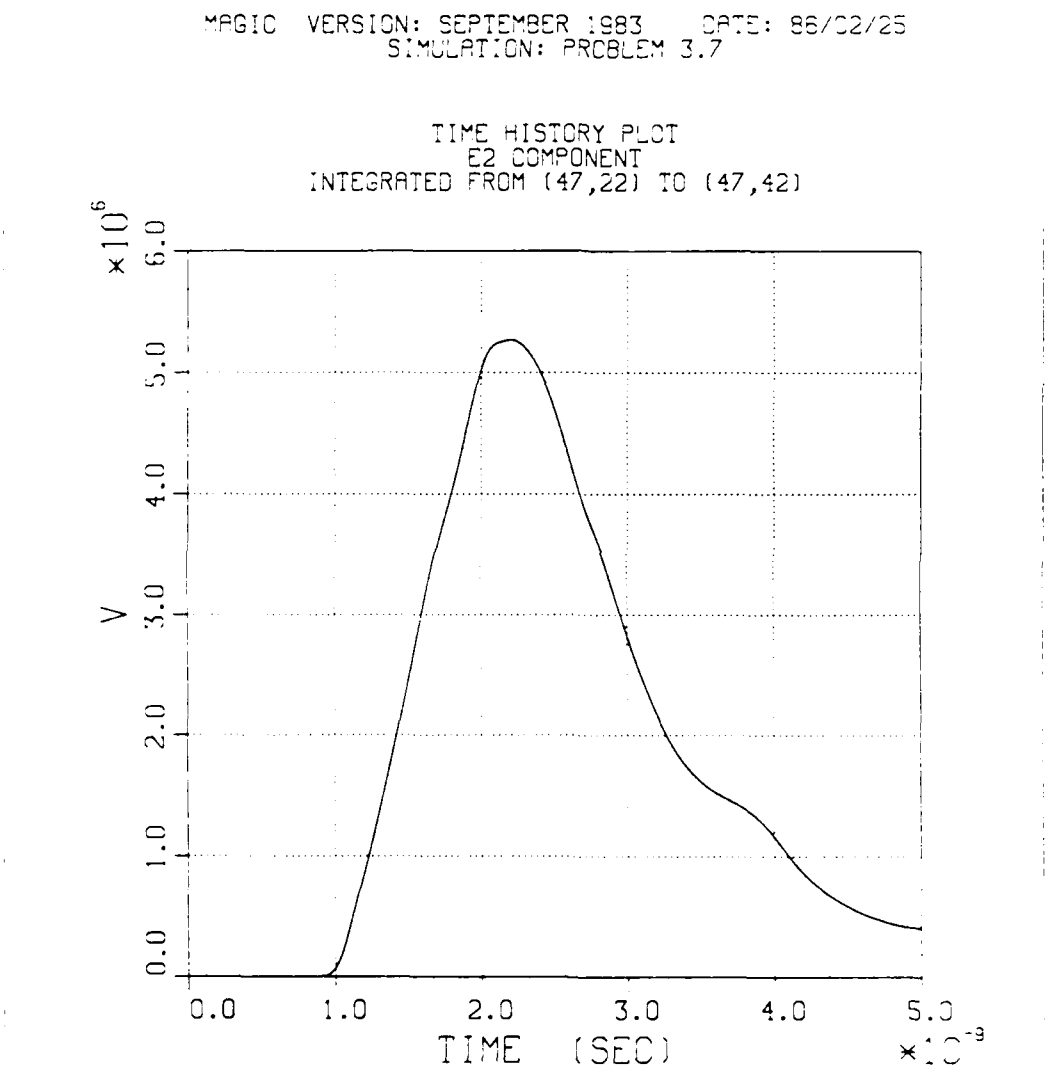

Figure 3.23. Midpoint voltage vs. time, Problem 3.7.

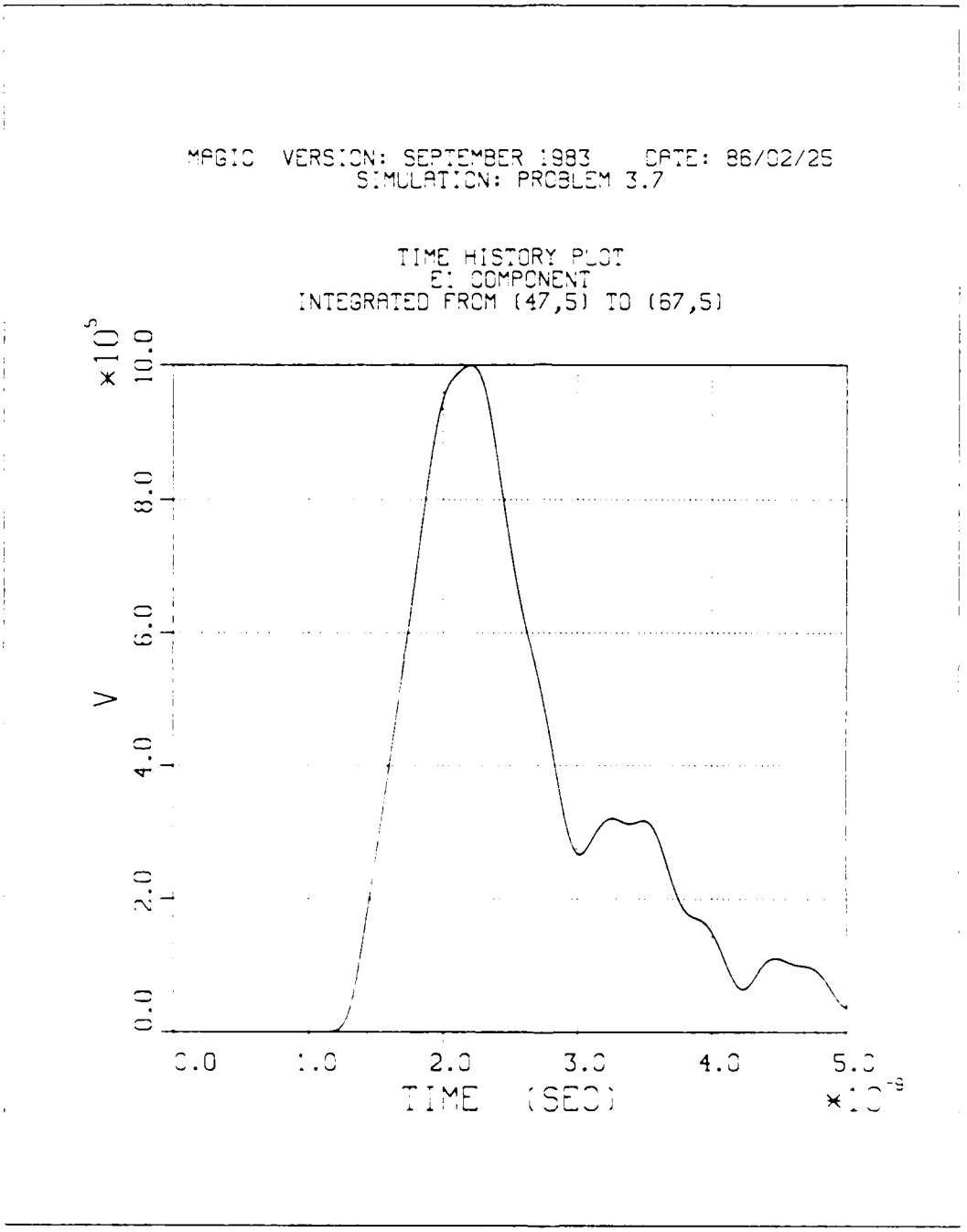

Figure 3.24. Axial voltage vs. time, Problem 3.7.

3.8 SHORTED DIODE WITH FIELD EMISSION.

3.8.1 Problem Description.

Problem 3.8 uses the shorted diode of Problem 3.7, but with cathode (electron) field emission reinstated on both conformal surfaces.

3.8.2 Suggested Approach.

A potential difficulty can result from electron trajectory calculations due to the large magnetic fields near axis. The standard kinematics algorithm will allow time steps consistent with up to $\pi/4$ radians in orbit. Beyond this, the algorithm becomes inaccurate, and artificial particle motion will result.† The onset of this difficulty can be estimated using previous results from Problems 2.2 and 3.7.

Input data for this simulation is shown in Table 3.8.

3.8.3 Analytical Solution.

Current through the short produces a magnetic field which varies inversely with radius. Thus, electrons tend to move in circular orbits, and tend to move toward the short due to ExB drift (see Problem 2.3). However, the short impedance is dominant, so that field emission affects the transient but not the steady state.

Figure 3.25 illustrates the voltage at inlet. Electron trajectory plots at 2.5 and 5.0 nsec are shown in Figures 3.26 and 3.27, respectively, where the tendency of electrons to orbit is clearly demonstrated.

† B. Goplen, J. Brandenburg, and R. Worl, "Particle Subcycling in Pulsed Power Simulations." MRC/WDC-R-125. April 1987.

Table 3.8. Input data for Problem 3.8.

```
title *problem 3.8* /
comment *problem 3.8 is a simulation of
         a diode like the one in problem 3.5,
         but with a short near the axis of symmetry* /
system 2 /
x1grid 1 67 2 0.0 25 0.008 0.2 20 0.008 0.1
                               20 0.002 0.1  /
x2grid 1 42 2 0.0 20 0.008 0.1 20 0.002 0.1 /
fields 1 3 800 6.25e-12 0.5 0.5 0.0
       4 1.0 0.29912 0.15022 0.11111 /
courant 0 0 /
conductor cathode 1 2 22 47 22 47  4 /
conductor short 1 47  4 67  4 /
conductor anode  -1 2 42 67 42 67  4/
symmetry axial 1 2  2 67  2 /
particles emission null electrons 0 0 6 1 1 2 1
          1.0e+7 6.25e-5 2.5e7 0.0 0.0 0.0 0.0 1  7 22 47 22 /
particles emission null electrons 0 0 6 1 1 2 1
          1.0e+7 6.25e-5 2.5e7 0.0 0.0 0.0 0.0 1 47 22 47  4 /
kinematics 1 0 0 0 0 /
currents 64 1.0 /
forces 0 0.5 1.0 1.0 /
voltage incident radial 1 twod 0 1.0 1 2 22 2 42 2 /
function incident 0 3 0.0 0.0 1.0e-9 4.0e6 1.0 4.0e6 /
function radial 5  -1 1 /
diagnose spacing 0 1 courant 0 1 /
statistics 200 /
trajectory 200 1 1 0.0 0.6 -0.15 0.45 /
observe 1 1 twod 1 0.0 1.0 0.0 1.0 2  2 22  2 42
            twod 1 0.0 1.0 0.0 1.0 2 47 22 47 42
            twod 1 0.0 1.0 0.0 1.0 1 47  5 67  5 /
range 200 1 2  2 22  2 42 1
          1 2 47 22 47 42 1
          1 1 47  5 67  5 1 /
display 0 0.0 0.6 -0.15 0.45 /
output 0 /
timeout 60 1 /
start /
stop /
```

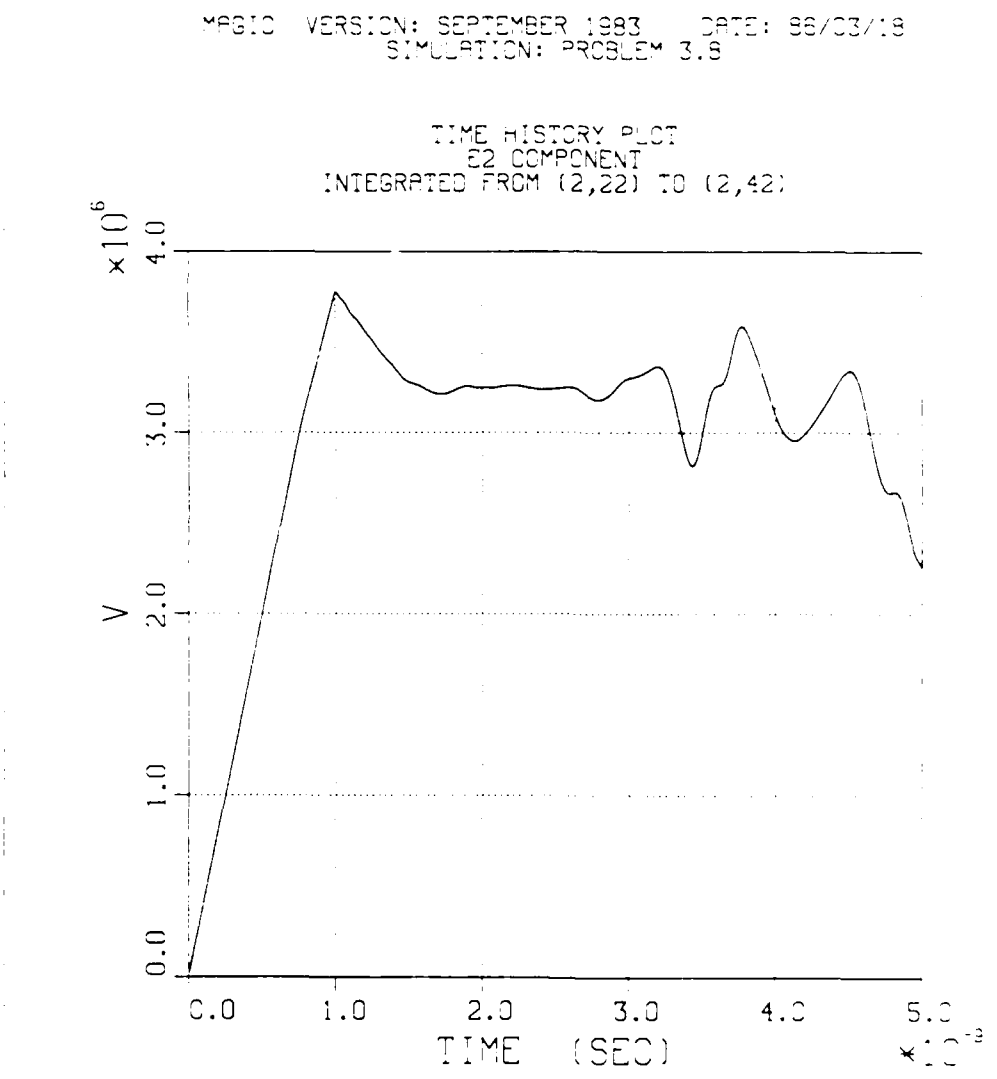

Figure 3.25. Inlet voltage vs. time, Problem 3.8.

MPGIC VERSION: SEPTEMBER 1983 DATE: 86/03/18
SIMULATION: PROBLEM 3.8

TRAJECTORY PLOT OF ELECTRONS (ISPE = 1)
AT TIME: 2.50E-09 SEC FOR 1 TIME STEPS

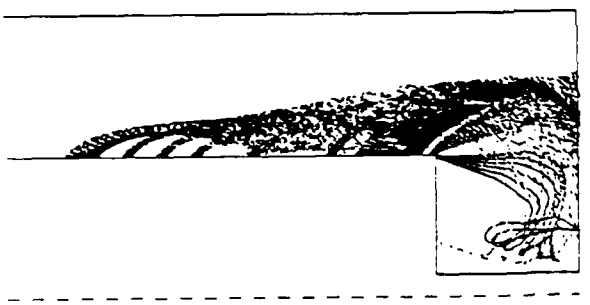

Figure 3.26. Trajectory plot at 2.5 nsec, Problem 3.8.

MAGIC VERSION: SEPTEMBER 1983 DATE: 86/03/18
SIMULATION: PROBLEM 3.8

TRAJECTORY PLOT OF ELECTRONS (ISPE = 1)
AT TIME: 5.00E-09 SEC FOR 1 TIME STEPS

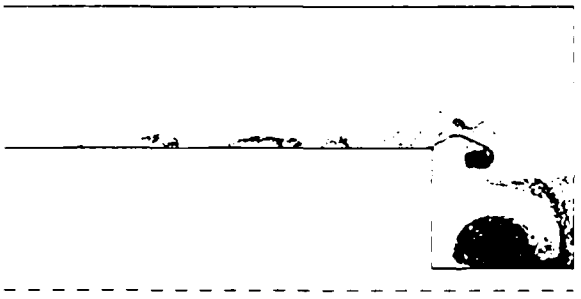

Figure 3.27. Trajectory plot at 5.0 nsec, Problem 3.8.

DISTRIBUTION LIST

DEPARTMENT OF DEFENSE

ASSISTANT TO THE SECRETARY OF DEFENSE
ATOMIC ENERGY
ATTN: EXECUTIVE ASSISTANT

DEFENSE INTELLIGENCE AGENCY
ATTN: RTS-2B

DEFENSE NUCLEAR AGENCY
ATTN: RAAE
ATTN: RAEE
2 CYS ATTN: RAEV
4 CYS ATTN: TITL

DEFENSE TECHNICAL INFORMATION CENTER
12 CYS ATTN: DD

FIELD COMMAND DEFENSE NUCLEAR AGENCY
ATTN: FCTXE
ATTN: FTTD
ATTN: FTTD W SUMMA

FIELD COMMAND/DNA
ATTN: FC-1

UNDER SECRETARY OF DEFENSE
ATTN: STRAT/SPACE SYS(OS)

DEPARTMENT OF THE ARMY

HARRY DIAMOND LABORATORIES
ATTN: SCHLD-NW-P
ATTN: SLCHD-NW-RA
ATTN: SLCHD-NW-RI KERVIS
ATTN: SLCIS-IM-TL (TECH LIB)

U S ARMY MISSILE COMMAND
ATTN: AMSMI-RD-CS-R (DOCS)

U S ARMY NUCLEAR & CHEMICAL AGENCY
ATTN: LIBRARY

U S ARMY TEST AND EVALUATION COMD
ATTN: AMSTE

DEPARTMENT OF THE NAVY

NAVAL RESEARCH LABORATORY
ATTN: CODE 2000 J BROWN
ATTN: CODE 4700 S OSSAKOW
ATTN: CODE 4701 I VITOKOVITSKY
ATTN: CODE 4720 J DAVIS
ATTN: CODE 4770 G COOPERSTEIN

NAVAL SURFACE WEAPONS CENTER
ATTN: CODE R40

NAVAL SURFACE WEAPONS CENTER
ATTN: CODE H-21

NAVAL WEAPONS CENTER
ATTN: CODE 343 (FKA6A2) TECH SVCS

DEPARTMENT OF THE AIR FORCE

AIR FORCE WEAPONS LABORATORY
ATTN: NT
ATTN: SUL

BALLISTIC MISSILE OFFICE
ATTN: ENSN

DEPUTY CHIEF OF STAFF/AF-RDQM
ATTN: AF/RDQI

SPACE DIVISION/XR
ATTN: XR (PLANS)

SPACE DIVISION/YA
ATTN: YAR
ATTN: YAS

SPACE DIVISION/YE
ATTN: SD/CWNZ

SPACE DIVISION/YG
ATTN: YGJ

SPACE DIVISION/YK
ATTN: YFF

SPACE DIVISION/YN
ATTN: YNV

DEPARTMENT OF ENERGY

DEPARTMENT OF ENERGY
ATTN: OFC OF INERT FUSION
ATTN: OFC OF INERT FUSION C HILLAND
ATTN: OFC OF INERT FUSION R SHRIEVER

LAWRENCE LIVERMORE NATIONAL LAB
ATTN: D MEEKER
ATTN: L-153
ATTN: TECH INFO DEPT LIBRARY
ATTN: J NUCKOLLS

LOS ALAMOS NATIONAL LABORATORY
ATTN: J BROWNELL

SANDIA NATIONAL LABORATORIES
ATTN J E POWELL
ATTN M J CLAUSER
ATTN D J ALLEN
ATTN TECH LIB 3141 (RPTS REC CLRK)

OTHER GOVERNMENT

CENTRAL INTELLIGENCE AGENCY
ATTN OSWR/NED

DEPARTMENT OF DEFENSE CONTRACTORS

ADVANCED RESEARCH & APPLICATIONS CORP
ATTN R ARMISTEAD

AEROSPACE CORP
ATTN LIBRARY ACQUISITION

BDM CORP
ATTN CORPORATE LIB

BDM CORP
ATTN L O HOEFT

EOS TECHNOLOGIES, INC
ATTN B GABBARD

GENERAL ELECTRIC CO
ATTN H ODONNELL

IRT CORP
ATTN J M WILKENFELD
ATTN R MERTZ

JAYCOR
ATTN E MENAAS

JAYCOR
ATTN R SULLIVAN

JAYCOR
ATTN C ROGERS

KAMAN SCIENCES CORP
ATTN S FACE

KAMAN SCIENCES CORP
ATTN E CONRAD

KAMAN SCIENCES CORPORATION
ATTN TECH LIB FOR/D PIRIO

KAMAN SCIENCES CORPORATION
ATTN DASIAC

KAMAN TEMPO
ATTN DASIAC

LOCKHEED MISSILES & SPACE CO, INC
ATTN L CHASE

LOCKHEED MISSILES & SPACE CO, INC
ATTN S TAIMUTY

MAXWELL LABS, INC
ATTN A KOLB
ATTN M MONTGOMERY

MCDONNELL DOUGLAS CORP
ATTN S SCHNEIDER

MISSION RESEARCH CORP
ATTN C LONGMIRE

MISSION RESEARCH CORP, SAN DIEGO
ATTN V VAN LINT

MISSION RESEARCH CORPORATION
2 CYS ATTN B GOPLEN
2 CYS ATTN R WORL

PACIFIC-SIERRA RESEARCH CORP
ATTN H BRODE, CHAIRMAN SAGE
ATTN L SCHLESSINGER

PHYSICS INTERNATIONAL CO
ATTN C GILMAN
ATTN C STALLINGS
ATTN G FRAZIER

PULSE SCIENCES, INC
ATTN I D SMITH
ATTN P W SPENCE
ATTN S PUTNOM

R & D ASSOCIATES
ATTN C KNOWLES
ATTN P TURCHI

RAND CORP
ATTN P DAVIS

RAND CORP
ATTN B BENNETT

S-CUBED
ATTN A WILSON

SCIENCE APPLICATIONS INTL CORP
ATTN K SITES

SCIENCE APPLICATIONS INTL CORP
ATTN W CHADSEY

TRW INC
ATTN D CLEMENT
ATTN TECH INFO CTR DOC ACQ

END

DATE

FILMED

5-88

DTIC